HUGHES

HUGHES DANBURY OPTICAL SYSTEMS, INC.
a subsidiary

PR D15-0013A

LUTE PRIMARY MIRROR
MATERIALS AND DESIGN STUDY REPORT

February 1993

Prepared for:
National Aeronautics and Space Administration
George C. Marshall Space Flight Center
Marshall Space Flight Center
Alabama 35812
Order No. H-11994D

HUGHES DANBURY OPTICAL SYSTEMS, INC.
100 WOOSTER HEIGHTS ROAD
DANBURY, CT 06810-7589

All or a portion of the Work Discussed herein was Supported by NASA/MSFC

HUGHES DANBURY OPTICAL SYSTEMS, INC.
a subsidiary

PR D15-0013A

LUTE PRIMARY MIRROR
MATERIALS AND DESIGN STUDY REPORT

February 1993

Prepared for:
National Aeronautics and Space Administration
George C. Marshall Space Flight Center
Marshall Space Flight Center
Alabama 35812
Order No. H-11994D

HUGHES DANBURY OPTICAL SYSTEMS, INC.
100 WOOSTER HEIGHTS ROAD
DANBURY, CT 06810-7589

All or a portion of the Work Discussed herein was Supported by NASA/MSFC

HUGHES

Hughes Danbury Optical Systems, Inc.
a subsidiary

PUBLICATION REVIEW:

Prepared by: _____ 2/26/93
Greg Ruthven, Project Engineer — Date

Approved by: _____ 26 Feb 93
Mark Stier, Program Manager — Date

_____ 2/26/93
George Bossers, Director Advanced Development Lab — Date

REVISION RECORD:

Revision	Date	Affected Pages
A	2-26-93	i through vi, 1-1, 2-1, 2-2, 3-1 through 3-12, 4-1 through 4-22, 5-1, 5-2, 6-1, 7-1, 8-1, A-1 through A-23, B-1 through B-29

TABLE OF CONTENTS

LIST OF ILLUSTRATIONS

LIST OF TABLES

SECTION 1
INTRODUCTION

The major objective of the Lunar Ultraviolet Telescope Experiment (LUTE) Primary Mirror Materials and Design Study is to investigate the feasibility of the LUTE telescope primary mirror. We took a systematic approach to accomplish this key goal by first understanding the optical, thermal and structural requirements and then deriving the critical primary mirror-level requirements for ground testing, launch, and lunar operations.

After summarizing our results in Section 2, Section 3 discusses those requirements which drove the selection of material and the design for the primary mirror. Most important of these are the optical design which we assumed to be the MSFC baseline (i.e. 3 mirror optical system), telescope wavefront error (WFE) allocations, the telescope weight budget, and the LUTE operational temperature ranges. Section 3 also discusses mechanical load levels, reflectance and microroughness issues, options for the LUTE metering structure and initiates an outline for the LUTE telescope sub-system design specification.

Section 4 presents our primary mirror analysis and results. We discuss the six material substrate candidates and show four distinct mirror geometries which we considered for our study. With these materials and configurations together with varying the location of the mirror support points, a total of 42 possible primary mirror designs resulted. We also investigated the polishability of each substrate candidate and present a usage history of 0.5 meter and larger precision cryogenic mirrors (the operational low end LUTE temperature of 60 K is the reason we feel a survey of cryogenic mirrors is appropriate) that have been flown or tested. Sections 4.3 and 4.4 present performance data in summary form via bar charts; more detailed analysis is provided in the data tables. Additional material is provided in Appendix A. Material cryogenic properties are provided in Appendix B. Section 4 concludes with a mass properties summary to aid both telescope feasibility and telescope material selection along with information required for launch vehicle applicability and performance. The active primary mirror design approach is also discussed and its impact on weight and performance is assessed.

We describe the leading mirror materials and configurations in Section 5 with rational on these selections and our assessment of producing such a primary mirror.

We conclude our study with a set of recommendations not only with respect to the LUTE primary mirror but also on other topics related to the overall feasibility of the LUTE telescope sub-system.

SECTION 2
SUMMARY OF RESULTS

The ability to design, build, test and successfully launch and operate a 1-meter class diffraction-limited telescope operating over a 200 K temperature range appears to be feasible, albeit very technically challenging. From our understanding of the requirements, a primary mirror areal density (mass per unit area) of 28 kg/m^2 is necessary and must have a wavefront error of less than ~1/30th wave rms at 0.6328 μm of which no more than ~1/46th wave rms can be caused by thermally induced distortions. The primary mirror can not have a 1-g to 1/6-g residual (after telescope re-alignment) distortion of more than ~ 1/200th wave rms. The ability to fabricate such a 1-m cryo mirror that weighs less than 22 kg and is diffraction limited is unproven at this time.

After evaluating all of the candidates in our trade space, a single arch mirror design, fabricated from beryllium is the leading candidate for the LUTE primary mirror. This design is marginally acceptable in terms of residual 1-g deformation. All other candidate designs have poorer performance. This leading candidate design is very strongly based on our engineering judgment that use of a cryogenic metrology mount (to simulate 1/6-g deformation in a 1-g environment) would be an excessively high risk approach. We believe a logical approach to 1-g testing and verification is one which does not utilize a cryo "met" mount.

We have briefly assessed an active primary mirror design option which uses figure control actuators to compensate for mirror distortions. In addition to a significant weight penalty we doubt that the level of figure error correction required (better than 90%) is attainable. A further disadvantage of an active primary mirror is the need to periodically determine what figure corrections are needed and the need to actuate them reliably over several years. We have, therefore, rejected the active primary mirror design option.

We have also briefly assessed the concept of fabricating the tertiary mirror directly on the same substrate as the primary mirror. This approach would avoid the need for a separate mount for the tertiary mirror and make the optical system less sensitive to thermally-induced misalignments. Although we have done no analysis, in the judgment of our optical fabrication experts it is feasible to fabricate the tertiary mirror and the primary mirror on the same substrate.

Thermally induced mirror deformations must be closely monitored. The ±100 K range of operating temperatures is an exceptionally severe environment for a precision optical system. Our analyses show that the allowable temperature gradient across the mirror diameter or through its thickness is highly dependent on the particular temperature at which the measurement is taking place. This is due to the fact that each candidate primary mirror material has a different temperature dependence of its coefficient of thermal expansion (CTE.) For a single arch design a lower operating temperature (e.g. 60 K) is preferred if the CTE at the lower temperatures is lower than its room temperature value.

At 60 K, a side-to-side (i.e. diametral) gradient of approximately 1 K is allowable. From our discussions with MSFC this value seems realistic based on preliminary thermal analyses. However an area which needs further investigation is the allowable variation in CTE (and $\Delta L/L$) of the substrate itself. Our calculations show that the beryllium $\Delta L/L$ inhomogeneity must be maintained to within less than 1%. This represents a technical challenge and further discussions with beryllium vendors is certainly warranted. This issue is also important in the overall architecture of the LUTE mission and may determine whether operating temperatures should be more closely controlled via a telescope thermal control system.

SECTION 3
PRIMARY MIRROR DESIGN AND PERFORMANCE REQUIREMENTS

Our derivation of the LUTE primary mirror top level requirements is based on the three-mirror telescope configuration as baselined by MSFC and shown in Figure 3-1. The driving requirements include both wavefront error and weight allocations. Mirror performance predictions were calculated using these allocations as guidelines in our design effort and these calculations ultimately resulted in a recommended substrate and mirror geometry design which we feel is warranted for further investigation.

Study logic flow is summarized in Figure 3-2. Efforts centered around the Primary Mirror Assembly design and, in particular, three aspects of this assembly: 1) the candidate mirror substrates, 2) candidate mirror designs, and 3) whether active mirror correction capability is required. To a lesser degree we evaluated whether LUTE should have active thermal control to minimize the large operational temperature range as currently baselined. We show further study logic and discuss analytical results in Sections 4.3 and 4.4.

SYSTEM DIMENSIONS:

PRIMARY O. DIAMETER	:	100 cm
PRIMARY I. DIAMETER	;	50 cm
SECONDARY DIAMETER	;	38 cm
SECONDARY HOLE	;	15 cm
TERTIARY DIAMETER	;	28 cm
MIRROR SEPARATION	:	65 cm
BACK FOCAL DISTANCE	:	65 cm
SYSTEM FOCAL LENGTH	:	300 cm
IMAGE DIAMETER	:	7.4 cm

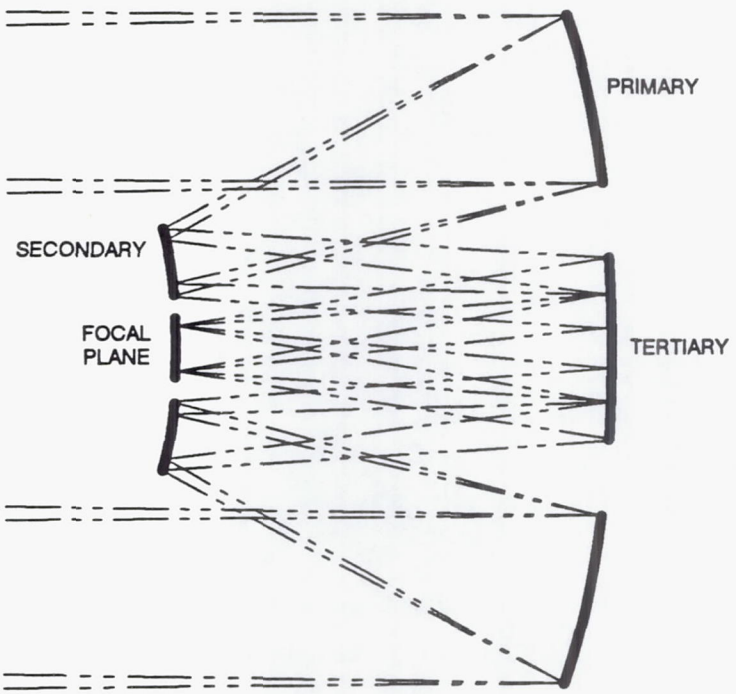

Figure 3-1. We Have Assumed the MSFC Optical Design Concept "LTT100" as the Baseline for Our Study.

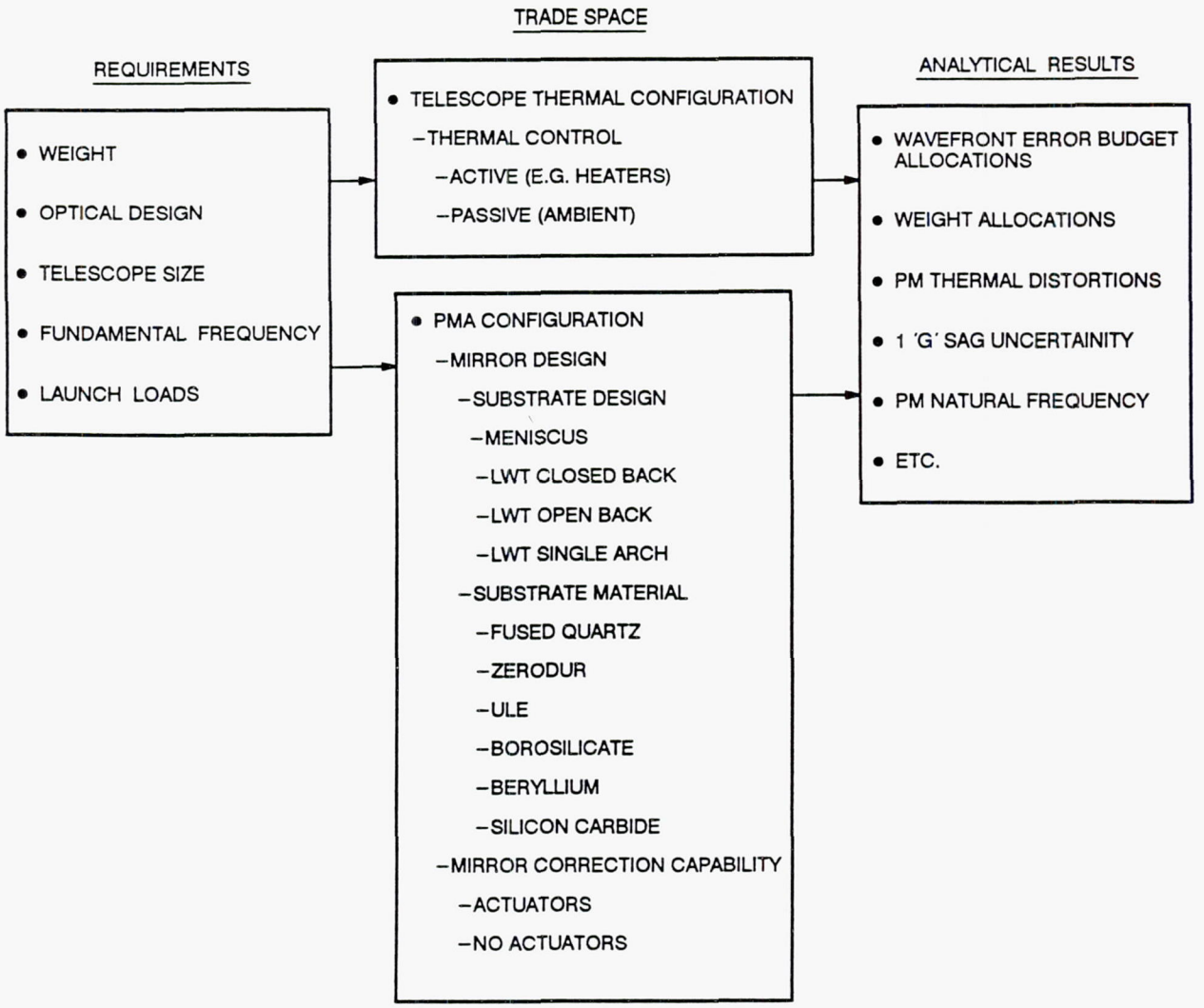

Figure 3-2. Critical Requirements Were Addressed to Ensure the Recommended Design(s) Meet Ground Testing and In-Operation Scenarios.

3.1 OPTICAL DESIGN

The optical design for LUTE was provided by MSFC. The need for a third optical element is derived from the need for a wide field of view. The LUTE concept is presently defined as a "transit" telescope that surveys the sky using only lunar rotation (and lunar precession.) It increases its effective sensitivity for faint objects by having a wide field of view to a focal plane fully populated with CCD's. This allows the integration time per object to be increased. The wide field system also increases the swath width of the sky that can be surveyed. No optical design analyses were performed as part of this study.

3.2 WAVEFRONT ERROR ALLOCATION

We developed a wavefront error allocation (Figure 3-3) for LUTE using that of the Hubble Space Telescope as a starting point. There are, however, significant differences in the two systems, and the LUTE allocation reflects its unique environment. The allocation forms a first-cut judgment of an equitable distribution of difficulty, but much more analytical work is required and considerable revisions to the allocation are likely to be needed in the future. Note that we have assumed that the secondary mirror has a re-alignment capability such that low-order wavefront errors are fully correctable.

The top-level value of 1/20 wave is a "round number" that, lacking analytical support, we believe will provide a reasonably good image quality at ultraviolet wavelengths. The majority of the budget has been allocated to the primary mirror. Only a small portion of the budget is available for primary mirror fabrication-related errors since we believe that the changes in the shape of the primary mirror from earth to moon may be particularly difficult to meet.

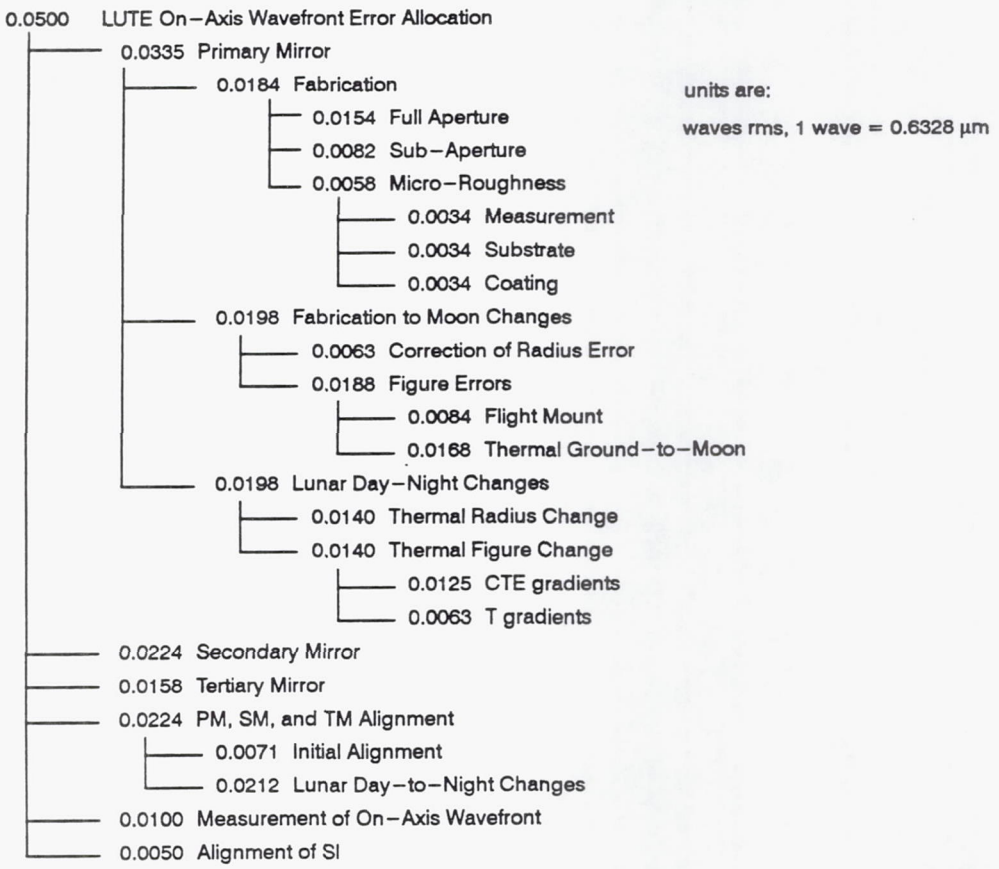

Figure 3-3. The LUTE Wavefront Error Allocation (Based on the HST WFE Budget).

There are three key contributors to post-launch changes in the shape of the primary mirror. First there is the change in deformation due to gravity. The HST mirror was precisely supported during fabrication/metrology such that it was measured in its 0-g configuration. As noted above, we believe that the use of a similar metrology mount for ground testing at LUTE's cryogenic operating temperatures would likely add more uncertainty to the interferometric data than an alternate approach that avoids the use of a cryo met mount. This decision has a very major impact on the mirror geometry selection as described below.

The second key contributor to wavefront errors is the "bulk" (mean) temperature change from the room temperature fabrication to the lunar environment. The primary effect of such a change is a radius of curvature change in the primary mirror that can be essentially eliminated by a focus mechanism at the secondary mirror. The budget allows for higher order errors, such as trefoil, spherical aberration, etc. that might be caused by CTE non-uniformities in the mirror substrate or residual effects of the mirror mount.

The third key contributor to wavefront error will be thermal gradients in the telescope. LUTE mass limitations preclude the use of a power system that can provide a stable thermal environment. Thus, as the 28 day long lunar "day" progresses there will be a changing thermal distribution in the telescope. If the mirror has a gradient in its CTE then a temperature change will produce a non-correctable figure error. Unfortunately, even if the mirror substrate has a perfectly uniform CTE, a thermal gradient in the mirror will produce a figure error. We have separated these two effects as an analytical tool for the study of primary mirror material and geometry.

3.3 WEIGHT ALLOCATION

Our weight budget allocations are based on our understanding of the LUTE telescope subsystem. We have assumed that an allocation of 84 kg total mass has been given to the telescope subsystem based on LUTE system engineering analyses done at MSFC. We have sub-allocated this 84 kg total into five major categories. They are:

- Mirrors
- Structure
- Electronics
- Thermal Control
- Alignment Sensor

These major categories and the weight allocations are shown in Table 3-1.

TABLE 3-1
LUTE TELESCOPE WEIGHT BUDGET DEFINED TO CONDUCT FEASIBILITY STUDY

Major Element	Sub-Assembly/Component	Weight (lbs)	Weight (kg)
1) Mirrors	Primary Mirror	48	21.9
	Secondary Mirror	6	2.7
	Tertiary Mirror	3	1.4
	Sub-Total	57	25.9
2) Structure	Baffle Subassembly		
	• Main	9	4.1
	• Central	2	0.9
	• SM	1	0.5
	Sub-Total	12	5.5
	Mirror Mounts		
	• PM	5	2.3
	• SM	3	1.4
	• TM	2	0.9
	Sub-Total	10	4.5
	Main Bulkhead Subassembly		
	• Main bulkhead	12	5.5
	• S/C interface fittings (3)	3	1.4
	Sub-Total	15	6.8
	Metering Bar Subassembly		
	• Metering bars (3)	3	1.4
	• Interface fittings (6)	3	1.4
	Sub-Total	6	2.7
	SM Subassembly		
	• Spider	4	1.8
	• Hub	3	1.4
	• Spider ring	3	1.4
	• Spider flexures (3)	3	1.4
	• Actuators (6)	6	2.7
	• Cabling	4	1.8
	Sub-Total	23	10.5
3) Electronics	ACE	3	1.4
	TCE	3	1.4
	DMS	3	1.4
	ASE	3	1.4
	Sub-Total	12	5.5
4) Thermal Control	Heaters	2	0.9
	Thermocouple	2	0.9
	MLI	3	1.4
	Sub-Total	7	3.2
5) Alignment Sensor	Sensor	10	4.5
	Sensor mount	2	0.9
	Sub-Total	12	5.5
	Total (w/o reserve):	154.0	70
	Reserve	31.6	14
	TOTAL	185.6	84

Based on our experience with other flight programs, we believe that a nominal value of 18% of the total 84 kg should be held in reserve for contingency factors. It is our experience that at this early stage in the development of a program, it is absolutely necessary to carry (at least) such a factor. As shown in Table 3-2, this schedule changes as a function of program maturity.

TABLE 3-2
WEIGHT CONTINGENCY SCHEDULE

Design Maturity	Contingency Factor (%)			
	Structures	Mechanisms	Wire/Cable	Therm. Control
Conceptual Estimate (Based on sketches, descriptions, experience, or finite element model)	18	18	33	18
Layout calculation (Equivalent to major mod's of existing hardware or soft mockup)	13	13	18	13
Prereleased drawings	3	3	8	8
Released drawings	1	1	2	2
Actual/measured weight	0	0	0	0

3.4 QUASI-STATIC LOADS

Once our weight allocations were established, we conducted a "zeroth order" stress analysis on several telescope components to ensure that some level of credibility existed for those allocations. We used a quasi-static load of 15-g's rms, applied singly in each of three orthogonal directions. The 15-g level is considered a limit load factor. Factors of safety of 1.25 and 1.5 for yield and ultimate criteria were used to assess the resulting design load factors. These design load factors are fully consistent with other flight programs that have used for expendable launch vehicles (ELV) including Titan IV, Delta II, and Atlas/Centaur.

A coupled loads analysis will eventually be required in order to attain more specific loads at each location of the telescope subsystem. This analysis will take into consideration the contribution of both "rigid" and "elastic" body effects due to transient, random vibration, steady state, and acoustic environments during ascent. However, this analysis may be deferred until a more definitive architecture for both the telescope subsystem and the spacecraft is in place.

The fundamental frequency of the telescope subsystem and each component is also a variable in the determination of flight load levels. There are generally two overriding concerns when trying to determine requirements for natural frequencies. The first is what is termed "avoidance frequencies." We desire the telescope to be sufficiently stiff relative to the ELV to avoid possible amplification of loads which might result if the elastic body (e.g. the telescope) dynamically couples into the launch vehicle modes. As an example, the Titan IV vehicle has two distinct avoidance frequencies; from 6-10 Hz in the lateral direction and 17-24 Hz in the axial (e.g. thrust) direction. If a high mass system's natural frequency is sitting between these bands, dynamically amplified loads will probably occur.

The second fundamental frequency requirement is derived from control system servo/structural interaction concerns. If the telescope has a closed loop servo system such as a fast steering mirror it is highly desirable that the structural modes be considerably higher than the bandwidth of the servo. Since we do not envision any closed loop active systems being implemented for LUTE, this requirement is not of concern here.

To address fundamental frequency requirements we have set as a guideline that we desire that the telescope be sufficiently stiff so that no amplification of loads will exist during ascent. To this end we have derived a requirement that the telescope, assuming a fixed base at the spacecraft interface (i.e. approximately 0.25 meters aft of the primary mirror virtual vertex), should have a fundamental frequency of at least 50 Hz. With this top level telescope requirement we have determined that a primary mirror natural frequency, assuming a three point rigid mount, should be greater than 150 Hz. This requirement has been used in our assessment of primary mirror substrates and designs.

3.5 MICROROUGHNESS

We have allocated a small portion of the LUTE wavefront error budget for the effects of mirror roughness at high spatial frequencies. The effects of microroughness become increasingly important as the operating wavelength decreases. Microroughness increases the amount of wide angle scatter that would increase the stray light seen by the focal plane detector. We have done no analysis in support of the allocation.

The applicability of beryllium mirror for the LUTE ultraviolet wavelengths also remains somewhat in question. We have considerable experience in polishing beryllium mirrors "bare" (uncoated) but they may exhibit too much scatter to be suitable for wavelengths as short as 0.1 μm. It is possible to overcoat beryllium mirrors with either beryllium or aluminum to reduce the amount of scatter, but one must then be careful about the magnitude of any thermal-induced "bi-metallic" effects. Analytical models of the effects of thin films have an additional uncertainty associated with the uncertainty in the

mechanical properties of very thin films. It is our judgment that beryllium mirrors can be polished to meet LUTE's scatter requirements but we currently lack physical proof.

The lunar environment is well-known to be dusty. Furthermore, dust particles are likely to travel very long distances in the airless environment. Thus, although it may be possible to fabricate a very smooth optical surface, lunar dust contamination could severely degrade system performance, both in terms of stray light rejection and throughput. Protection from dust, perhaps including sensors, a protective cover, and a means for *in situ* cleaning may be required by LUTE, but we have not included such subsystems in the weight budget.

3.6 COATING REFLECTANCE

We have computed the normal incidence reflectance of several candidate coatings for the LUTE telescope. The reflectances (plotted for a single reflection; note that LUTE requires three reflections) are shown in Figure 3-4. For the majority of materials that are well-known to be good reflectors at visible wavelengths, the UV reflectance shows a dramatic decrease. Silicon carbide and beryllium are somewhat exceptions to this trend, but neither exhibit excellent UV reflectance.

Aluminum appears to be an excellent reflector at wavelengths as short as 0.1 μm. However, it must be emphasized that the plotted values are for bare aluminum, without an oxide layer as would result if an aluminized mirror were exposed even to very small amounts of oxygen. A typical approach to this problem is to immediately follow the aluminum deposition with, for example, magnesium fluoride, while the mirror remains under high vacuum. The overcoating prevents oxidation of the aluminum without significantly absorbing UV photons. We have not computed reflectances for overcoated materials as part of this study.

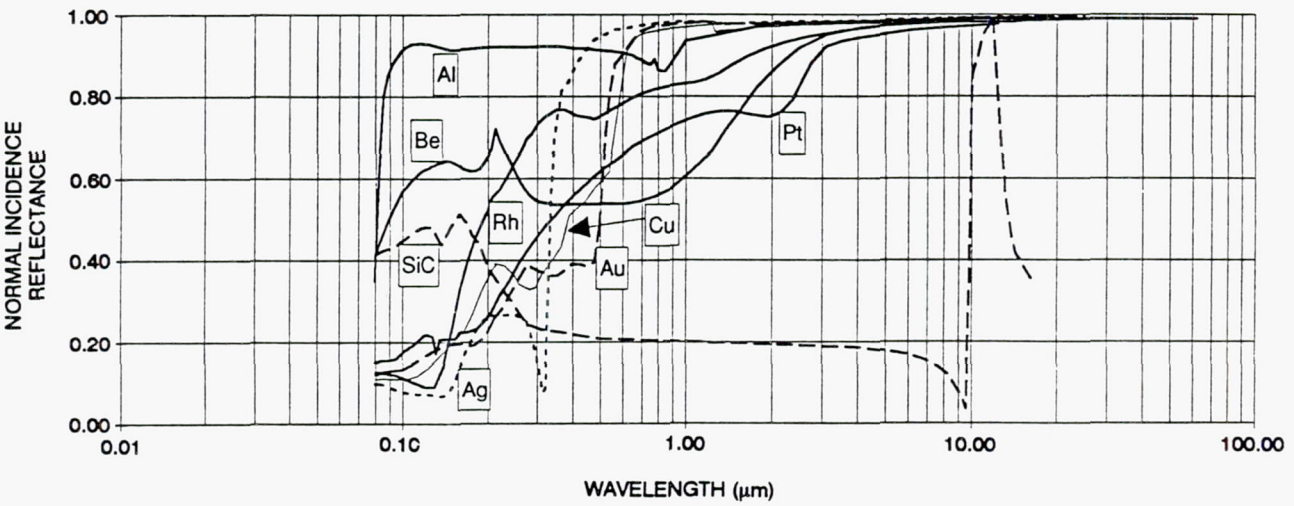

Figure 3-4. UV-to-IR Normal Incidence Reflectances of Candidate Coatings.

Optical coating of the LUTE mirrors remains a key issue for wavefront error performance. That is, since the operating temperature is far below the coating deposition temperature, and since the coating material will probably have a very different CTE than the substrate, coating stresses may deform the mirrors. The addition of an overcoat compounds this problem since it adds a third material. Analytical study of the wavefront effects of coatings is difficult since it is unclear that thin films have the same mechanical properties as the bulk material.

An alternative to overcoating remains a possibility for LUTE, but it is as-yet, an untried approach. Future LUTE studies should consider re-coating the mirror(s) in situ. Presumably there is insufficient oxygen in the lunar environment to oxidize the freshly-coated aluminum, and there would be no need for an overcoat layer.

3.7 METERING STRUCTURE

Several candidate metering structures are available to use for the LUTE telescope subsystem. These candidates are summarized in Figure 3-5.

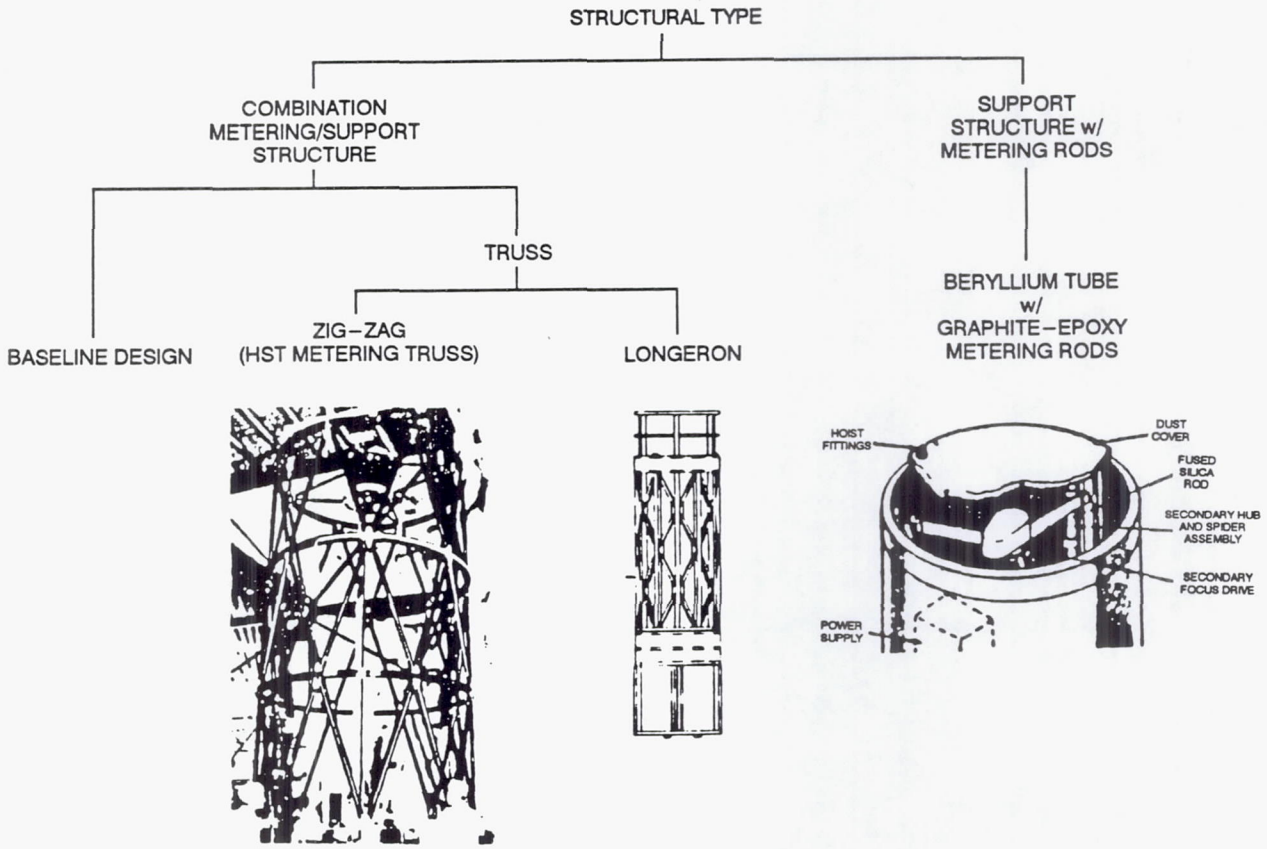

Figure 3-5. Various Candidate Metering Truss Designs Are Available for LUTE. Active thermal control could dictate preference. "Baseline Design" is a ring stiffened tube.

Although we did not conduct analyses on the LUTE metering structure, results conducted on other programs showing the optimum truss design for a given weight (see Figure 3-6) are directly applicable when considering a design which yields a high fundamental frequency for low weight. It is of interest that the "baseline design" (i.e. a ring-stiffened tube) for this particular trade space far surpasses both truss designs.

A variation of the metering structure is a support structure with metering rods. This design concept was successfully implemented on the OAO-C, an 80-cm UV orbiting telescope. Schematically shown

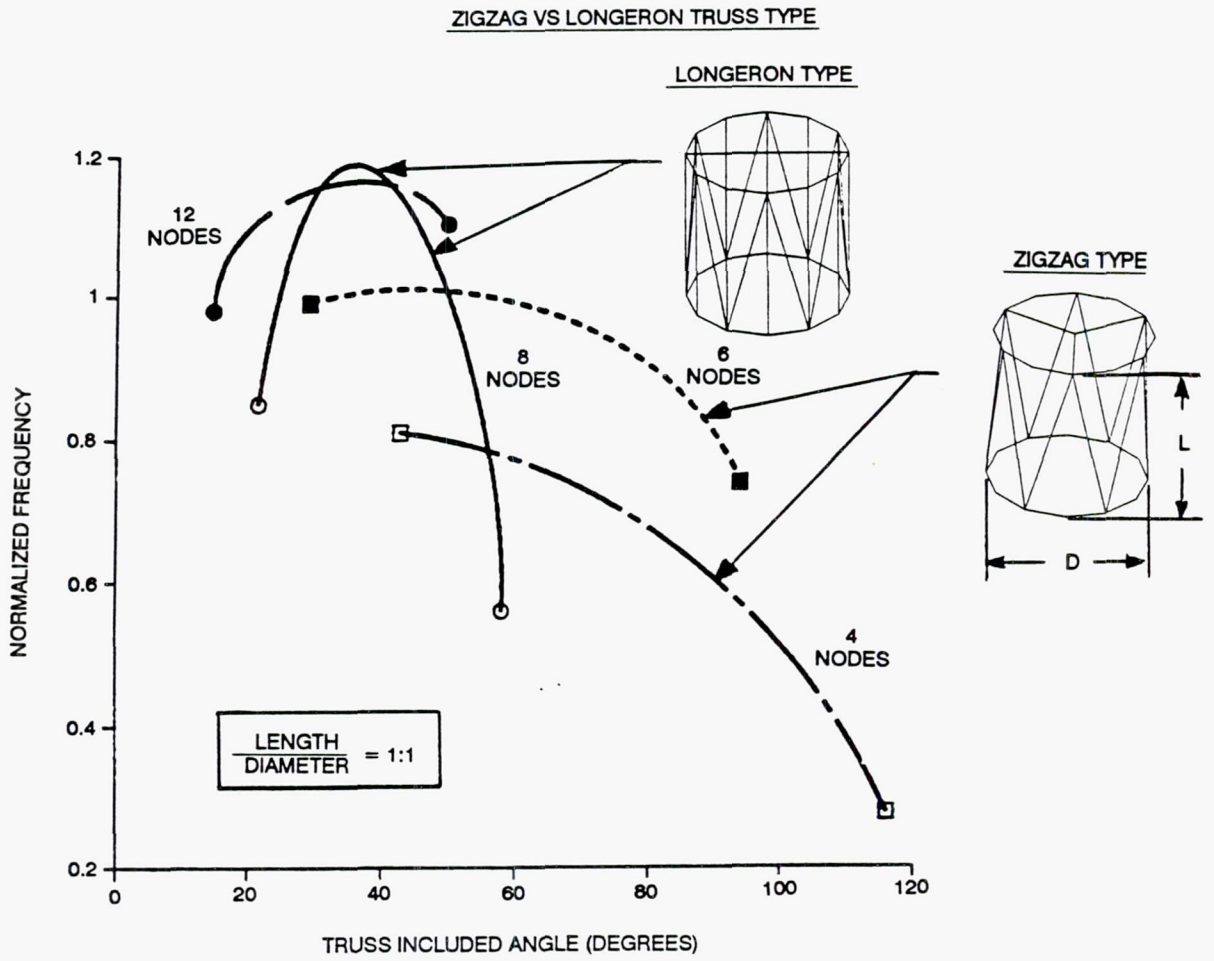

Figure 3-6. Results from Other Programs Can Be Applied to LUTE Specific Investigations. Metering structure type trades obtain high frequency and low weight.

in Figure 3-7 (for a Gregorian Telescope), this design is especially attractive if fabricated from beryllium, due to its outstanding stiffness to weight ratio. However, since beryllium's CTE properties would require the telescope to maintain very tight lateral temperature control, low CTE metering rods are employed to maintain primary mirror to secondary mirror despace and decenter within acceptable limits. These metering rods are attached to the main baffle by axial flexures at their centers and tangential flexures at their ends. With this design, should the structure "hot-dog" due to a side-to-side temperature gradient, both primary and secondary mirrors would decenter equal amounts with no relative tilts.

- ALLOWS THE USE OF BERYLLIUM FOR MAIN SUPPORT STRUCTURE
  - –OUTSTANDING STIFFNESS TO WEIGHT PERFORMANCE
  - –HIGH CTE
- APPROACH EMPLOYS LOW CTE METERING RODS TO MAINTAIN MIRROR SPACING

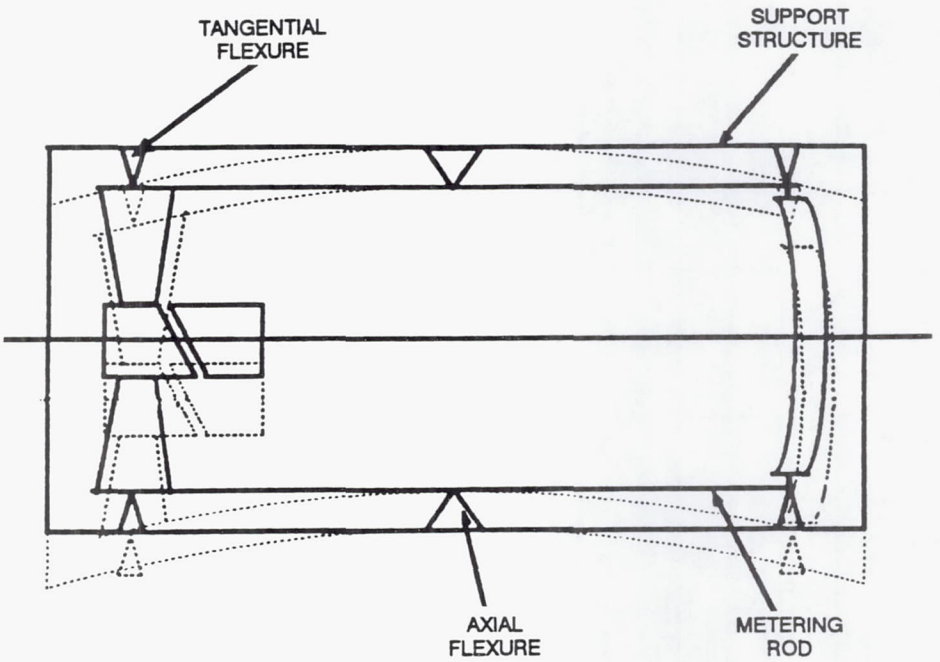

Figure 3-7. The Support Structure with Metering Rod Design Allows A High CTE Material to Be Used in the Presence of Large Side-To-Side Temperature Gradients.

3.8 DESIGN SPECIFICATION

Our design specification for the LUTE primary mirror is the combination of information described in the preceding paragraphs. The driving requirements which form the basis of this specification are shown in Table 3-3.

TABLE 3-3
SPECIFICATIONS FOR LUTE PRIMARY MIRROR

Item	Requirements/Goals
Optical Design	3 mirror telescope Diffraction limited @ 0.6328 μm 1 meter class Operating wavelength = 0.1 to 0.35 μm Throughput: > TBD BRDF: < TBD PM WFE: < 1/30 waves rms @ 0.6328 μm
Mechanical Configuration	Passive primary mirror Passive telescope thermal control Mass < 84 kg (including contingency)
Environment	Operating temperature range: - 260 K to 60 K - lunar day/night period Launch loads: - 15 g's (limit) x FOS Yield FOS = 1.25 Ultimate FOS = 1.5
Fundamental Frequency	Telescope: > 50 Hz Primary mirror: > 150 Hz

SECTION 4
PRIMARY MIRROR CANDIDATE MATERIALS AND CONFIGURATIONS

We conducted an extensive investigation of candidate primary mirror substrate materials and geometries which was then evaluated against the requirements, as stated in Section 3.8, to assess their suitability for the LUTE telescope.

4.1 SUBSTRATE MATERIALS AND DESIGNS

A broad range of substrate materials were investigated and evaluated against the applicable LUTE telescope requirements. The substrate materials we investigated are shown in Table 4-1.

TABLE 4-1
LUTE SUBSTRATE MATERIALS

Materials/Supplier	Evaluation Criteria
1) Glasses	
• Fused Quartz/Silica	• Repeatability
- Corning 7940	• Homogeneity
- Heraeus Suprasil	• Isotropy
- Heraeus Herasil	• Size Availability
• Ultra-Low Expansion (ULE)	• Inspectability
- Corning 7971	• Specific Stiffness
• Borosilicate	• Lightweighting Compatibility
- Corning Pyrex	• Cryogenic Heritage
- Ohara E6	• Polishability
2) Ceramics	• Conductivity and Specific Heat
• Zerodur	• Coating Compatibility
- Schott Glaswerks	• Strength
• Silicon Carbide (Reaction Bonded)	• Cost
- Carborundum	• Schedule
3) Metallics	
• HIP Beryllium	
- Battelle	

Fused quartz and fused silica are both amorphous silicon dioxide (SiO2) but differ in that fused quartz is manufactured from mined, high purity quartz crystals while fused silica is synthetic. From prior programs we have obtained an extensive library on the CTE, ΔL/L, Young's Modulus, and Poisson's Ratio characteristics as a function of temperature, ranging from room temperature (293 K) to ~ 1 K. Although our library on these parameters for the remaining materials is not as extensive as for fused quartz, the data on hand is from several sources and, we feel, is a good representation of actual values.

We continue to develop our experience base in both silicon carbide and beryllium substrates (see Paragraph 4.2). Although there are a number a candidate silicon carbide vendors, we have worked closely with Carborundum Specialty Products (CSP) Corporation using their reaction-bonded SiC. Reaction bonded SiC is an open network of alpha SiC crystals which has its pores completely filled with silicon, thereby producing a material which is 100% dense.

Our beryllium substrate candidate design is centered around the fabrication technique termed hot isostatic pressing (HIP) which uses beryllium powder in a high temperature, high pressure environment to produce near-net-shape optics.

Along with the substrate candidates mentioned above we also evaluated a number a primary mirror geometries. Figure 4-1 shows that a large range of structural designs are available for use as the LUTE primary mirror.

4.2 USAGE HISTORY

Performance data from demonstrated telescopes and mirrors with apertures greater than or equal to 0.5 meter in diameter that are exposed to cryogenic environments is summarized in Table 4-2. This information was employed in areal density (mass per unit area) surveys along with understanding the cryogenic cooling-induced deformation of the mirror. Our survey of demonstrated mirrors at cryogenic temperatures revealed a wide range of substrate material, mirror design and performance.

4.3 THERMAL PERFORMANCE

Figure 4-2 shows the flow of our approach to evaluating mirror materials and geometries for thermal distortion effects. There are two outputs, the allowable thermal gradient and the allowable ΔL/L gradient that would meet the wavefront error budget. We emphasize here that the structural analysis sensitivities were scaled from analyses done for another cryogenic telescope program.

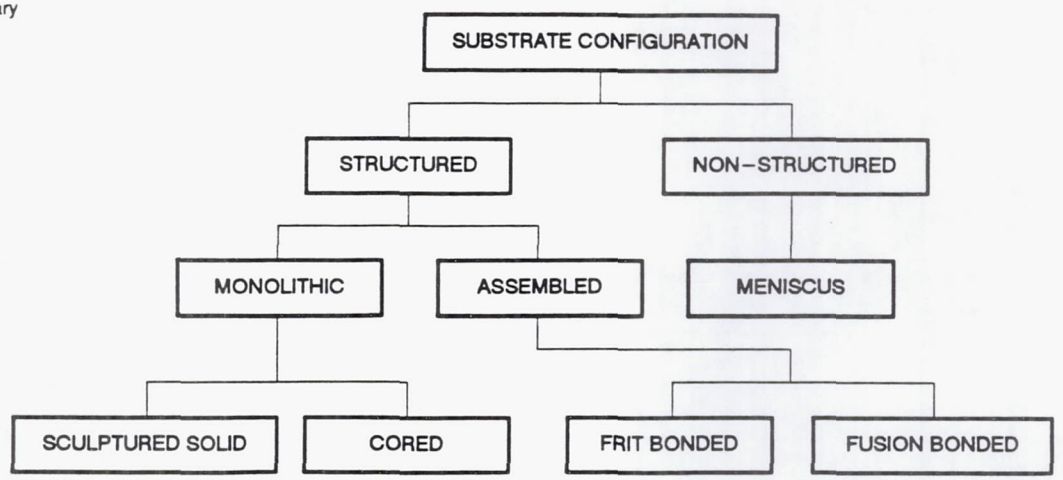

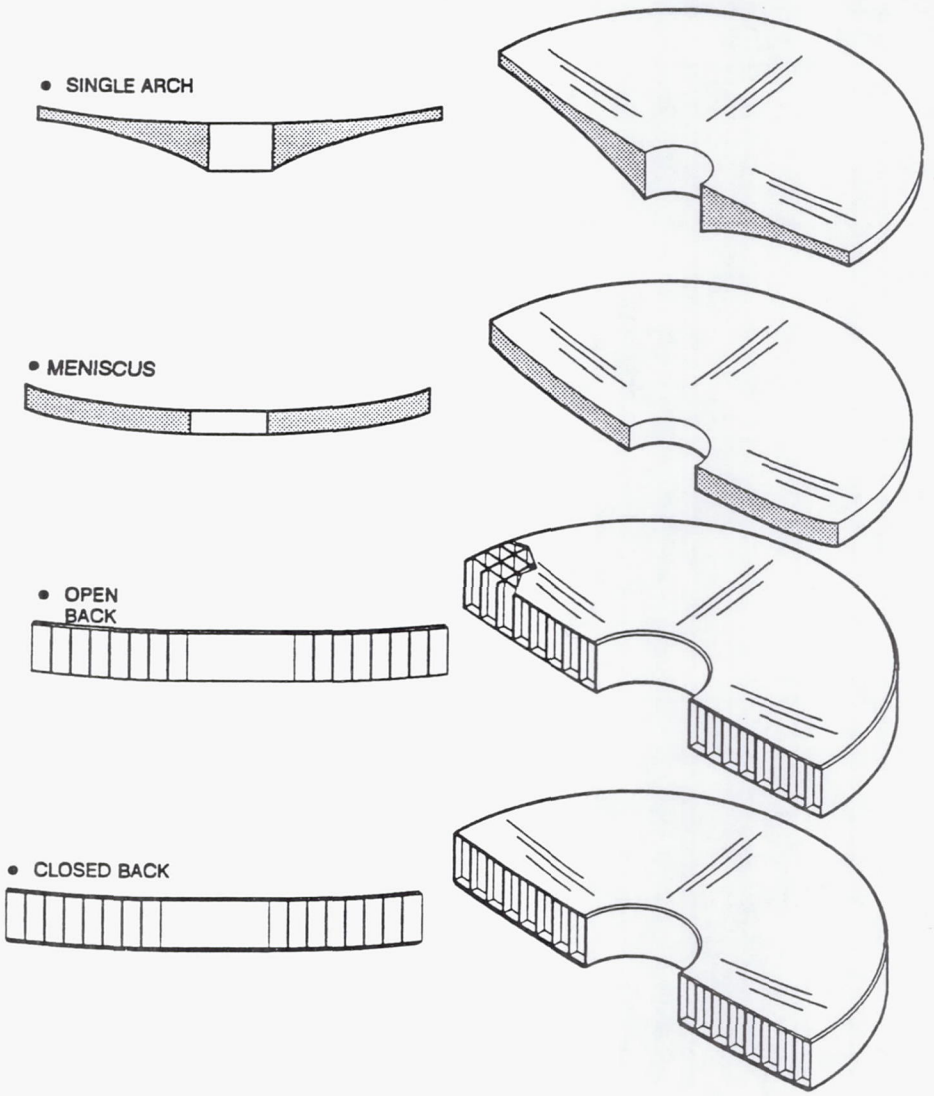

Figure 4-1. The Lute Study Investigation Yielded Various Mirror Geometries.

TABLE 4-2
CRYOGENIC MIRROR PERFORMANCE DATA

Name	Dia. (m)	Density (kg/m^2)	Temp. (K)	Cryo WF Distor'n (rms @ 0.63 μm)	Config/Mat'l
RADC/HDOS	0.4	23	110	n/a	Closed Back HIP Beryllium
ARC/Steward	0.4	55	80	0.18	Closed Back Pyrex
ARC/U of A	0.5	96	6	0.30	Double Arch Fused Silica
ARC/U of A	0.5	78	10	0.26	Single Arch Heraeus TO8E
GIRL	0.5	127	8	n/a	Open Back Zerodur
DARPA/EK	0.5	23	8	0.19	Closed Back Fused Silica
ARC/HDOS	0.5	28	8	0.46	Single Arch Beryllium
Aerosp./ISO	0.6	70	10	0.16	Open Back Fused Quartz
IRAS/HDOS	0.6	45	25	0.68	Open Back HIP Beryllium
Heraeus/Itek	0.7	57	15	0.52	Closed Back Fused Quartz
HAC/AOA	0.7×0.6	52	80	0.50	Open Back Fused Quartz
HAC/AOA	0.9×0.4	70	80	0.50	Open Back Fused Quartz
RADC/HDOS	1.0	23	110	0.37	Open Back HIP Beryllium

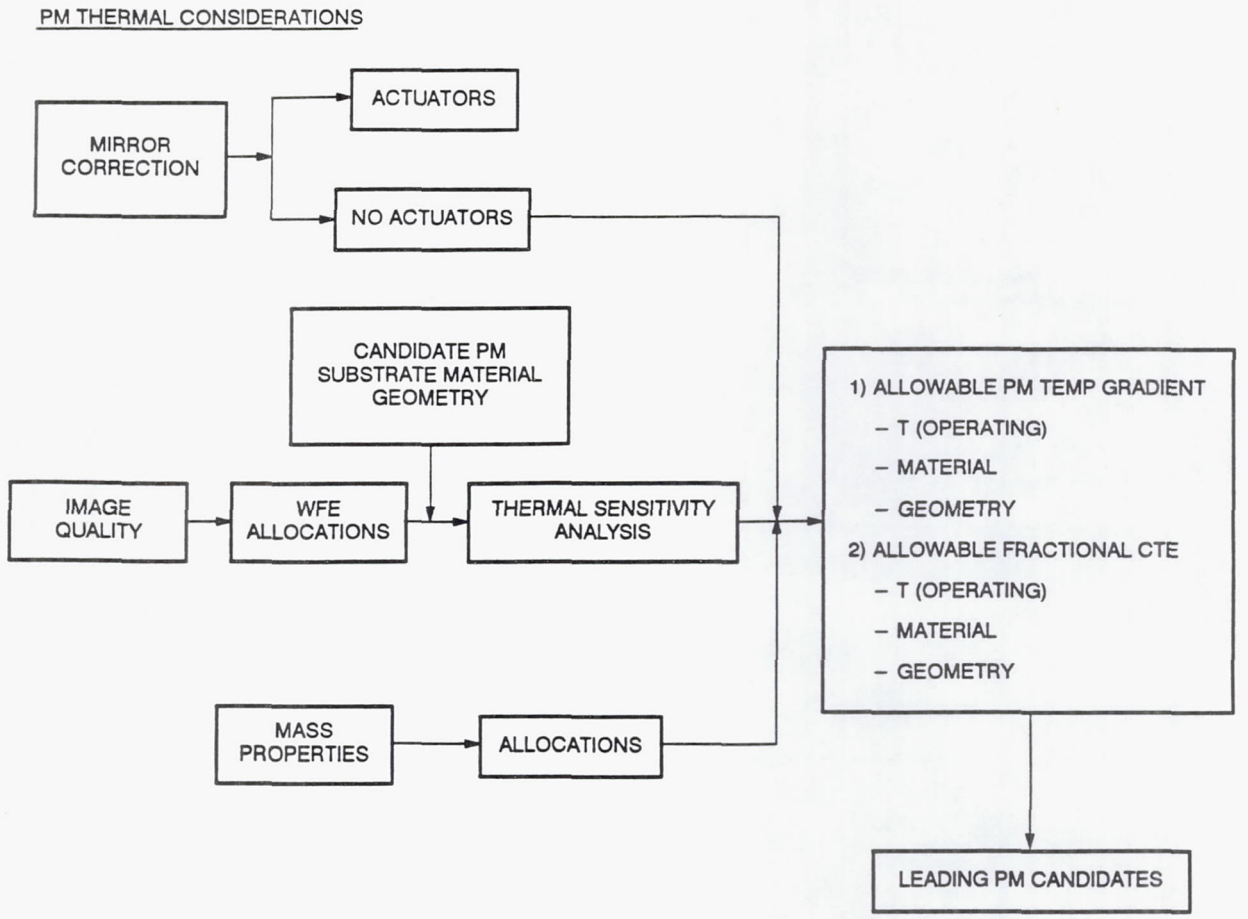

Figure 4-2. LUTE PM Materials and Design Study Thermal Considerations.

We did not generate new finite element models specifically for the LUTE study and the results are only approximate. Unfortunately, the effects of a thermal gradient that may exist in the primary mirror is also a function of the thermal conductivity of the mirror material. Both beryllium and silicon carbide have extremely high thermal conductivities compared to the glassy materials. Thus, beryllium and silicon carbide mirrors would not tend to develop significant thermal gradients. As part of this study we did not compute the thermal gradients that would actually be developed in the primary mirror in the lunar environment. This portion of the study is therefore based upon choosing materials and geometries based upon relative sensitivities and not on predicted deformations.

Figure 4-3 shows several examples of the results of our investigation into thermal gradient effects on the primary mirror wavefront error. The intent of the investigation was to determine if one material and one mirror geometry exhibited a particular insensitivity to thermal gradients. The wavefront error

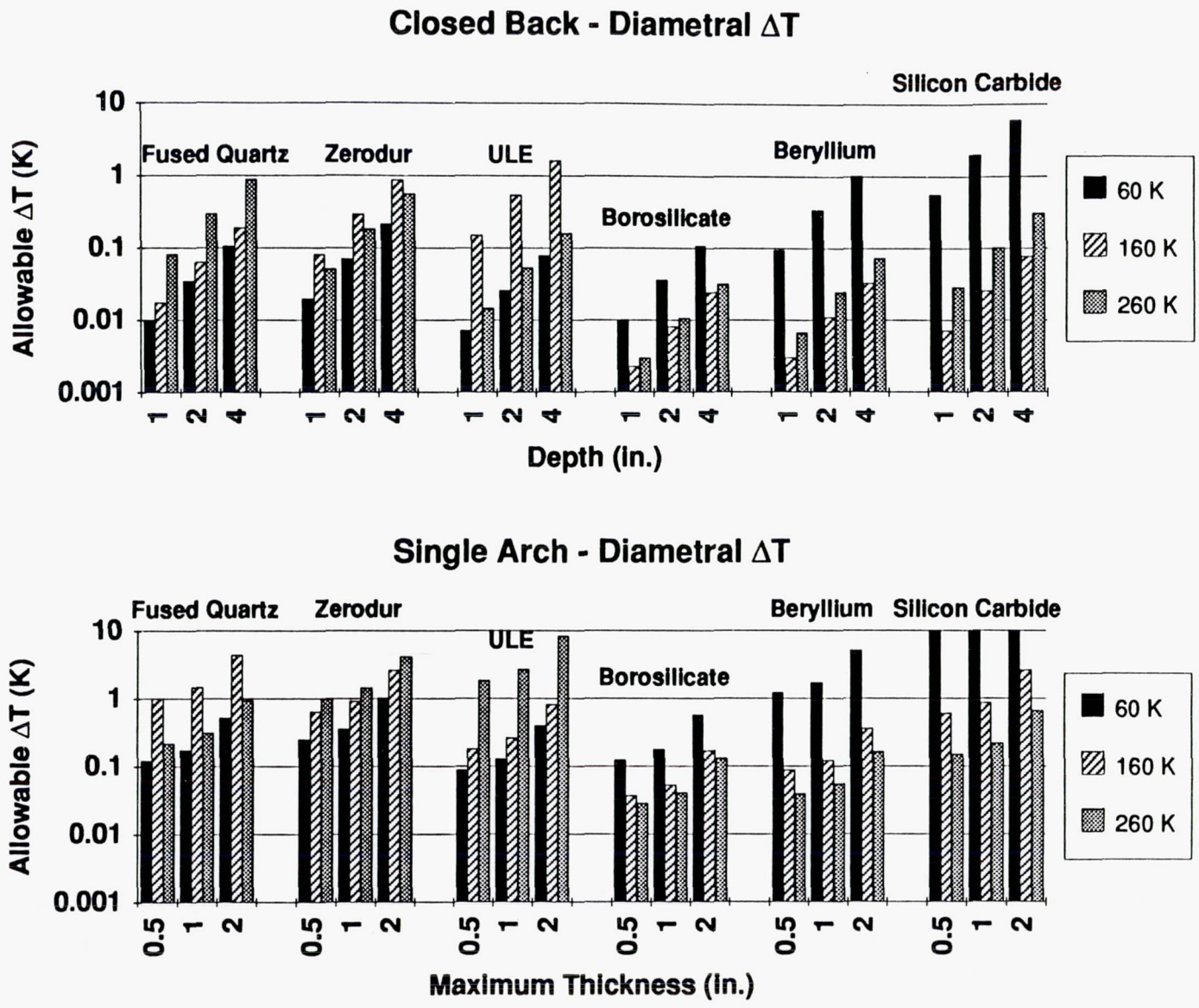

Figure 4-3. LUTE PM Materials and Design Study Performance Results (Closed Back and Single Arch-Diametral ΔT.)

budget used for this effect was 0.0063 waves rms (1 wave=0.6328 μm.) We computed the wavefront deformation assuming that the lowest order deformations could be removed by realignment of the secondary mirror.

The analysis uses the CTE of each material at the designated temperatures. We chose 60 K (the coldest temperature), 160 K (the "mean" temperature) and 260 K (the highest temperature) for the comparisons.

Inspection of Figure 4-3 shows that the single arch mirror has a consistently lower sensitivity to diametral thermal gradients than does the closed back mirror geometry. That is, the single arch mirror can tolerate larger thermal gradients than the closed back mirror before exceeding the wavefront error budget for this effect. Note that one limitation of this comparison is that mass is not constant between the various cases.

It is clear from Figure 4-3 that materials with a lower CTE can tolerate larger thermal gradients than materials with higher CTE's. For example, borosilicate (e.g. Pyrex) has a higher CTE at all three temperatures than beryllium and has a lower modulus. Therefore borosilicate mirrors are particularly sensitive to optical deformation from thermal gradients. Silicon carbide has an even lower CTE than beryllium, and combined with its high modulus it has superior low temperature performance. However, note that at 260 K, fused quartz is superior due to its very low CTE at that temperature. Thus, it is clear that the preferred material and geometry are a function of operating temperature and operating temperature range.

Figure 4-4 compares the sensitivities of a meniscus geometry with that of a single arch in terms of the effects of gradients in CTE (actually $\Delta L/L$.) We have used the actual CTE's of the various materials, integrated over three different temperature ranges. The wavefront error budget for the bulk ΔT (293 K to 160 K) was 0.0168 waves rms. The budget for 60 K to 160 K and for 160 K to 260 K was 0.0125 waves. In all cases the lowest order aberrations were neglected as they were assumed to be correctable using a secondary mirror mechanism.

The single arch geometry is more tolerant of a radially symmetric CTE variation than the meniscus geometry. In the 60 K to 160 K range the material most tolerant of CTE gradients is silicon carbide. In that temperature range it has an exceptionally low $\Delta L/L$, even lower than the glass and its high stiffness is an additional advantage.

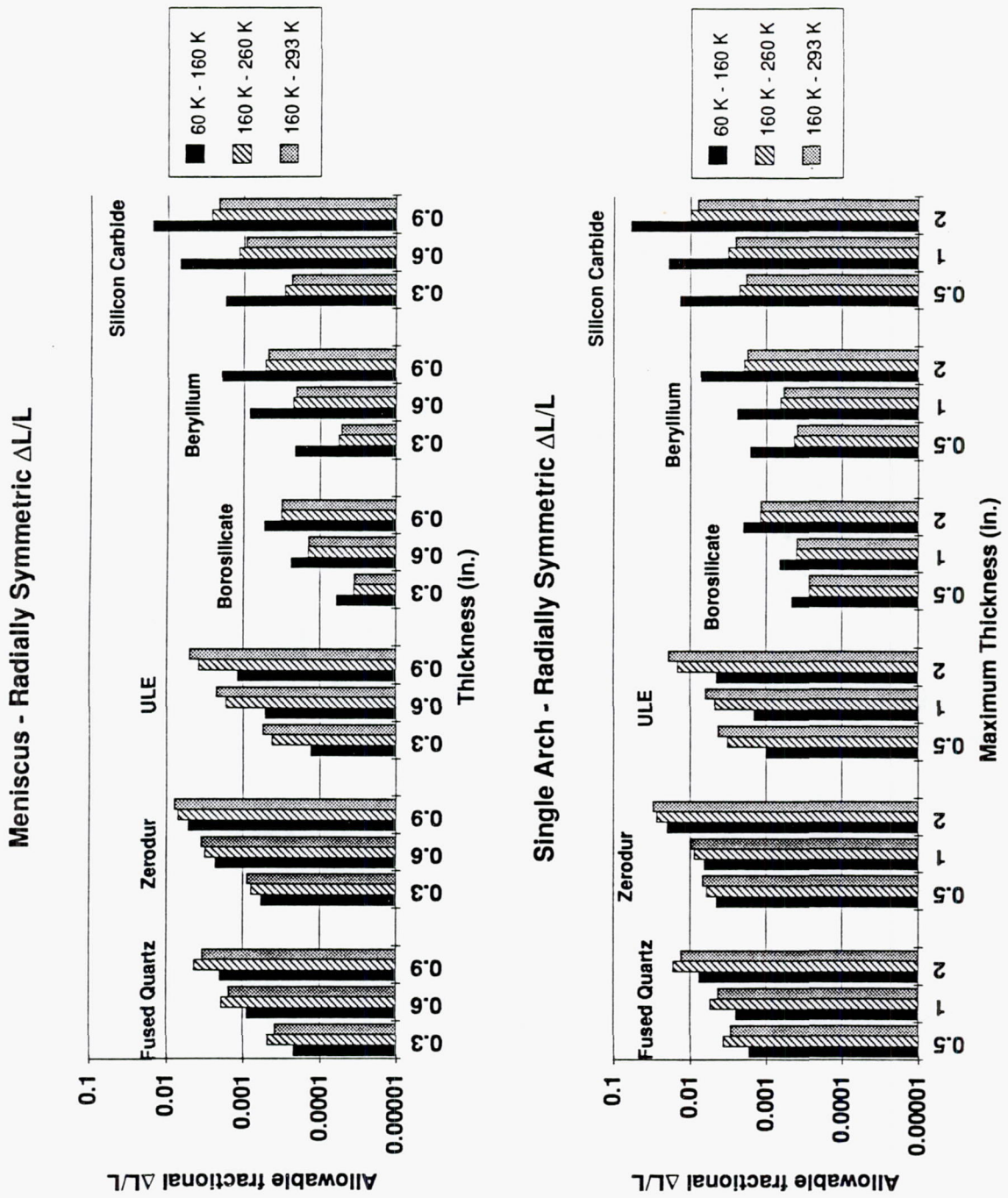

Figure 4-4. LUTE PM Materials and Design Study Performance Results (Meniscus and Single Arch-Radially Symmetric ΔL/L).

However, at the higher temperatures the glasses have the largest tolerance for CTE gradients. Beryllium, the preferred material from a structural (mass) viewpoint, does not fare very well in this comparison. It requires that the center to edge $\Delta L/L$ variation not exceed about 0.1%. Such a tolerance on a beryllium mirror's CTE gradient may be achievable but we have confirmed this as part of our study.

4.4 STRUCTURAL PERFORMANCE AND MASS PROPERTIES ESTIMATES

The logic used to assess the structural applicability of a particular substrate and mirror design for use as the LUTE primary mirror is shown in Figure 4-5. The critical requirements when making this assessment is the weight allocation of 21.8 kg (see paragraph 3.3), fundamental frequency greater than 150 Hz, and a 5/6-g release uncertainty of less than 0.0063 waves rms at 0.6328 μm.

The structural analyses conducted to assess each candidate design against the above requirements is summarized in Tables 4-3 through 4-6. These results present 1 g sag, fundamental frequency, and weight estimate results for each mirror geometry and substrate material investigated. For the meniscus, closed back and open back mirror designs, the effects of varying the mirror mount locations (e.g. at the 2/3 radius points versus edge supported) is also presented. These results are very good indicators for the relative performance of one design versus another. However, as previously stated, we

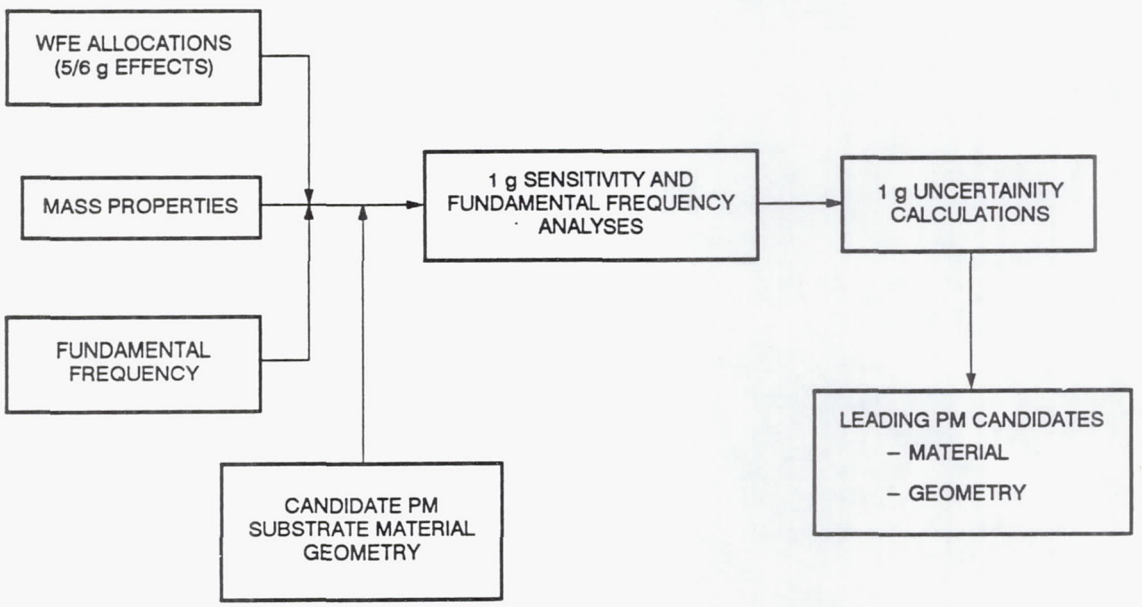

Figure 4-5. Major Structural Considerations Were Quantified to Determine Leading Candidate Designs.

TABLE 4-3
MENISCUS MIRROR - THREE POINT SUPPORTED - PERFORMANCE RESULTS

				Spread Sheet for Calculating 1-g Sag & Fund. Frequency									G. Ruthven 12/10/92	
							Mirror Supported at Outer Diameter				Mirror Supported at 2/3 Radius			
Mirror Type	Radius (inch)	Equiv. Thickness (inch)	Density (lbs/in^3)	Weight (lbs)	Young's (psi)	Nu	Defl'n (in)	Defl'n (um)	Est. WFE (um) Z(5-23)-um	Freq (Hz)	Defl'n (in)	Defl'n (um)	Est. WFE (um) Z(5-23)-um	Freq (Hz)
1) Meniscus	20.69	0.3	0.079	24.53	10200000	0.17	0.01608	408.5	51.1	24.7	0.00366	92.8	23.2	51.8
• Fused Quartz	20.69	0.6	0.079	49.06	10200000	0.17	0.00402	102.1	12.8	49.4	0.00091	23.2	5.8	103.5
	20.69	0.9	0.079	73.59	10200000	0.17	0.00179	45.4	5.7	74.0	0.00041	10.3	2.6	155.3
• Zerodur	20.69	0.3	0.091	28.26	13200000	0.24	0.01389	352.9	44.1	26.6	0.00316	80.2	20.1	55.7
	20.69	0.6	0.091	56.51	13200000	0.24	0.00347	88.2	11.0	53.1	0.00079	20.1	5.0	111.4
	20.69	0.9	0.091	84.77	13200000	0.24	0.00154	39.2	4.9	79.7	0.00035	8.9	2.2	167.1
• ULE	20.69	0.3	0.079	24.53	9800000	0.22	0.01640	416.7	52.1	24.4	0.00373	94.7	23.7	51.3
	20.69	0.6	0.079	49.06	9800000	0.22	0.00410	104.2	13.0	48.9	0.00093	23.7	5.9	102.5
	20.69	0.9	0.079	73.59	9800000	0.22	0.00182	46.3	5.8	73.3	0.00041	10.5	2.6	153.8
• Borosilicate	20.69	0.3	0.085	26.39	9500000	0.22	0.01821	462.5	57.8	23.2	0.00414	105.1	26.3	48.7
	20.69	0.6	0.085	52.79	9500000	0.22	0.00455	115.6	14.5	46.4	0.00103	26.3	6.6	97.3
	20.69	0.9	0.085	79.18	9500000	0.22	0.00202	51.4	6.4	69.6	0.00046	11.7	2.9	146.0
• Beryllium	20.69	0.3	0.067	20.80	42000000	0.07	0.00339	86.2	10.8	53.7	0.00077	19.6	4.9	112.7
	20.69	0.6	0.067	41.61	42000000	0.07	0.00085	21.6	2.7	107.4	0.00019	4.9	1.2	225.4
	20.69	0.9	0.067	62.41	42000000	0.07	0.00038	9.6	1.2	161.2	0.00009	2.2	0.5	338.1
• Silicon Carbide	20.69	0.3	0.106	32.91	47000000	0.2	0.00463	117.6	14.7	46.0	0.00105	26.7	6.7	96.5
	20.69	0.6	0.106	65.83	47000000	0.2	0.00116	29.4	3.7	92.0	0.00026	6.7	1.7	193.0
	20.69	0.9	0.106	98.74	47000000	0.2	0.00051	13.1	1.6	138.0	0.00012	3.0	0.7	289.5

TABLE 4-4
OPEN BACK MIRROR - THREE POINT SUPPORTED - PERFORMANCE RESULTS

				Spread Sheet for Calculating 1-g Sag & Fund. Frequency									G. Ruthven 12/10/92	
							Mirror Supported at Outer Diameter				Mirror Supported at 2/3 Radius			
Mirror Type	Radius (inch)	Depth (inch)	Density (lbs/in^3)	Weight (lbs)	Young's (psi)	Nu	Defl'n (in)	Defl'n (um)	Est. WFE (um) Z(5-23)-um	Freq (Hz)	Defl'n (in)	Defl'n (um)	Est. WFE (um) Z(5-23)-um	Freq (Hz)
2) Open Back	20.69	1	0.079	32.71	10200000	0.17	0.00228	58.0	19.3	65.5	0.00052	13.19	4.62	137.4
• Fused Quartz	20.69	2	0.079	49.06	10200000	0.17	0.00074	18.7	6.2	115.4	0.00017	4.25	1.49	242.0
	20.69	4	0.079	81.77	10200000	0.17	0.00018	4.5	1.5	236.3	0.00004	1.01	0.35	495.8
• Zerodur	20.69	1	0.091	37.67	13200000	0.24	0.00197	50.1	16.7	70.5	0.00045	11.39	3.99	147.8
	20.69	2	0.091	56.51	13200000	0.24	0.00064	16.2	5.4	124.1	0.00014	3.67	1.28	260.4
	20.69	4	0.091	94.19	13200000	0.24	0.00015	3.8	1.3	254.3	0.00003	0.87	0.31	533.4
• ULE	20.69	1	0.079	32.71	9800000	0.22	0.00233	59.2	19.7	64.8	0.00053	13.45	4.71	136.0
	20.69	2	0.079	49.06	9800000	0.22	0.00075	19.1	6.4	114.2	0.00017	4.33	1.52	239.6
	20.69	4	0.079	81.77	9800000	0.22	0.00018	4.5	1.5	234.0	0.00004	1.03	0.36	490.9
• Borosilicate	20.69	1	0.085	35.19	9500000	0.22	0.00259	65.7	21.9	61.6	0.00059	14.93	5.22	129.1
	20.69	2	0.085	52.79	9500000	0.22	0.00083	21.2	7.1	108.4	0.00019	4.81	1.68	227.5
	20.69	4	0.085	87.98	9500000	0.22	0.00020	5.0	1.7	222.1	0.00005	1.15	0.40	465.9
• Beryllium	20.69	1	0.067	27.74	42000000	0.07	0.00048	12.2	4.1	142.6	0.00011	2.78	0.97	299.0
	20.69	2	0.067	41.61	42000000	0.07	0.00016	3.9	1.3	251.1	0.00004	0.90	0.31	526.6
	20.69	4	0.067	69.35	42000000	0.07	0.00004	0.9	0.3	514.4	0.00001	0.21	0.07	1079.1
• Silicon Carbide	20.69	1	0.106	43.88	47000000	0.2	0.00066	16.7	5.6	122.1	0.00015	3.80	1.33	256.0
	20.69	2	0.106	65.83	47000000	0.2	0.00021	5.4	1.8	215.0	0.00005	1.22	0.43	451.0
	20.69	4	0.106	109.71	47000000	0.2	0.00005	1.3	0.4	440.5	0.00001	0.29	0.10	924.0

TABLE 4-5
CLOSED BACK MIRROR - THREE POINT SUPPORTED - PERFORMANCE RESULTS

				Spread Sheet for Calculating 1-g Sag & Fund. Frequency									G. Ruthven 12/10/92	
							Mirror Supported at Outer Diameter				Mirror Supported at 2/3 Radius			
Mirror Type	Radius (inch)	Depth (inch)	Density (lbs/in^3)	Weight (lbs)	Young's (psi)	Nu	Defl'n (in)	Defl'n (um)	Est. WFE (um) Z(6-23)-um	Freq (Hz)	Defl'n (in)	Defl'n (um)	Est. WFE (um) Z(6-23)-um	Freq (Hz)
3) Closed Back	20.69	1	0.079	36.98	10200000	0.17	0.00139	35.19	11.73	84.1	0.00031	8.00	2.80	176.4
• Fused Quartz	20.69	2	0.079	52.33	10200000	0.17	0.00039	9.84	3.28	159.0	0.00009	2.24	0.78	333.6
	20.69	4	0.079	85.04	10200000	0.17	0.00012	3.12	1.04	282.5	0.00003	0.71	0.25	592.5
• Zerodur	20.69	1	0.091	41.44	13200000	0.24	0.00120	30.39	10.13	90.5	0.00027	6.91	2.42	189.8
	20.69	2	0.091	60.28	13200000	0.24	0.00033	8.50	2.83	171.1	0.00008	1.93	0.68	358.9
	20.69	4	0.091	97.95	13200000	0.24	0.00011	2.69	0.90	303.9	0.00002	0.61	0.21	637.5
• ULE	20.69	1	0.079	35.98	9800000	0.22	0.00141	35.89	11.96	83.3	0.00032	8.16	2.85	174.7
	20.69	2	0.079	52.33	9800000	0.22	0.00040	10.04	3.35	157.5	0.00009	2.28	0.80	330.3
	20.69	4	0.079	85.04	9800000	0.22	0.00013	3.18	1.06	279.7	0.00003	0.72	0.25	586.7
• Borosilicate	20.69	1	0.085	38.71	9500000	0.22	0.00157	39.83	13.28	79.0	0.00036	9.05	3.17	165.6
	20.69	2	0.085	56.30	9500000	0.22	0.00044	11.14	3.71	149.5	0.00010	2.53	0.89	313.5
	20.69	4	0.085	91.49	9500000	0.22	0.00014	3.53	1.18	265.5	0.00003	0.80	0.28	556.9
• Beryllium	20.69	1	0.067	30.51	42000000	0.07	0.00029	7.43	2.48	183.1	0.00007	1.69	0.59	384.0
	20.69	2	0.067	44.38	42000000	0.07	0.00008	2.08	0.69	346.2	0.00002	0.47	0.17	726.1
	20.69	4	0.067	72.12	42000000	0.07	0.00003	0.66	0.22	614.9	0.00001	0.15	0.05	1289.7
• Silicon Carbide	20.69	1	0.106	48.27	47000000	0.2	0.00040	10.13	3.38	156.7	0.00009	2.30	0.81	328.8
	20.69	2	0.106	70.21	47000000	0.2	0.00011	2.83	0.94	296.4	0.00003	0.64	0.23	621.8
	20.69	4	0.106	114.10	47000000	0.2	0.00004	0.90	0.30	526.5	0.00001	0.20	0.07	1104.4

TABLE 4-6
SINGLE ARCH MIRROR - THREE POINT SUPPORTED - PERFORMANCE RESULTS

				Spread Sheet for Calculating 1-g Sag & Fund. Frequency						G. Ruthven 12/10/92
							Mirror Supported at Inner Diameter			
Mirror Type	Radius (inch)	Max Thickness (inch	Density (lbs/in^3)	Weight (lbs)	Young's (psi)	Nu	Defl'n (in)	Defl'n (um)	Est. WFE (um) Z(5-23)-um	Freq (Hz)
4) Single Arch	20.69	0.5	0.079	24.8	10200000	0.17	0.00090	22.9	0.62	104.3
• Fused Quartz	20.69	1	0.079	49.5	10200000	0.17	0.00062	15.7	0.43	119.4
	20.69	2	0.079	99.1	10200000	0.17	0.00021	5.3	0.14	187.9
• Zerodur	20.69	0.5	0.091	28.1	13200000	0.24	0.00079	20.0	0.54	111.5
	20.69	1	0.091	56.2	13200000	0.24	0.00054	13.8	0.37	127.5
	20.69	2	0.091	112.3	13200000	0.24	0.00018	4.7	0.13	200.8
• ULE	20.69	0.5	0.079	24.8	9800000	0.22	0.00103	26.1	0.71	97.6
	20.69	1	0.079	49.5	9800000	0.22	0.00071	18.0	0.49	111.6
	20.69	2	0.079	99.1	9800000	0.22	0.00024	6.1	0.16	175.6
• Borosilicate	20.69	0.5	0.085	26.4	9500000	0.22	0.00103	26.1	0.71	97.6
	20.69	1	0.085	52.8	9500000	0.22	0.00071	18.0	0.49	111.6
	20.69	2	0.085	105.7	9500000	0.22	0.00024	6.1	0.16	175.6
• Beryllium	20.69	0.5	0.067	21.5	42000000	0.07	0.00019	4.8	0.13	227.4
	20.69	1	0.067	42.9	42000000	0.07	0.00013	3.3	0.09	260.3
	20.69	2	0.067	85.8	42000000	0.07	0.00004	1.1	0.03	409.8
• Silicon Carbide	20.69	0.5	0.106	32.2	47000000	0.2	0.00025	6.4	0.17	196.6
	20.69	1	0.106	64.4	47000000	0.2	0.00018	4.4	0.12	224.7
	20.69	2	0.106	128.8	47000000	0.2	0.00006	1.5	0.04	353.8

did not generate detailed finite element models (FEM) for every candidate. We developed scaling laws and applied them where applicable. The results generated by these scaling laws were occasionally checked with a FEM to ensure that we obtained reasonable results. An example of one such model is shown in Figure 4-6 and the resulting 1-g sag results shown graphically in Figure 4-7.

The uncertainty in the primary mirror deformation caused by the 5/6-g change in acceleration is a critical requirement in our overall approach to the LUTE telescope design. The 5/6-g uncertainty budget item is that amount of wavefront error which the mirror can exhibit when going from a 1-g earth environment to the lunar surface environment of 1/6-g.

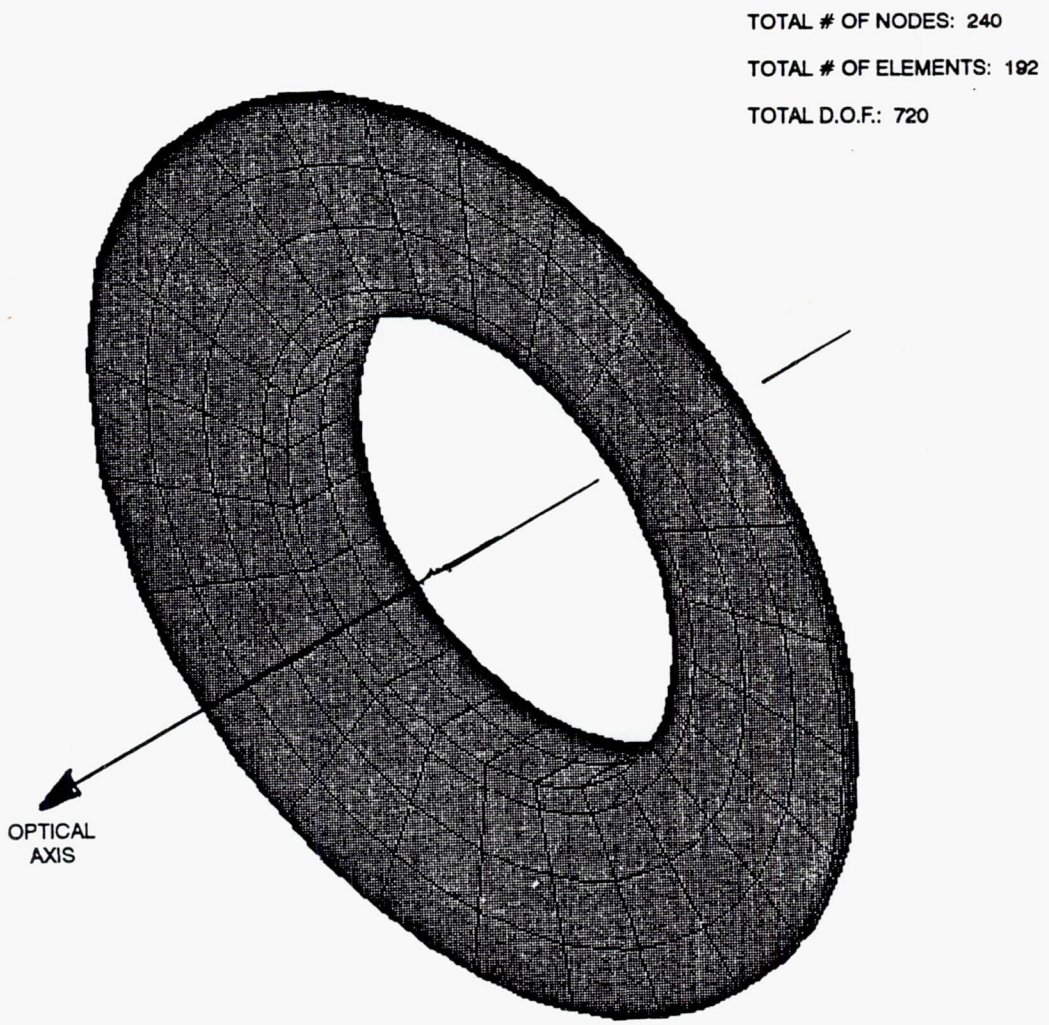

Figure 4-6. Existing Mirror Finite Element Models Used as Cross-Check for Scaling Laws.

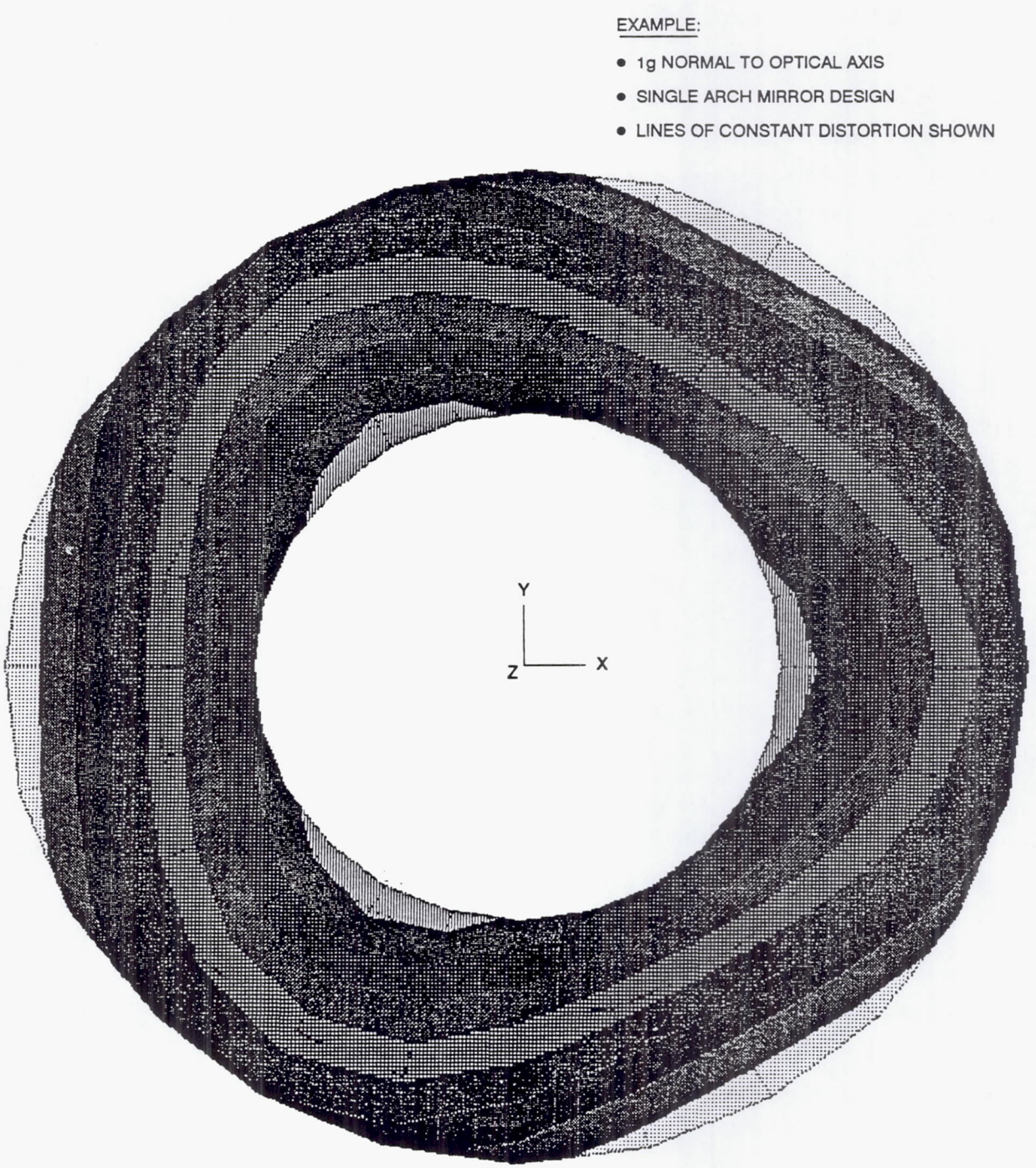

Figure 4-7. Mirror Deformation Patterns Decomposed to Determine Wavefront Error after Tilt and Focus is Removed.

The Hubble Space Telescope (HST) program used a "0-g metrology mount" to simulate the on-orbit 0-g environment. Because the metrology mount is always somewhat imperfect some residual error will exist. HDOS conducted a number of tests to correlate the HST metrology mount/mirror with a FEM of that system. We were able to correlate very well with test data. For instance, when the mirror was deformed in an astigmatic shape (sometimes referred to as "saddle") the mirror was interferometrically measured and compared to the predicted deformation. The mirror and FEM correlated to within 4%. For the LUTE primary mirror our wavefront error allocation for this effect is 0.0063 waves rms at 0.6328 μm.

For the LUTE telescope the scenario of using a metrology mount is in question since LUTE operates over a very wide temperature range compared with HST is ± 4° F. It is our judgment that the ability to design, fabricate and test a cryogenic metrology mount for LUTE would be a high risk approach. That is, the uncertainty of the metrology mount's performance operating over such a large temperature range could easily overshadow the 1-g effects we would be trying to measure. A similar concern affected the approach we used on the Infrared Astronomical Satellite (IRAS) program. We believe that a conservative approach to the LUTE primary mirror would be to have a mirror sufficiently stiff (at least in so far as non-realignable wavefront errors are concerned) that one can do without a cryogenic metrology mount.

If a cryogenic metrology mount is not used the question remains as to what is the uncertainty value for the 5/6-g effects. We believe, based on HST and other programs that we will be able to correlate the physical mirror characteristics to a FEM model to within 10%. Thus we can analytically predict how the mirror will deform in a 1/6-g cryogenic environment by correlating our model to 1-g cryogenic tests that do not utilize a metrology mount. We note here that it will be necessary to know the Young's modulus and Poisson's ratio of the mirror material throughout its operating temperature range.

Figure 4-8 shows the 1g uncertainty factors for the mirror candidates. Several items are noteworthy. The results shown are for 1-g; they should be multiplied by 5/6 to reflect the moon's 1/6-g environment. The second item to note is our assumption that LUTE will employ despace, decenter, and tilt capabilities via the secondary mirror subassembly. With this assumption, all the results shown in Table 4-3 through 4-6 and Figure 4-8 have piston, tilt and focus contributions removed from the estimated wavefront error.

From Figure 4-8 it is clearly seen that a beryllium single arch mirror is superior to all other candidates in terms of 1-g wavefront error uncertainty. The reason for this is that for the single arch the 1-g

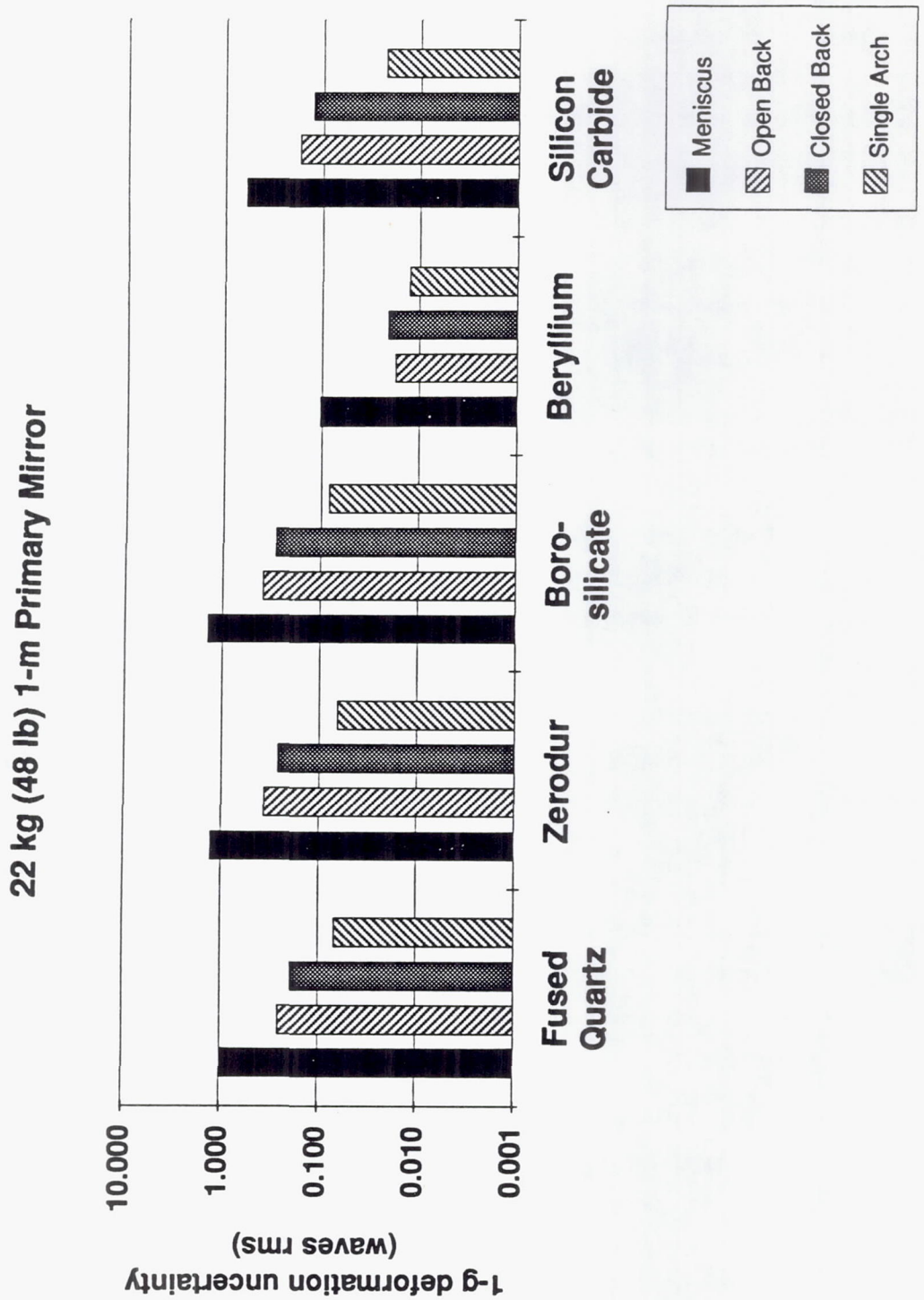

Figure 4-8. A Beryllium, Single Arch Primary Mirror Design is Clearly Superior for 1g-to-1/6g Effects.

results are dominated by focus error (i.e. Zernike polynomial terms Z4.) Our assumption of a focus mechanism makes focus error inconsequential. However, even though the single arch design has superior performance it is still just marginally acceptable in terms of the 0.0063 waves-rms requirement. In a future study a more refined investigation of this configuration and a revisiting of the overall error budget is warranted.

The mass properties estimates are presented in Table 4-7. The coordinate system used for the mass properties determination is such that the "X" direction is along the telescope optical axis (i.e. along the thrust axis of the launch vehicle) and the "Y" and "Z" axes are perpendicular to the "X" axis. The spacecraft interface in assumed to be 0.25 m aft of the (virtual) location of the primary mirror's vertex.

4.5 ACTIVE PRIMARY MIRROR DESIGN OPTION

The passive telescope design results presented show that due to the extreme operating temperature ranges, the ability to meet the top level primary mirror wavefront error budget of 0.0335 waves rms (at 0.6328 μm) is very challenging. An alternative design approach would be to employ figure control actuators which provide the ability to correct the mirror's surface figure in a closed loop fashion via an alignment/wavefront sensor.

We have conducted a first order analysis on the effects of figure control actuators on overall performance. Shown in Figure 4-9, the residual error which exists after correction has taken place as a function of mirror spatial frequency error suggests that for the anticipated low frequency errors associated with both temperature and substrate $\Delta L/L$ variations, a large portion (~ 80%) of these errors can be negated with the use of figure control actuators. This correction capability prediction is for a meniscus mirror design where a moderate number of actuators (approximately 16) are located on the rear surface of the primary mirror. The number of actuators could be optimized by targeting a specific set of aberrations caused by the thermal distortion sources (i.e material CTE gradients and variations in the mirror's thermal environment.)

A schematic of the figure control actuators is provided in Figure 4-10. This design employs a dual mode approach which provides large dynamic range while simultaneously providing fine adjustment capability. HDOS actuator technology has been demonstrated on several DoD programs, on the NASA HST Program and in HDOS laboratories.

TABLE 4-7
LUTE TELESCOPE MASS PROPERTIES

		LUTE Telescope							
		Hardware Family Tree & Mass Properties Estimates							
				Determine CG Location			*Inertia Properties (in-lbs-sec^2)*		
Major Element	**Sub-Ass'y/Component**	**Weight (lbs)**	**Weight (kg)**	**Datum Dist.(x) (in)**	**Wt * x (in-lbs)**	**r(x) (in)**	**Mr(x)^2**	**Ixo**	**Iyo=Izo**
1) Mirrors									
	- Primary Mirror	48	21.8	9	432.0	-7.3	6.7	26.6	13.5
	- Secondary Mirror	6	2.7	33	198.0	16.7	4.3	0.6	0.3
	- Tertiary Mirror	3	1.4	6	18.0	-10.3	0.8	0.1	0.1
	Sub-Total:	**57**	**25.9**		**648.0**		**11.8**	**27.3**	**13.8**
2) Structure	**Baffle Sub-Ass'y**								
	- Main	9	4.1	18	162.0	1.7	0.1	10.0	8.1
	- Central	2	0.9	5	10.0	-11.3	0.7	0.5	0.3
	- SM	1	0.5	30	30.0	13.7	0.5	0.3	0.2
	Sub-Total:	**12**	**5.5**		**202.0**		**1.2**	**10.7**	**8.5**
	Mirror Mounts								
	- PM	5	2.3	6	30.0	-10.3	1.4	0	0
	- SM	3	1.4	33	99.0	16.7	2.2	0	0
	- TM	2	0.9	5	10.0	-11.3	0.7	0	0
	Sub-Total:	**10**	**4.5**		**139.0**		**4.2**	**0**	**0**
	Main Bulkhead Sub-Ass'y								
	- Main bulkhead	12	5.5	2	24.0	-14.3	6.4	9.6	4.8
	- S/C interface fittings (3)	3	1.4	2	6.0	-14.3	1.6	0	0
	Sub-Total:	**15**	**6.8**		**30.0**		**8.0**	**9.6**	**4.8**
	Metering Bar Sub-Ass'y								
	- Metering bars (3)	3	1.4	18	54.0	1.7	0.0	0	1.1
	- Interface fittings (6)	3	1.4	18	54.0	1.7	0.0	0	0
	Sub-Total:	**6**	**2.7**		**108.0**		**0.0**	**0**	**1.1**
	SM Sub-Ass'y								
	- Spider	4	1.8	36	144.0	19.7	4.0	0	0
	- Hub	3	1.4	36	108.0	19.7	3.0	1	0.5
	- Spider ring	3	1.4	36	108.0	19.7	3.0	3.3	1.5
	- Spider flexures (3)	3	1.4	36	108.0	19.7	3.0	0	0
	- Actuators (6)	6	2.7	34	204.0	17.7	4.8	0	0
	- Cabling	4	1.8	18	72.0	1.7	0.0	0	0
	Sub-Total:	**23**	**10.5**		**744.0**		**17.9**	**4.3**	**2**

TABLE 4-7 (Continued)
LUTE TELESCOPE MASS PROPERTIES

3) Electronics	• ACE	3	1.4	1	3.0	-15.3	1.8	0	0
	• TCE	3	1.4	1	3.0	-15.3	1.8	0	0
	• DMS	3	1.4	1	3.0	-15.3	1.8	0	0
	• ASE	3	1.4	1	3.0	-15.3	1.8	0	0
	Sub-Total:	**12**	**5.5**		**12.0**		**7.3**	**0.3**	**0.1**
4) Thermal Control	• Heaters	2	0.9	18	36.0	1.7	0.0	0	0
	• Thermocouples	2	0.9	18	36.0	1.7	0.0	0	0
	• MLI	3	1.4	18	54.0	1.7	0.0	0	0
	Sub-Total:	**7**	**3.2**		**126.0**		**0.0**	**0**	**0**
5) Alignment Sensor	• Sensor	10	4.5	38	380.0	21.7	12.1	2	1
	• Sensor mount	2	0.9	38	76.0	21.7	2.4	0	0
	Sub-Total:	**12**	**5.5**		**456.0**		**14.6**	**2**	**1**
	Total (w/o Reserve):	**154.0**	**70**		**2465.0**		**65.1**	**54.2**	**31.4**
	Reserve:	**31.6**	**14**	**18**	**569.16**	1.7	**0.2**		
	Total:	**185.6**	**84**				**65.3**		
				CG Location:	**16.3**	**Total Inertia:**			
				(in)		**Ix=Ixo**		**54.2**	
				(WRT S/C I/F)		**Iy=Iz=Mr^2+Iy(o)**			**96.5**

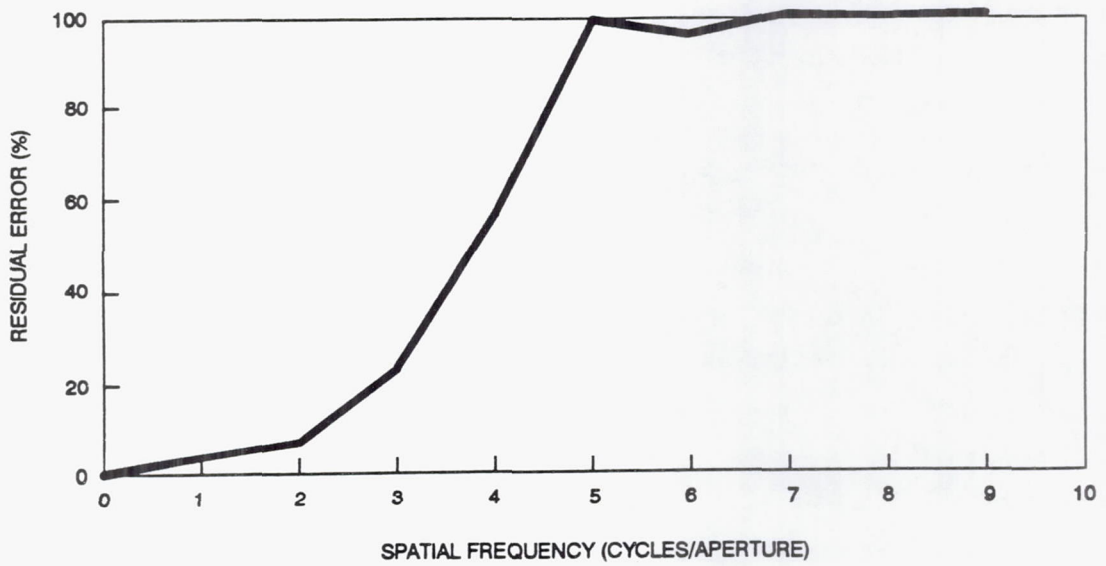

Figure 4-9. Primary Mirror Residual Distortion After Active Correction Via Figure Control Actuators. Additional analyses are required to determine LUTE specific performance.

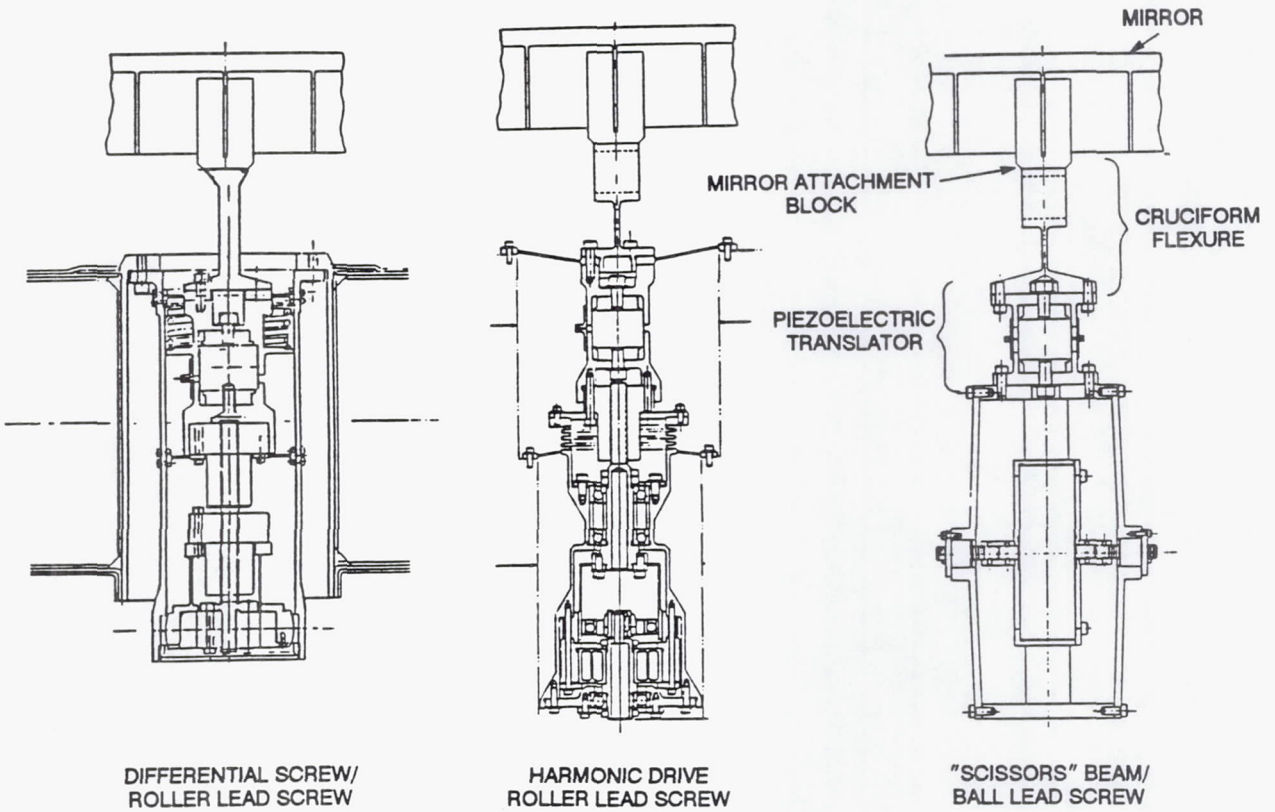

Figure 4-10. Several Design Concepts Exist for Primary Mirror Figure Control Actuators.

Our mass estimate for each actuator is about 1 kg. With approximately 16 actuators needed for 80% wavefront error correction capability a total mass of about 18 kg would be required. The weight allocations as presented in Figure 3-3 would need to be modified if an active mirror approach is adopted.

Our preliminary assessment of active figure compensation for the primary mirror shows that, along with a weight penalty, the ability to adequately compensate for the mirror distortion would be seriously in question. The residual 5/6-g effects of a beryllium meniscus design (a meniscus mirror is probably required if figure control actuators are to be used) with a weight consistent with the mass allocation is still three times larger than the error budget allocation of 0.0063 waves-rms at 0.6328 μm. All other substrate material candidates would yield even poorer results because of their lower specific stiffness (E/ρ) values. For instance, a fused quartz meniscus design would require a correction factor of better than 99%, a value which is certainly not attainable. We have tentatively concluded that the option of active control the primary mirror distortions is not viable.

SECTION 5
SELECTION CRITERIA AND EVALUATION

5.1 RECOMMENDED CANDIDATES

A beryllium single arch design is the leading candidate for the LUTE primary mirror. The next tier of leading candidates would include an open or closed back beryllium design. All glass and ceramic candidates of suitable low mass exhibit excessive 1-g deformations and thus cannot be considered viable materials. Mass is the key driver for the choice of beryllium.

5.2 BASIS OF SELECTION

The premise that leads us to recommend a beryllium single arch design is that a cryogenic metrology mount is a high risk approach which, in our engineering judgment, is not required to verify primary mirror 1-g to 1/6-g performance. The performance uncertainty of a cryogenic metrology mount may dwarf the mirror deformation effects which we would be trying to measure.

Verification of 1-g to 1/6-g effects can be predicted using 1-g interferometric test measurements of the mirror. These results, using both a room temperature metrology mount (for mirror fabrication) and other support fixturing, can be correlated to a finite element model of the mirror. The degree to which the model and interferometric measurement results do not correlate is the level of uncertainty which will exist when transitioning from earth to lunar gravity environments. We have recommended a slightly conservative correlation uncertainty factor of 10% for LUTE. This being the case, a single arch beryllium mirror design is the only candidate which approaches the allowable 1-g to 1/6-g uncertainty level of 0.0084 waves-rms (0.084 waves times 0.10) for the allowable primary mirror mass of 22 kg.

The thermal performance of the single arch beryllium mirror is good. In general, the mirror candidate geometries are more sensitive to a diametral variation of $\Delta L/L$ than a radial or axial variation. At the lower operating temperatures an allowable diametral temperature gradient of ~1 K is acceptable for the single arch beryllium candidate. However at higher operating temperatures an allowable gradient of only ~0.1 K is tolerable. LUTE system level trades must address this issue and whether an active telescope thermal control system should be considered. With the active thermal control system, an increase in the allowable temperature gradient as well as an increase in the allowable variation in material CTE would be realized.

5.3 CANDIDATE DESIGN PRODUCIBILTY STATUS

The ability to fabricate a 1-m class diffraction limited cryogenic primary mirror with an areal density of 28 kg/m^2 has not been proven to date. HDOS has designed and fabricated a 0.5 m, 28 kg/m^2 optic and cryogenically tested it to 8 K. The cryogenic distortion (i.e the amount of distortion transitioning from room temperature to cryogenic temperatures) was approximately 0.5 waves rms. This suggests that cryo null figuring will be required to meet the LUTE wavefront requirements. Note that the repeatability of the thermally-induced distortion must be exceptionally high for cryo null figuring to be successful. Such high repeatability has not been shown to date but may nonetheless be achievable in beryllium.

Cryo null figuring is an extension of traditional metrology and mirror fabrication techniques. In this process, metrology data is gathered at a discreet cryogenic temperature (this temperature is chosen based on worst case predicted mirror deformations.) The inverse wavefront error is figured into the mirror at room temperature so that subsequent further cooling the mirror wavefront is optimized at this discreet temperature. The advantages of using a cryo-null figuring approach are further enhanced if the operating temperature range of the telescope is reduced by the use of an active thermal control system.

Our current beryllium facilities can easily handle a 1-m class optic. Most recently we fabricated and tested a 1-m, closed back HIP beryllium optic. A low scatter surface roughness of approximately 20Å rms was achieved.

SECTION 6
CONCLUSIONS

No areas were identified in this study that would indicate that the LUTE mission is not feasible. Nonetheless, development of an ultra-lightweight, 1-m telescope with visible wavelength diffraction-limited performance for operation at cryogenic temperatures with a ±100 K temperature range would undoubtedly prove to be exceptionally difficult. We are unaware of any existing hardware that has met such requirements. No 1-m beryllium mirror has even been polished to such stringent wavefront error requirements.

The choice of beryllium was driven by the mass budget. For the currently allowable mass, beryllium is the only material that has a sufficiently small 1-g to 1/6-g deformation uncertainty.

The ability of beryllium to meet the LUTE primary mirror requirement is perhaps most uncertain due to the possibility that any cryogenic deformation will not be sufficiently repeatable to be able to be removed adequately with cryo null figuring. Furthermore a beryllium mirror cannot tolerate more than about 0.1% $\Delta L/L$ variation throughout the mirror substrate.

There are at least two LUTE system parameters that should be considered for revision following the results of this study; the first, being the LUTE mass budget. Should a substantial increase in lunar lander payload mass become available the selection of beryllium must be revisited. Other materials, particularly fused quartz, have shown a much higher degree of thermal cycling-induced deformation repeatability. They are likewise known to be suitable for exceptionally high performance optical systems.

The second LUTE system parameter that has had a major impact on this study is the temperature range over which the telescope must operate. Mirror substrate material properties such as coefficient of thermal expansion, thermal conductivity, etc. are strong functions of temperature. Any change to the LUTE operating temperature will require that the choice of optical materials be re-evaluated. This is clearly an iterative process since the evaluation of primary mirror thermal gradients requires knowledge of the material, while knowledge of the thermal gradients is required for the evaluation of the mirror wavefront deformation.

SECTION 7
CANDIDATE TOPICS FOR FURTHER STUDY

The following tasks remain as high priority candidates for further study to support the LUTE program.

- Re-evaluation of mirror material and geometry trades based upon revisions to the lunar lander payload mass budget and revisions to the operating temperature range.
- Analysis of three candidate beryllium mirror concepts (single arch, structured open back, and structured closed back) to identify the optimum geometry.
- Optical analysis to determine mirror alignment sensitivities in support of the concept to fabricate the tertiary mirror on same substrate as primary mirror.
- Ultraviolet scatter measurements on small (3-5 cm diameter) polished and coated beryllium mirrors.
- Analysis of the candidate materials to identify the optimum temperature range for each material to achieve its optimum performance.
- Structural analysis of the entire telescope assembly (in addition to the primary mirror) to show that the weight allocations are feasible.
- Further investigation into the utility of active correction of primary mirror surface deformations.
- Investigation into the CTE and $\Delta L/L$ uniformity of hot isostatic pressed beryllium.
- Optical analysis to support a re-evaluation of the existing wavefront error allocation to check its suitability for an ultraviolet wavelength telescope.
- Optical design trades to support optimization of the location of the focal plane.

SECTION 8
ACKNOWLEDGEMENTS

Mike Krim's help in many areas has been immeasurable. We would also like to thank Aaron Turner for the normal incidence ultraviolet reflectance computations, Alan Green and Bill Meyer for insightful discussions regarding optical fabrication, and Charlie Schaub for comments on the suitability of beryllium mirrors for UV applications.

APPENDIX A
ALLOWABLE THERMAL AND CTE GRADIENTS

Appendix A contains a set of tables and charts that support the trades between the candidate mirror materials and geometries. The materials evaluated include fused quartz, Zerodur, ULE, borosilicate, beryllium, and silicon carbide. For each mirror material we evaluated four mirror geometries: meniscus, open back, closed back, and single arch.

The charts are simply a graphical representation of the tabulated values and do not contain any additional information. However, the charts enable one to quickly detect trends.

The last set of tables document the mirror deformation sensitivities used in the previous tables and charts. Note that the sensitivity values do not include the lowest order primary mirror wavefront errors associated with rigid body motions or focus error because we assume that a secondary mirror alignment mechanism will be available. Also note that we computed more deformation sensitivities than were plotted in the previous charts; these data are provided for completeness.

TABLE A-1
MENISCUS RADIAL GRADIENT SENSITIVITY

			budget (waves rms, 1 wave = 0.6328 μm)					
			0.0168	0.0125	0.0125	0.0063	0.0063	0.0063
	Meniscus							
	Radial Gradient Sensitivity		T range			operating T		
	for 1E-6 ΔL/L		293 K-160 K	160 K-60 K	160 K-260 K	160 K	60 K	260 K
		Z5-Z23						
Material	Thickness (in.	μm rms	allowable fractional ΔL/L			allowable center-to-edge radial ΔT (K)		
Fused Quartz	0.3	0.748	0.00039	0.00023	0.00049	0.059	0.007	0.013
	0.6	0.188	0.00155	0.00090	0.00196	0.235	0.028	0.050
	0.9	0.084	0.00348	0.00202	0.00439	0.526	0.063	0.113
Zerodur	0.3	0.578	0.00090	0.00059	0.00080	0.037	0.014	0.058
	0.6	0.146	0.00358	0.00234	0.00317	0.147	0.057	0.231
	0.9	0.065	0.00805	0.00525	0.00713	0.331	0.128	0.520
ULE	0.3	0.779	0.00057	0.00013	0.00043	0.011	0.005	0.109
	0.6	0.196	0.00226	0.00053	0.00171	0.042	0.021	0.431
	0.9	0.087	0.00509	0.00120	0.00385	0.095	0.047	0.972
Borosilicate	0.3	0.803	0.00004	0.00006	0.00004	0.002	0.007	0.002
	0.6	0.202	0.00014	0.00024	0.00015	0.009	0.029	0.007
	0.9	0.090	0.00032	0.00054	0.00033	0.019	0.064	0.015
Beryllium	0.3	0.182	0.00005	0.00022	0.00006	0.005	0.068	0.002
	0.6	0.046	0.00021	0.00086	0.00023	0.019	0.269	0.009
	0.9	0.020	0.00049	0.00198	0.00053	0.044	0.619	0.020
Silicon Carbid	0.3	0.162	0.00024	0.00177	0.00030	0.035	0.676	0.009
	0.6	0.041	0.00095	0.00700	0.00118	0.138	2.670	0.035
	0.9	0.018	0.00216	0.01594	0.00269	0.314	6.082	0.079

TABLE A-2
MENISCUS DIAMETRAL GRADIENT SENSITIVITY

			budget (waves rms, 1 wave = 0.6328 μm)					
			0.0168	0.0125	0.0125	0.0063	0.0063	0.0063
	Meniscus							
	Diametral Gradient Sensiti		T range			operating T		
	for 1E-6 ΔL/L		293 K-160 K	160 K-60 K	160 K-260 K	160 K	60 K	260 K
		Z5-Z23						
Material	Thickness (in.	μm rms	allowable fractional ΔL/L			allowable diametral ΔT (K)		
Fused Quartz	0.3	0.066	0.00443	0.00257	0.00558	0.670	0.080	0.144
	0.6	0.017	0.01718	0.00996	0.02167	2.601	0.309	0.557
	0.9	0.007	0.04173	0.02420	0.05262	6.318	0.751	1.354
Zerodur	0.3	0.051	0.01026	0.00668	0.00909	0.422	0.163	0.663
	0.6	0.013	0.04023	0.02623	0.03565	1.655	0.638	2.600
	0.9	0.006	0.08717	0.05682	0.07724	3.586	1.382	5.633
ULE	0.3	0.069	0.00642	0.00151	0.00486	0.120	0.059	1.225
	0.6	0.017	0.02606	0.00614	0.01972	0.488	0.238	4.974
	0.9	0.008	0.05537	0.01305	0.04190	1.037	0.506	10.569
Borosilicate	0.3	0.071	0.00041	0.00069	0.00041	0.024	0.082	0.019
	0.6	0.018	0.00161	0.00272	0.00163	0.096	0.322	0.074
	0.9	0.008	0.00362	0.00613	0.00367	0.216	0.725	0.166
Beryllium	0.3	0.016	0.00061	0.00247	0.00067	0.055	0.774	0.025
	0.6	0.004	0.00243	0.00989	0.00266	0.222	3.095	0.100
	0.9	0.002	0.00486	0.01978	0.00533	0.444	6.190	0.200
Silicon Carbid	0.3	0.014	0.00278	0.02050	0.00346	0.404	7.819	0.101
	0.6	0.004	0.00974	0.07174	0.01211	1.413	27.367	0.354
	0.9	0.002	0.01948	0.14349	0.02423	2.826	54.734	0.708

TABLE A-3
OPEN BACK DIAMETRAL GRADIENT SENSITIVITY

			budget (waves rms, 1 wave = 0.6328 μm)					
			0.0168	0.0125	0.0125	0.0063	0.0063	0.0063
	Open Back							
	Diametral Gradient Sensiti		T range			operating T		
	for 1E-6 ΔL/L		293 K-160 K	160 K-60 K	160 K-260 K	160 K	60 K	260 K
		Z5-Z23						
Material	Depth (in.)	μm rms	allowable fractional ΔL/L			allowable diametral ΔT (K)		
Fused Quartz	1	0.849	0.00034	0.00020	0.00043	0.052	0.006	0.011
	2	0.272	0.00107	0.00062	0.00135	0.163	0.019	0.035
	4	0.066	0.00443	0.00257	0.00558	0.670	0.080	0.144
Zerodur	1	0.656	0.00080	0.00052	0.00071	0.033	0.013	0.052
	2	0.210	0.00249	0.00162	0.00221	0.102	0.039	0.161
	4	0.051	0.01026	0.00668	0.00909	0.422	0.163	0.663
ULE	1	0.884	0.00050	0.00012	0.00038	0.009	0.005	0.096
	2	0.283	0.00157	0.00037	0.00118	0.029	0.014	0.299
	4	0.069	0.00642	0.00151	0.00486	0.120	0.059	1.225
Borosilicate	1	0.912	0.00003	0.00005	0.00003	0.002	0.006	0.001
	2	0.292	0.00010	0.00017	0.00010	0.006	0.020	0.005
	4	0.071	0.00041	0.00069	0.00041	0.024	0.082	0.019
Beryllium	1	0.206	0.00005	0.00019	0.00005	0.004	0.060	0.002
	2	0.066	0.00015	0.00060	0.00016	0.013	0.188	0.006
	4	0.016	0.00061	0.00247	0.00067	0.055	0.774	0.025
Silicon Carbid	1	0.184	0.00021	0.00156	0.00026	0.031	0.595	0.008
	2	0.059	0.00066	0.00486	0.00082	0.096	1.855	0.024
	4	0.014	0.00278	0.02050	0.00346	0.404	7.819	0.101

TABLE A-4
CLOSED BACK DIAMETRAL GRADIENT SENSITIVITY

			budget (waves rms, 1 wave = 0.6328 μm)					
			0.0168	0.0125	0.0125	0.0063	0.0063	0.0063
	Closed Back							
	Diametral Gradient Sensiti		T range			operating T		
	for 1E-6 ΔL/L		293 K-160 K	160 K-60 K	160 K-260 K	160 K	60 K	260 K
		Z5-Z23						
Material	Depth (in.)	μm rms	allowable fractional ΔL/L			allowable diametral ΔT (K)		
Fused Quartz	1	0.534	0.00055	0.00032	0.00069	0.083	0.010	0.018
	2	0.148	0.00197	0.00114	0.00249	0.299	0.036	0.064
	4	0.049	0.00596	0.00346	0.00752	0.903	0.107	0.193
Zerodur	1	0.413	0.00127	0.00083	0.00112	0.052	0.020	0.082
	2	0.115	0.00455	0.00296	0.00403	0.187	0.072	0.294
	4	0.038	0.01376	0.00897	0.01220	0.566	0.218	0.889
ULE	1	0.556	0.00080	0.00019	0.00060	0.015	0.007	0.152
	2	0.154	0.00288	0.00068	0.00218	0.054	0.026	0.549
	4	0.051	0.00869	0.00205	0.00657	0.163	0.079	1.658
Borosilicate	1	0.573	0.00005	0.00009	0.00005	0.003	0.010	0.002
	2	0.159	0.00018	0.00031	0.00018	0.011	0.036	0.008
	4	0.053	0.00055	0.00092	0.00055	0.033	0.109	0.025
Beryllium	1	0.130	0.00007	0.00030	0.00008	0.007	0.095	0.003
	2	0.036	0.00027	0.00110	0.00030	0.025	0.344	0.011
	4	0.012	0.00081	0.00330	0.00089	0.074	1.032	0.033
Silicon Carbid	1	0.193	0.00020	0.00149	0.00025	0.029	0.567	0.007
	2	0.054	0.00072	0.00531	0.00090	0.105	2.027	0.026
	4	0.018	0.00216	0.01594	0.00269	0.314	6.082	0.079

TABLE A-5
SINGLE ARCH RADIAL GRADIENT SENSITIVITY

			budget (waves rms, 1 wave = 0.6328 μm)					
			0.0168	0.0125	0.0125	0.0063	0.0063	0.0063
	Single Arch							
	Radial Gradient Sensitivity		T range			operating T		
	for 1E-6 ΔL/L		293 K-160 K	160 K-60 K	160 K-260 K	160 K	60 K	260 K
		Z5-Z23						
Material	Max. Thick. (in	μm rms	allowable fractional ΔL/L			allowable center-to-edge ΔT (K)		
Fused Quartz	0.5	0.098	0.00298	0.00173	0.00376	0.451	0.054	0.097
	1	0.067	0.00436	0.00253	0.00550	0.660	0.078	0.141
	2	0.022	0.01328	0.00770	0.01674	2.010	0.239	0.431
Zerodur	0.5	0.075	0.00697	0.00455	0.00618	0.287	0.111	0.451
	1	0.052	0.01006	0.00656	0.00891	0.414	0.159	0.650
	2	0.017	0.03077	0.02005	0.02726	1.266	0.488	1.988
ULE	0.5	0.102	0.00434	0.00102	0.00329	0.081	0.040	0.829
	1	0.070	0.00633	0.00149	0.00479	0.118	0.058	1.208
	2	0.023	0.01926	0.00454	0.01457	0.361	0.176	3.676
Borosilicate	0.5	0.105	0.00028	0.00047	0.00028	0.016	0.055	0.013
	1	0.072	0.00040	0.00068	0.00041	0.024	0.081	0.018
	2	0.024	0.00121	0.00204	0.00122	0.072	0.242	0.055
Beryllium	0.5	0.024	0.00041	0.00165	0.00044	0.037	0.516	0.017
	1	0.016	0.00061	0.00247	0.00067	0.055	0.774	0.025
	2	0.005	0.00180	0.00733	0.00197	0.164	2.292	0.074
Silicon Carbid	0.5	0.021	0.00186	0.01367	0.00231	0.269	5.213	0.067
	1	0.015	0.00260	0.01913	0.00323	0.377	7.298	0.094
	2	0.005	0.00812	0.05979	0.01009	1.177	22.806	0.295

TABLE A-6
SINGLE ARCH DIAMETRAL GRADIENT SENSITIVITY

			budget (waves rms, 1 wave = 0.6328 μm)					
			0.0168	0.0125	0.0125	0.0063	0.0063	0.0063
	Single Arch							
	Diametral Gradient Sensitiv		T range			operating T		
	for 1E-6 ΔL/L		293 K-160 K	160 K-60 K	160 K-260 K	160 K	60 K	260 K
		Z5-Z23						
Material	Max. Thick. (ir	μm rms	allowable fractional ΔL/L			allowable diametral ΔT (K)		
Fused Quartz	0.5	0.043	0.00679	0.00394	0.00857	1.028	0.122	0.220
	1	0.030	0.00974	0.00565	0.01228	1.474	0.175	0.316
	2	0.010	0.02921	0.01694	0.03683	4.422	0.526	0.948
Zerodur	0.5	0.033	0.01585	0.01033	0.01404	0.652	0.251	1.024
	1	0.023	0.02274	0.01482	0.02015	0.936	0.360	1.469
	2	0.008	0.06538	0.04262	0.05793	2.690	1.036	4.225
ULE	0.5	0.045	0.00984	0.00232	0.00745	0.184	0.090	1.879
	1	0.031	0.01429	0.00337	0.01081	0.267	0.131	2.728
	2	0.010	0.04430	0.01044	0.03352	0.829	0.405	8.455
Borosilicate	0.5	0.046	0.00063	0.00107	0.00064	0.038	0.126	0.029
	1	0.032	0.00091	0.00153	0.00092	0.054	0.181	0.041
	2	0.010	0.00290	0.00490	0.00293	0.173	0.580	0.132
Beryllium	0.5	0.010	0.00097	0.00396	0.00107	0.089	1.238	0.040
	1	0.007	0.00135	0.00550	0.00148	0.123	1.719	0.056
	2	0.002	0.00405	0.01649	0.00444	0.370	5.158	0.167
Silicon Carbid	0.5	0.009	0.00419	0.03086	0.00521	0.608	11.771	0.152
	1	0.006	0.00609	0.04484	0.00757	0.883	17.104	0.221
	2	0.002	0.01855	0.13665	0.02307	2.691	52.127	0.674

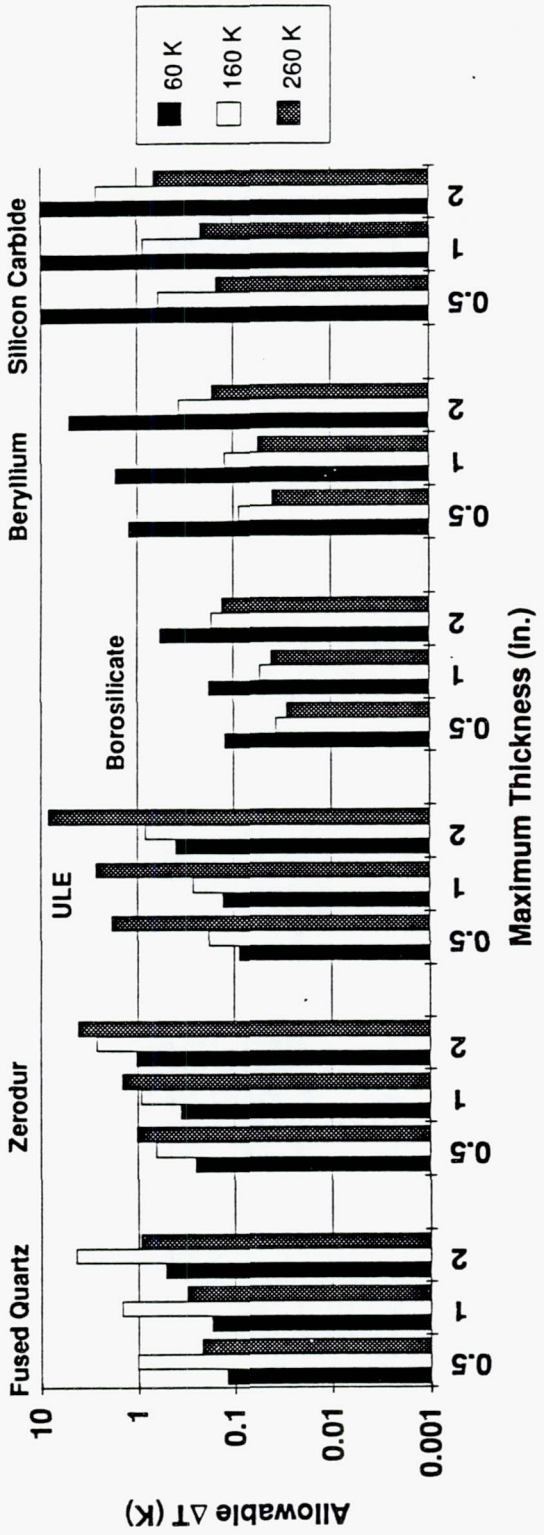

Figure A-1. Single Arch-Diametral ΔT.

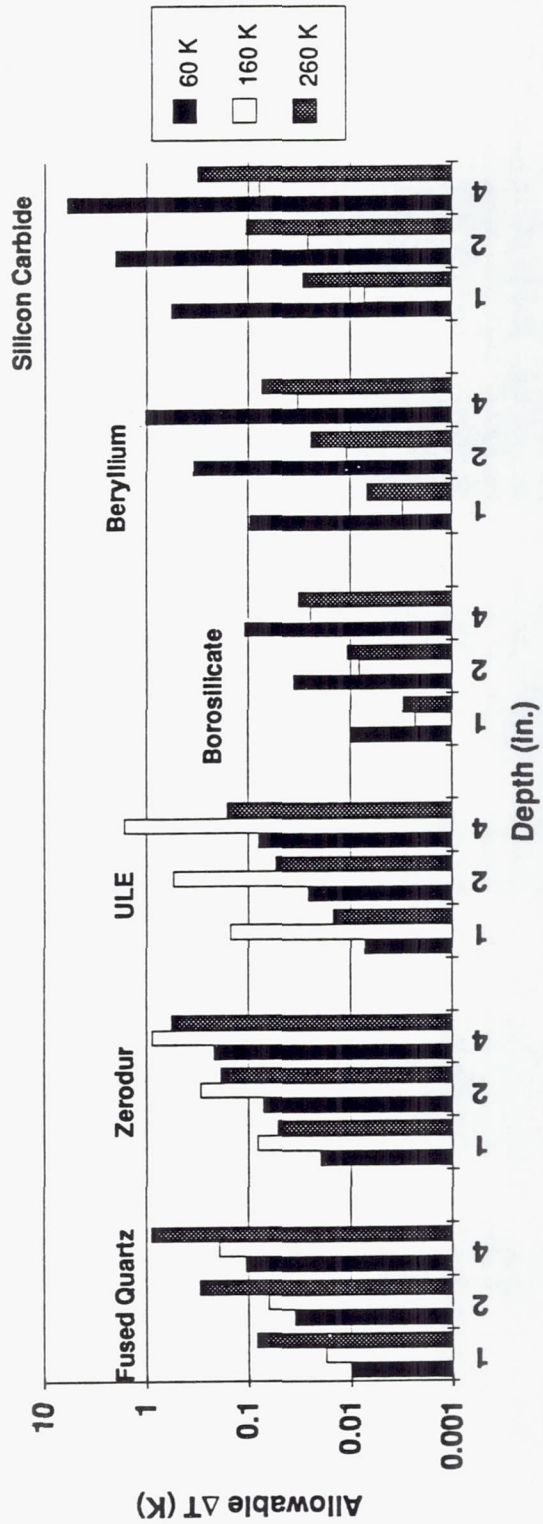

Figure A-2. Closed Back-Diametral ΔT.

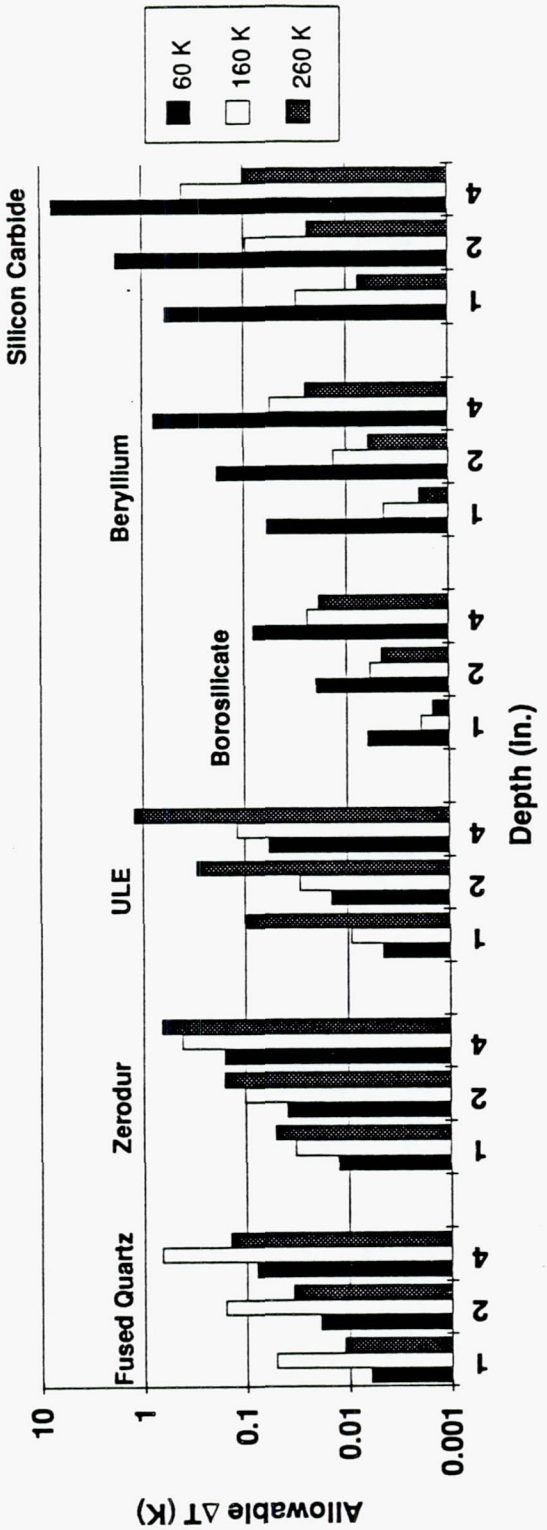

Figure A-3. Open Back-Diametral ΔT.

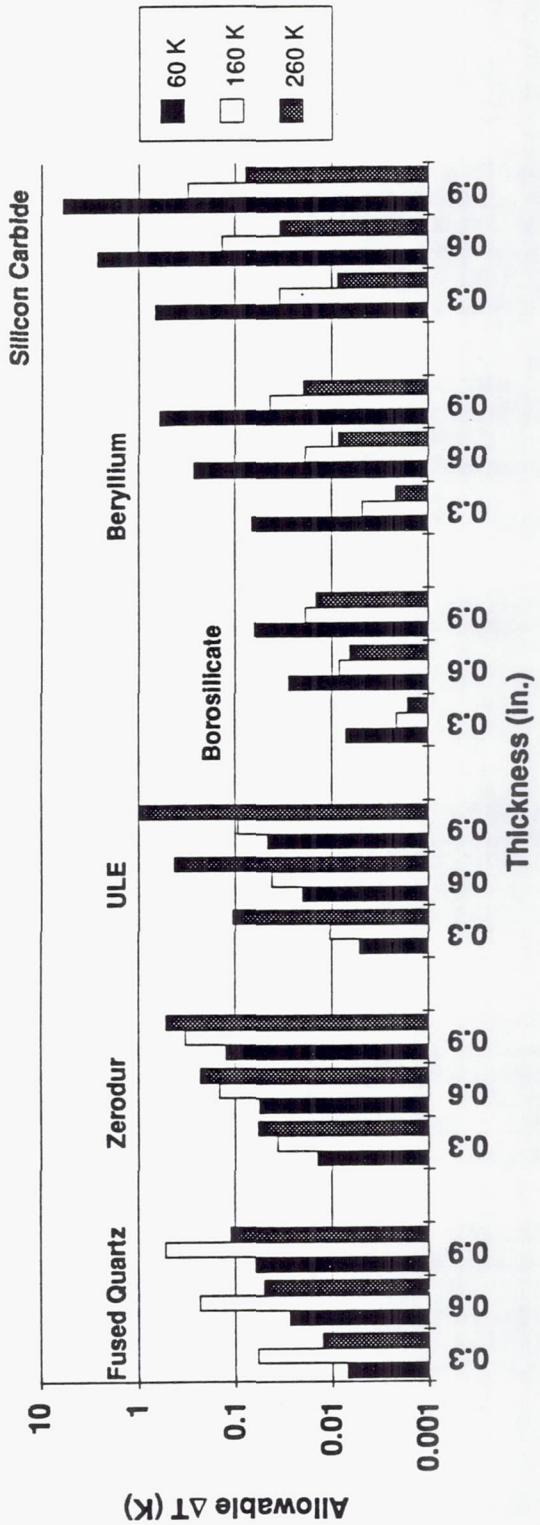

Figure A-4. Meniscus-Radially Symmetric ΔT.

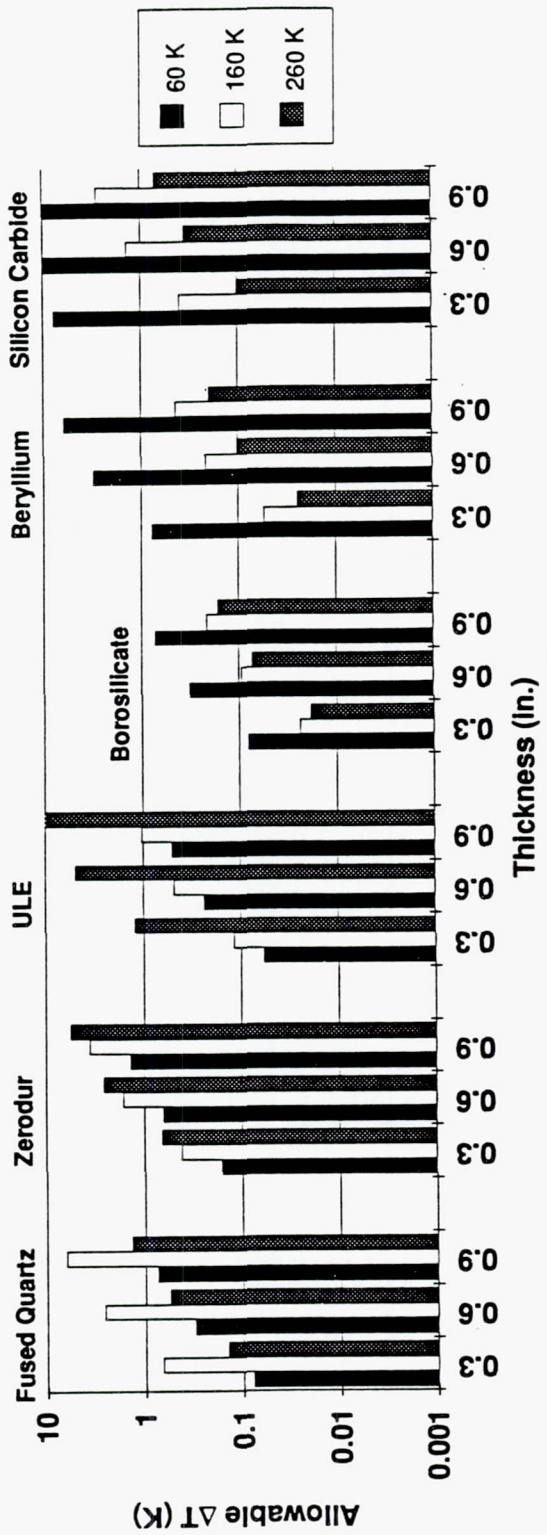

Figure A-5. Meniscus-Diametral ΔT.

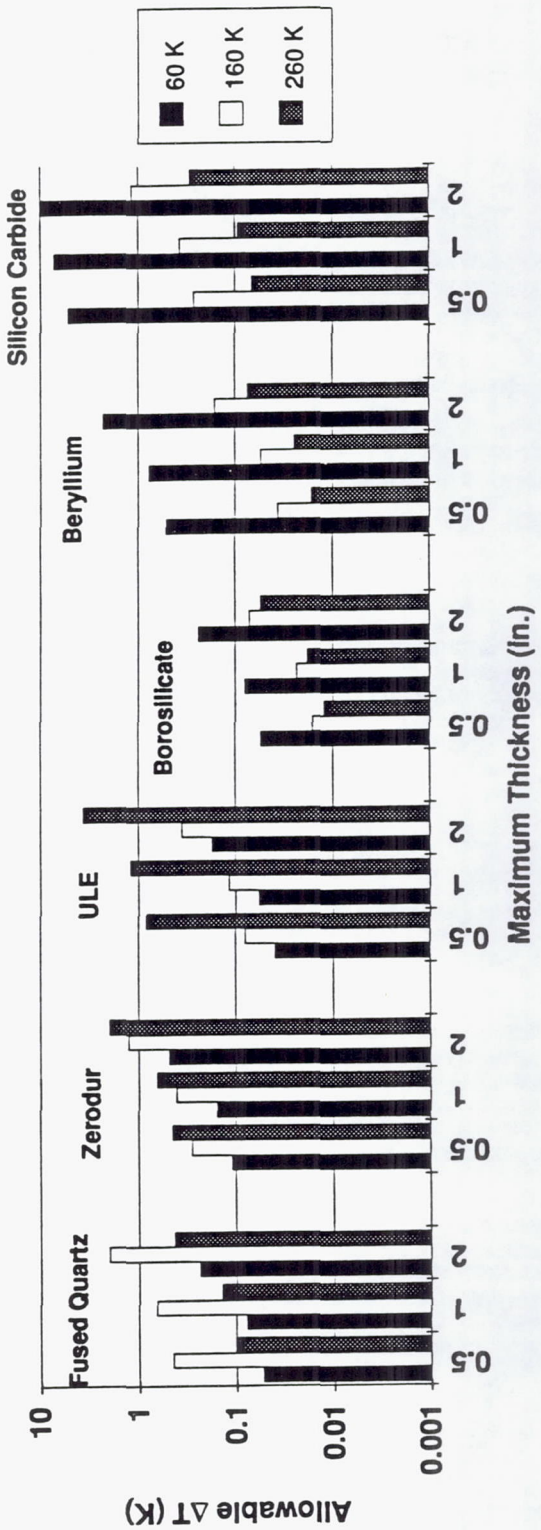

Figure A-6. Single Arch-Radially Symmetric ΔT.

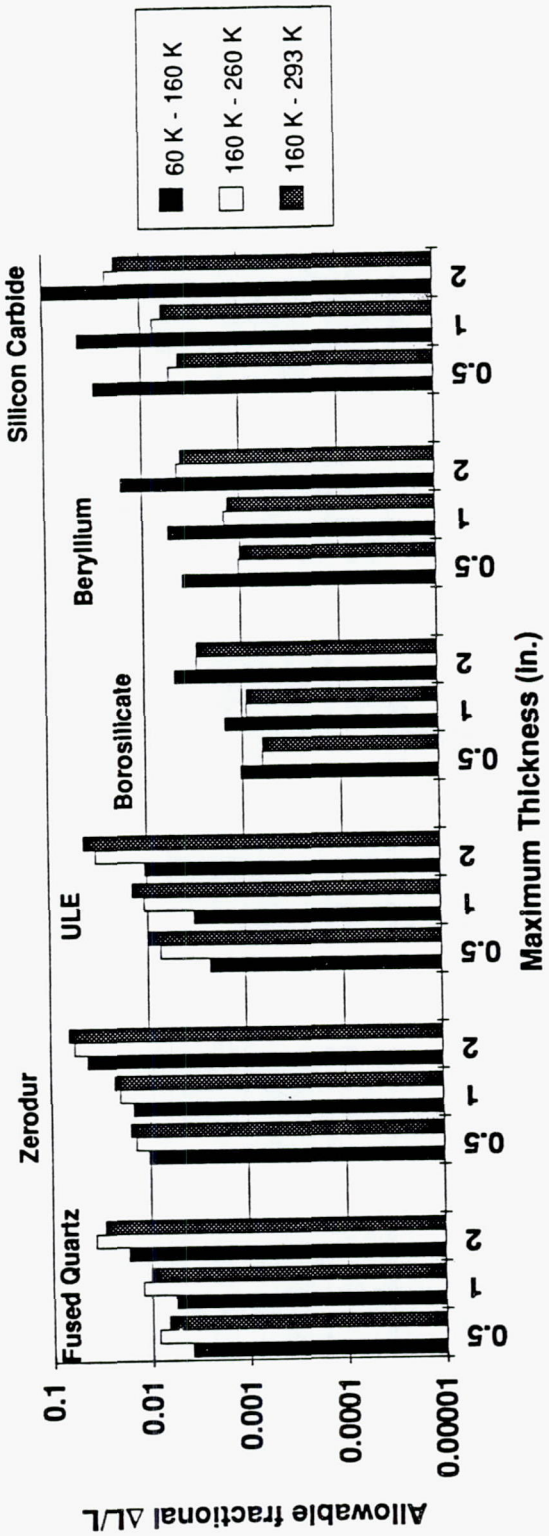

Figure A-7. Single Arch-Diametral ΔL/L.

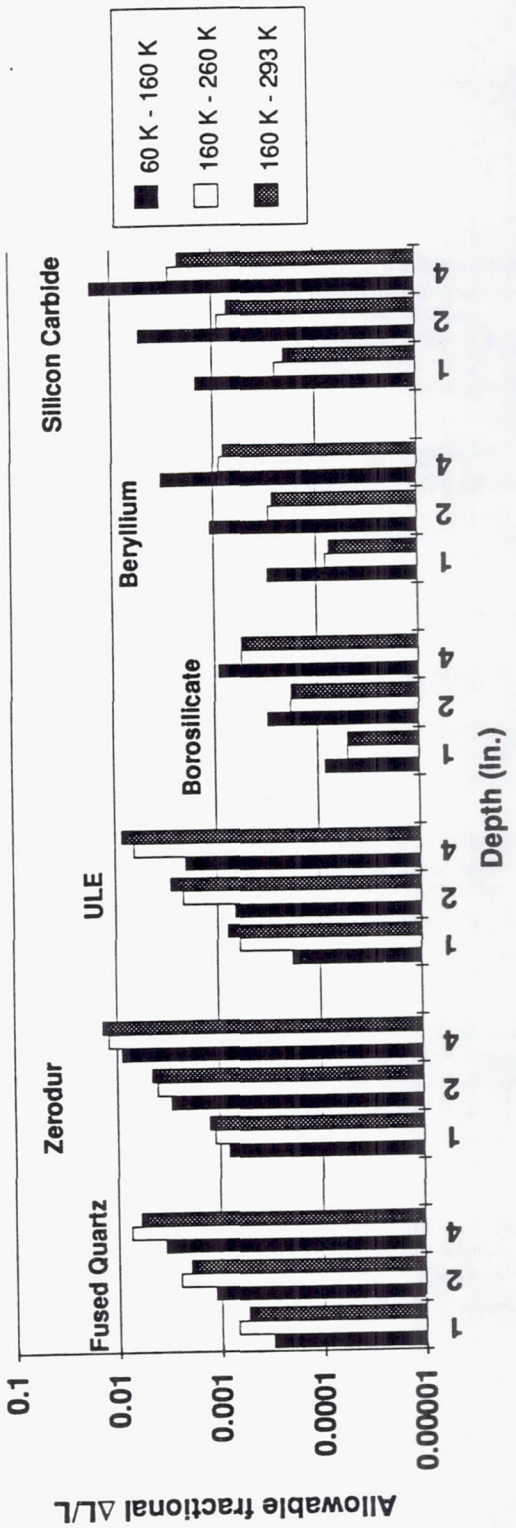

Figure A-8. Closed Back-Diametral ΔL/L.

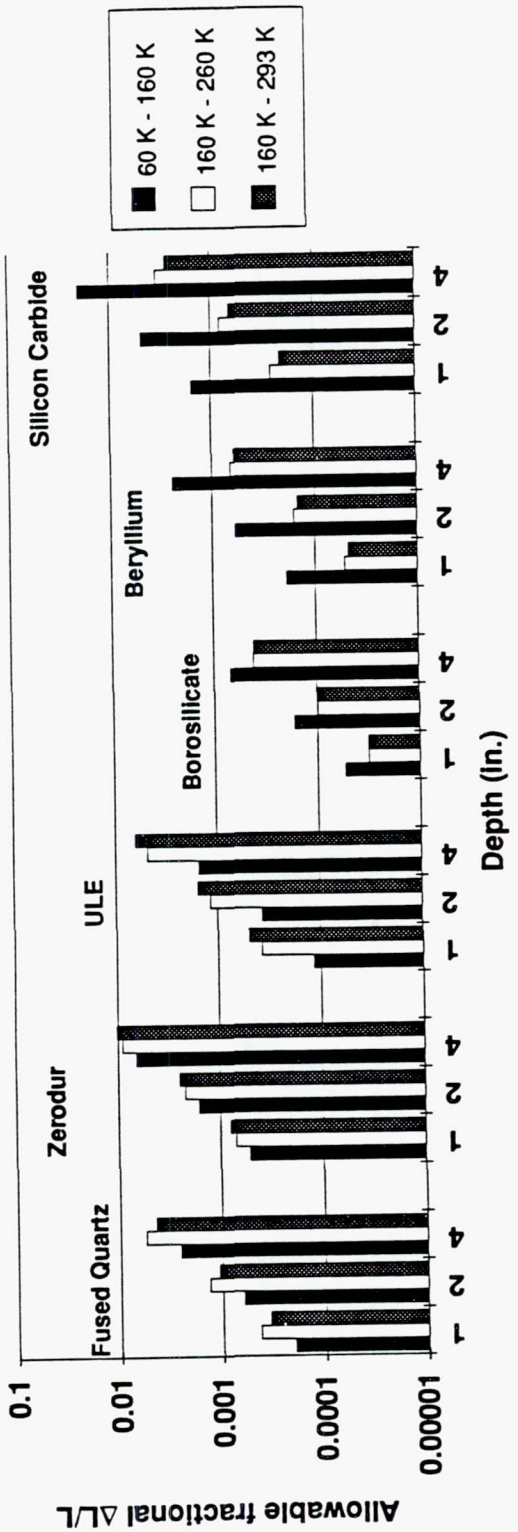

Figure A-9. Open Back-Diametral ΔL/L.

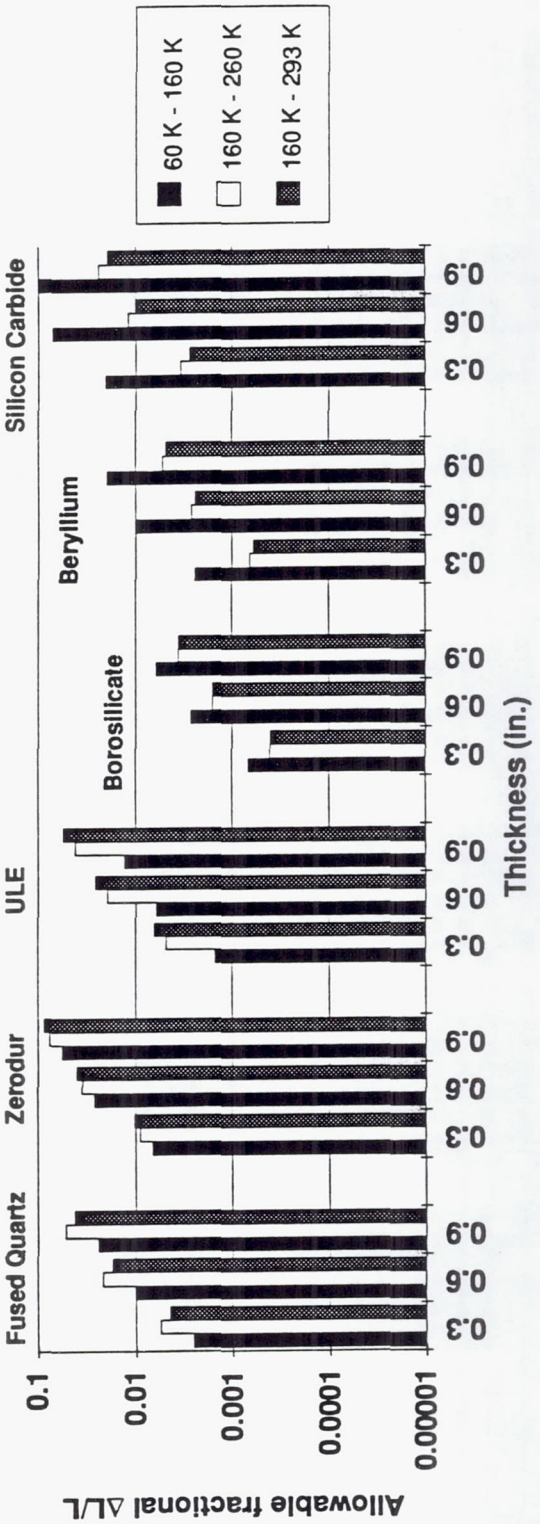

Figure A-10. Meniscus-Diametral ΔL/L.

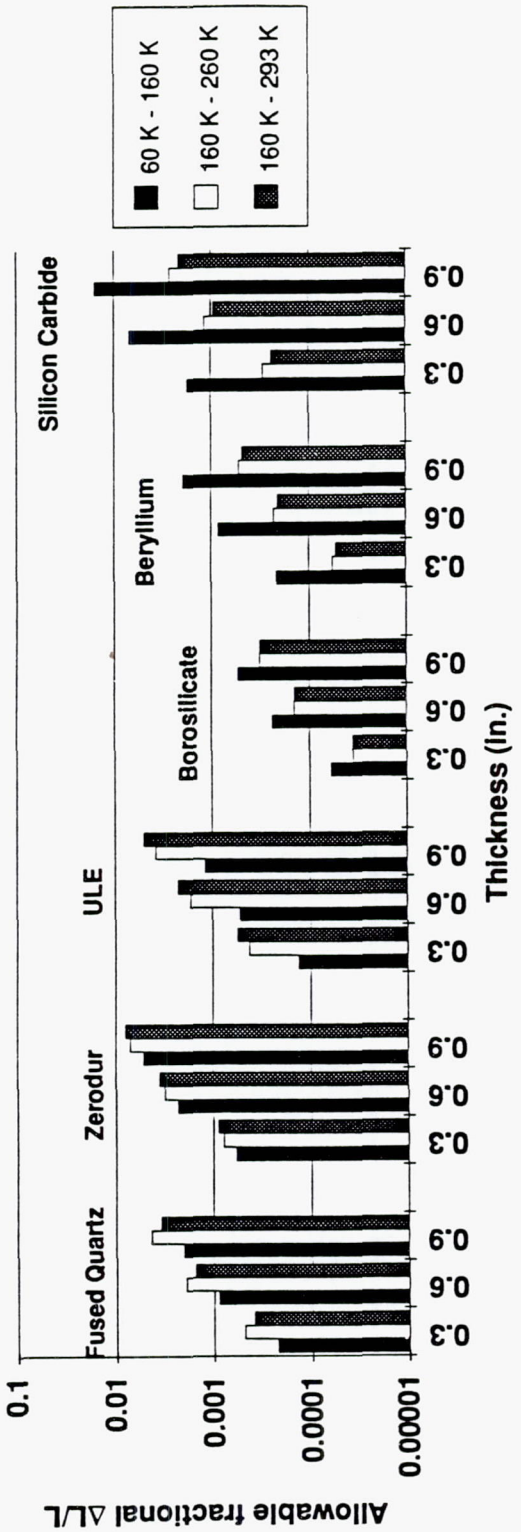

Figure A-11. Meniscus-Radially Symmetric ΔL/L.

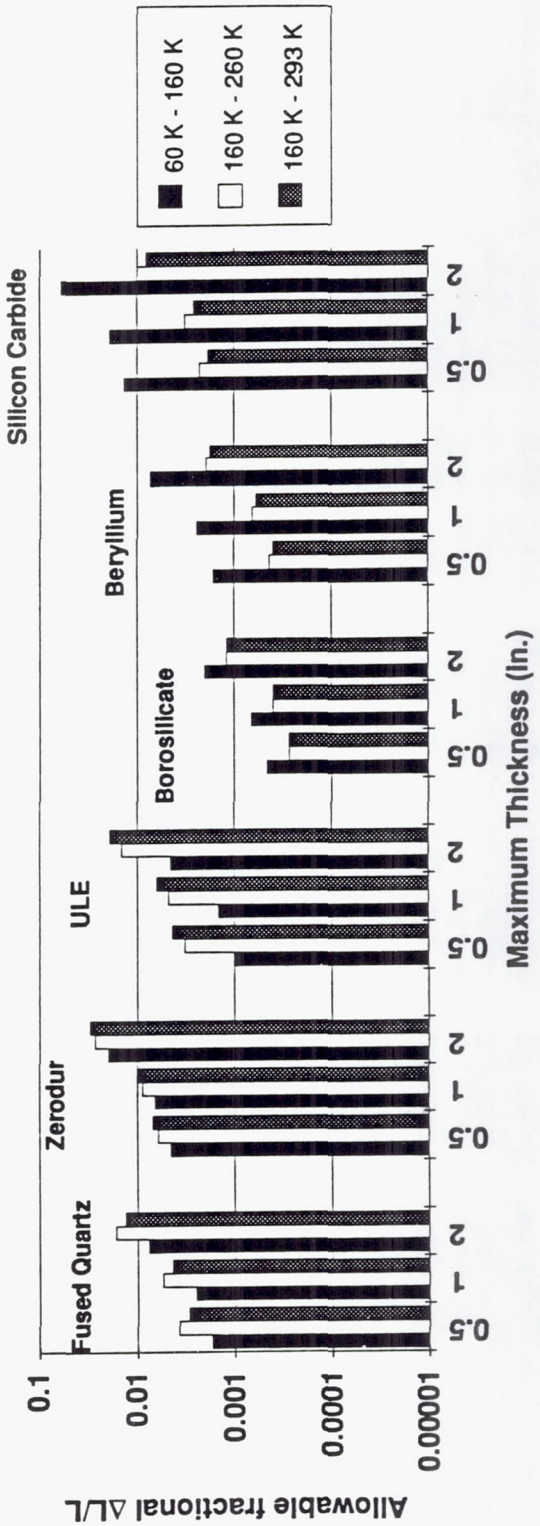

Figure A-12. Single Arch-Radially Symmetric ΔL/L.

TABLE A-7
PRIMARY MIRROR MENISCUS - ΔL/L

		Primary Mirror ΔL/L = (CTE * ΔT) Sensitivities		
		Diametral Gradient	Radial Gradient	Axial Gradient
		ΔL/L = 1.0e-6	ΔL/L = 1.0e-6	ΔL/L = 1.0e-6
		Est. WFE (um-rms)	Est. WFE (um-rms)	Est. WFE (um-rms)
Mirror Type	Thickness (Inch)	Z(5-23)	Z(5-23)	Z(5-23)
1) Meniscus	0.3	0.066	0.748	0.0555
• Fused Quartz	0.6	0.017	0.188	0.0140
	0.9	0.007	0.084	0.0062
• Zerodur	0.3	0.051	0.578	0.0429
	0.6	0.013	0.146	0.0108
	0.9	0.006	0.065	0.0048
• ULE	0.3	0.069	0.779	0.0578
	0.6	0.017	0.196	0.0146
	0.9	0.008	0.087	0.0065
• Borosilicate	0.3	0.071	0.803	0.0596
	0.6	0.018	0.202	0.0150
	0.9	0.008	0.090	0.0067
• Beryllium	0.3	0.016	0.182	0.0135
	0.6	0.004	0.046	0.0034
	0.9	0.002	0.020	0.0015
• Silicon Carbide	0.3	0.014	0.162	0.0121
	0.6	0.004	0.041	0.0030
	0.9	0.002	0.018	0.0013

TABLE A-8
PRIMARY MIRROR OPEN BACK - ΔL/L

		Primary Mirror ΔL/L = (CTE * ΔT) Sensitivities		
		Diametral Gradient	Radial Gradient	Axial Gradient
		ΔL/L = 1.0e-6	ΔL/L = 1.0e-6	ΔL/L = 1.0e-6
		Est. WFE (um-rms)	Est. WFE (um-rms)	Est. WFE (um-rms)
Mirror Type	Depth (inch)	Z(5-23)	Z(5-23)	Z(5-23)
2) Open Back	1	0.849	0.145	0.0093
• Fused Quartz	2	0.272	0.046	0.0030
	4	0.066	0.011	0.0007
• Zerodur	1	0.656	0.112	0.0072
	2	0.210	0.036	0.0023
	4	0.051	0.009	0.0006
• ULE	1	0.884	0.151	0.0097
	2	0.283	0.048	0.0031
	4	0.069	0.012	0.0008
• Borosilicate	1	0.912	0.155	0.0100
	2	0.292	0.050	0.0032
	4	0.071	0.012	0.0008
• Beryllium	1	0.206	0.035	0.0023
	2	0.066	0.011	0.0007
	4	0.016	0.003	0.0002
• Silicon Carbide	1	0.184	0.031	0.0020
	2	0.059	0.010	0.0006
	4	0.014	0.002	0.0002

TABLE A-9
PRIMARY MIRROR CLOSED BACK - ΔL/L

		Primary Mirror ΔL/L = (CTE * ΔT) Sensitivities		
Mirror Type	Depth (inch)	Diametral Gradient ΔL/L = 1.0e-6 Est. WFE (um-rms) Z(5-23)	Radial Gradient ΔL/L = 1.0e-6 Est. WFE (um-rms) Z(5-23)	Axial Gradient ΔL/L = 1.0e-6 Est. WFE (um-rms) Z(5-23)
3) Closed Back	1	0.534	0.087	0.0063
• Fused Quartz	2	0.148	0.024	0.0018
	4	0.049	0.008	0.0006
• Zerodur	1	0.413	0.068	0.0049
	2	0.115	0.019	0.0014
	4	0.038	0.006	0.0005
• ULE	1	0.556	0.091	0.0066
	2	0.154	0.025	0.0018
	4	0.051	0.008	0.0006
• Borosilicate	1	0.573	0.094	0.0068
	2	0.159	0.026	0.0019
	4	0.053	0.009	0.0006
• Beryllium	1	0.130	0.021	0.0015
	2	0.036	0.006	0.0004
	4	0.012	0.002	0.0001
• Silicon Carbide	1	0.193	0.019	0.0014
	2	0.054	0.005	0.0004
	4	0.018	0.002	0.0001

TABLE A-10
PRIMARY MIRROR SINGLE ARCH - ΔL/L

		Primary Mirror ΔL/L = (CTE * ΔT) Sensitivities		
		Diametral Gradient	Radial Gradient	Axial Gradient
		ΔL/L = 1.0e-6	ΔL/L = 1.0e-6	ΔL/L = 1.0e-6
		Est. WFE (um-rms)	Est. WFE (um-rms)	Est. WFE (um-rms)
Mirror Type	Max. Thick. (inch)	Z(5-23)	Z(5-23)	Z(5-23)
4) Single Arch	0.5	0.043	0.098	0.0151
• Fused Quartz	1	0.030	0.067	0.0104
	2	0.010	0.022	0.0034
• Zerodur	0.5	0.033	0.075	0.0117
	1	0.023	0.052	0.0081
	2	0.008	0.017	0.0026
• ULE	0.5	0.045	0.102	0.0157
	1	0.031	0.070	0.0109
	2	0.010	0.023	0.0036
• Borosilicate	0.5	0.046	0.105	0.0162
	1	0.032	0.072	0.0112
	2	0.010	0.024	0.0037
• Beryllium	0.5	0.010	0.024	0.0037
	1	0.0072	0.016	0.0025
	2	0.0024	0.0054	0.00083
• Silicon Carbide	0.5	0.0093	0.021	0.0033
	1	0.0064	0.015	0.0023
	2	0.0021	0.0048	0.00074

APPENDIX B
MIRROR MATERIAL CRYOGENIC PROPERTIES AND FIGURES OF MERIT

Appendix B contains a series of figures that describe the variation in mirror material properties with temperature. Since LUTE will operate over a very wide temperature range, and since mirror material properties at cryogenic temperatures can differ dramatically from the room temperature values, we used the following data in the analyses presented in this report.

How do they vary with temperature?

	Density	*Young's Modulus*	*Specific Stiffness*	*Poisson's Ratio*	*Coefficient of Thermal Expansion*	*Fractional Dimensional Change*	*Thermal Conductivity*
Preferred Magnitude	small	large	large	large	small	small	large
metric units	kg/(m^3)	Pa	(m^2)/(s^2)	---	1/K	[ref. 293 K]	W/(m K)
symbol	rho	E	E/rho	nu	alpha	ΔL/L	k

St. State Thermal Distortion	*Specific Heat*	*Thermal Diffusivity*	*Transient Thermal Distortion*
small	large	large	small
m/W	J/(kg K)	(m^2)/s	s/[(m^2) K]
alpha/k	C	D = k/(rho C)	alpha/D

Figure B-1. Material Property Figures of Merit.

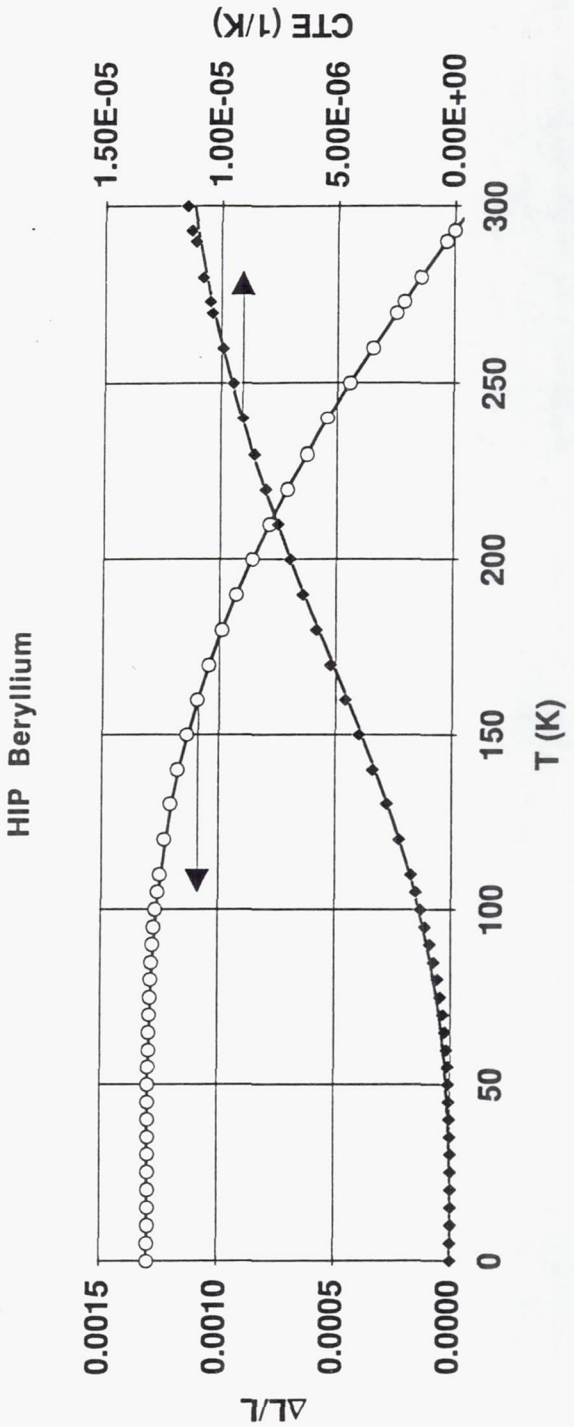

Figure B-2. Hot Isostatic Pressed Beryllium Coefficient of Thermal Expansion and Integrated Thermal Contraction.

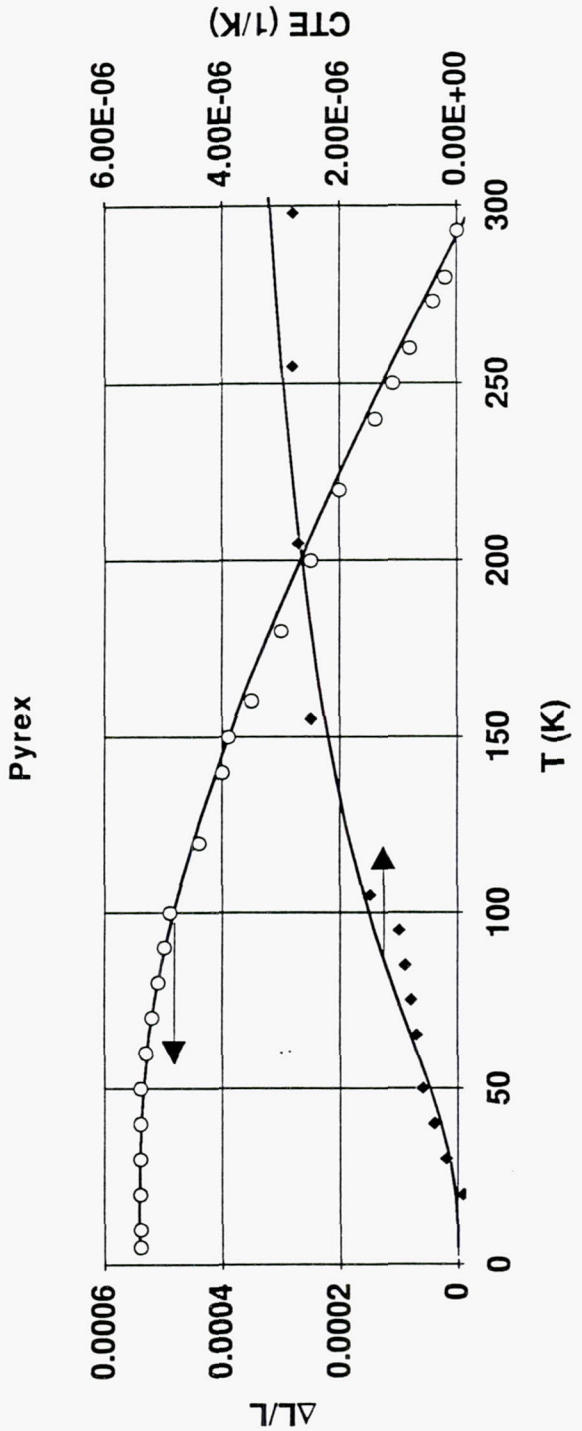

Figure B-3. Pyrex Coefficient of Thermal Expansion and Integrated Thermal Contraction.

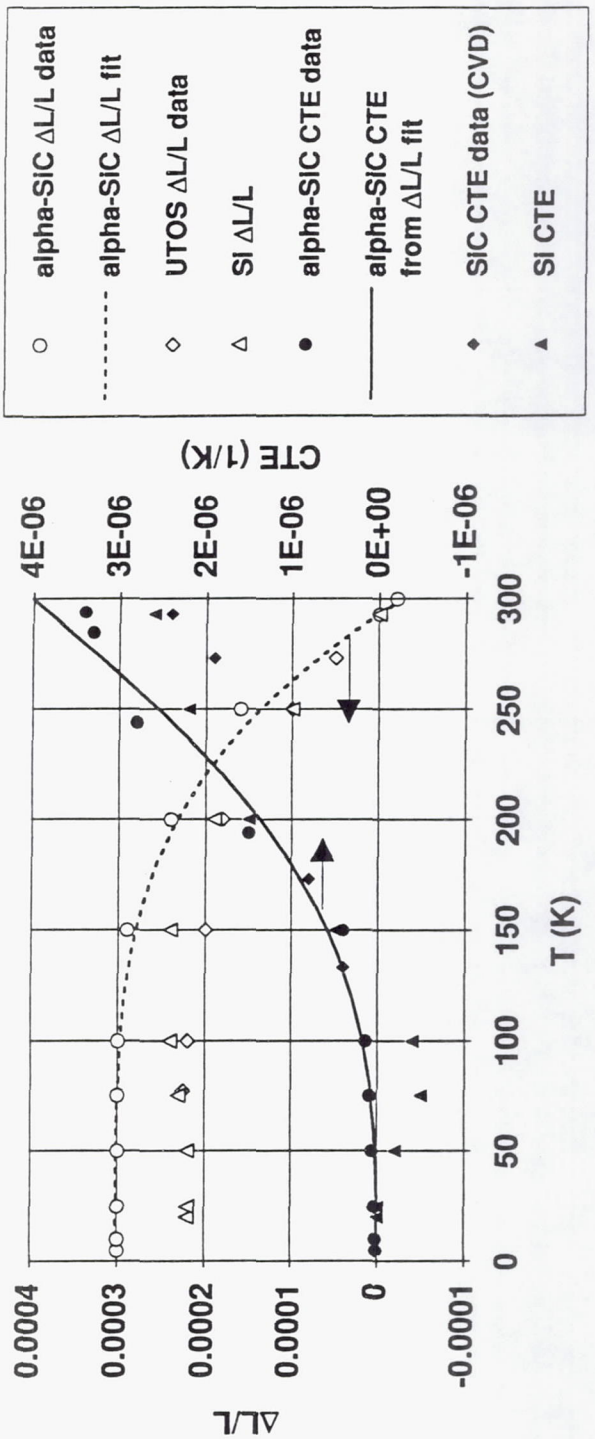

Figure B-4. Silicon Carbide and Silicon Coefficients of Thermal Expansion and Integrated Thermal Contraction. (Data is for the alpha form of silicon carbide and is only approximately correct for reaction-bonded silicon carbide.)

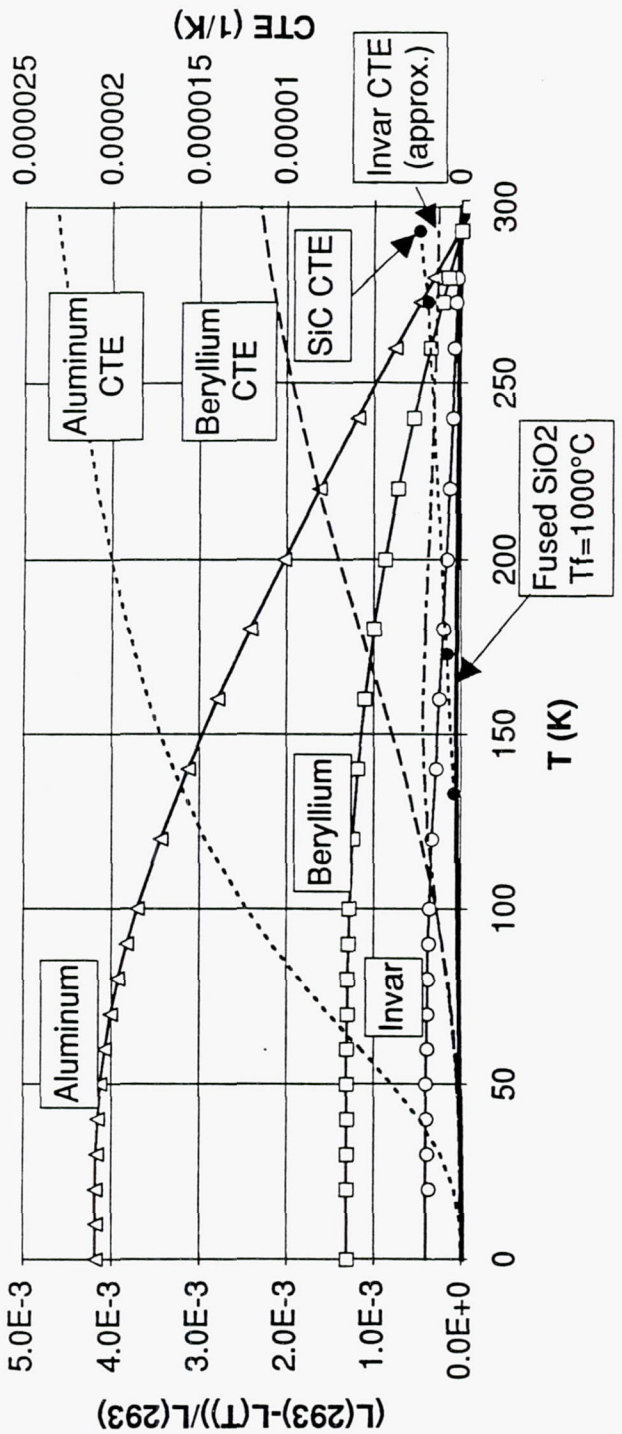

Figure B-5. Comparison of Coefficients of Thermal Expansion and Integrated Thermal Contraction for Metals, Silicon Carbide, and Fused Quartz.

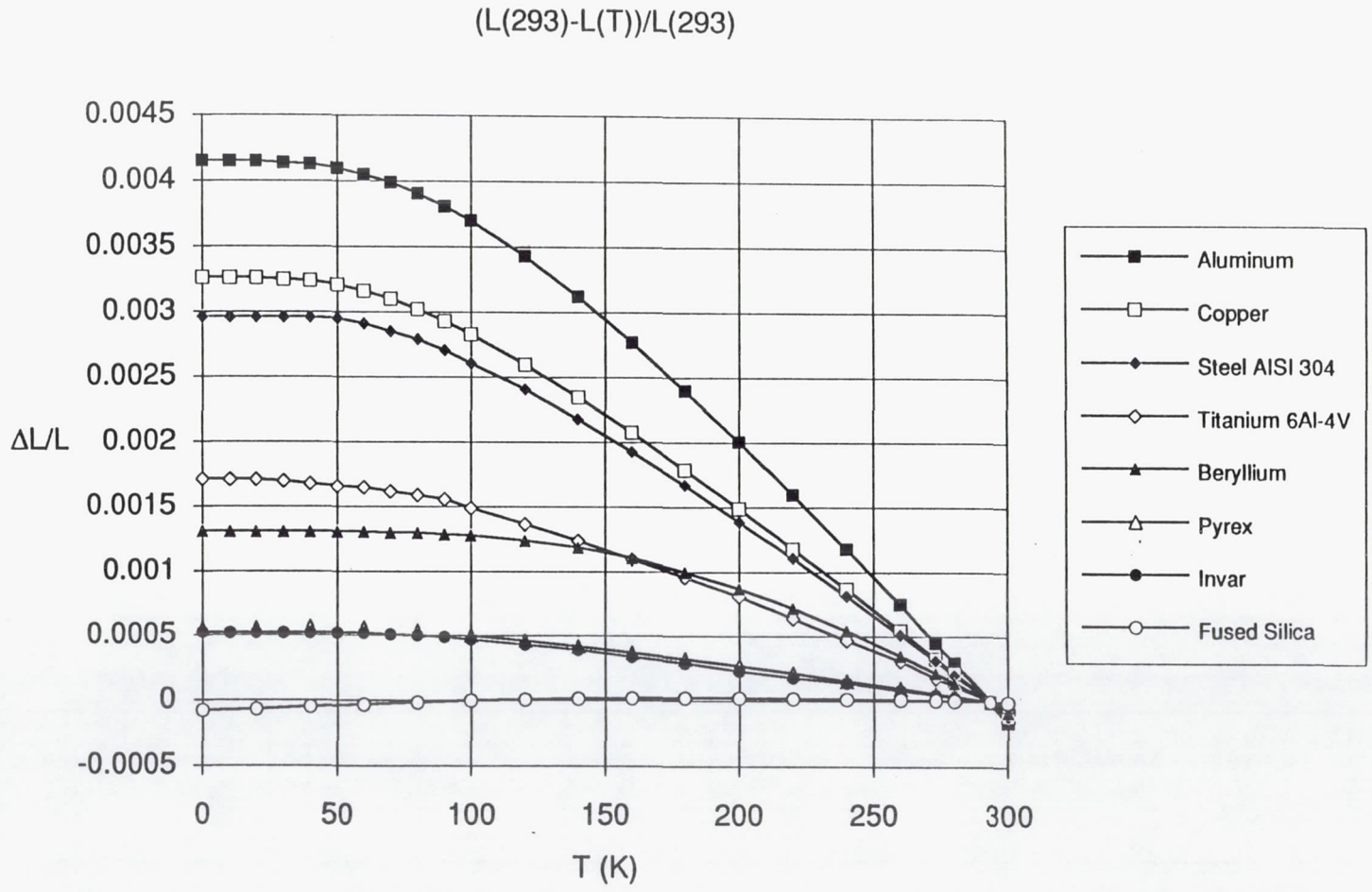

Figure B-6. Comparison of Integrated Thermal Contraction for Metals and Fused Quartz.

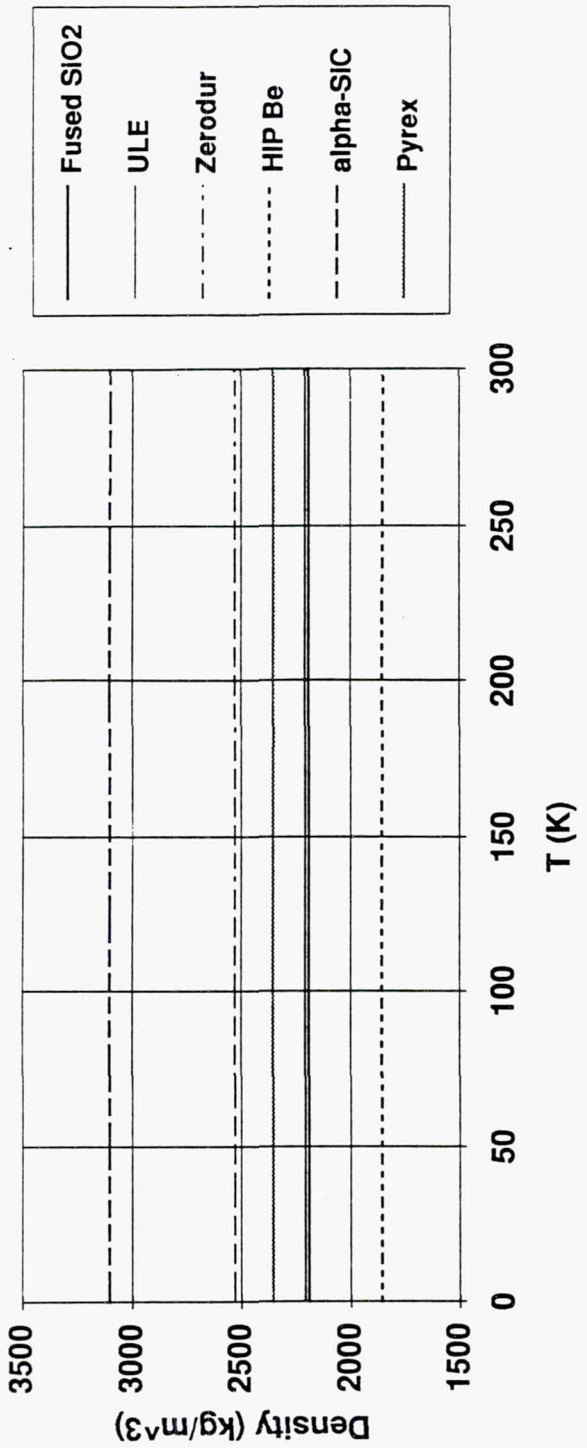

Figure B-7. Density of Candidate Mirror Materials.

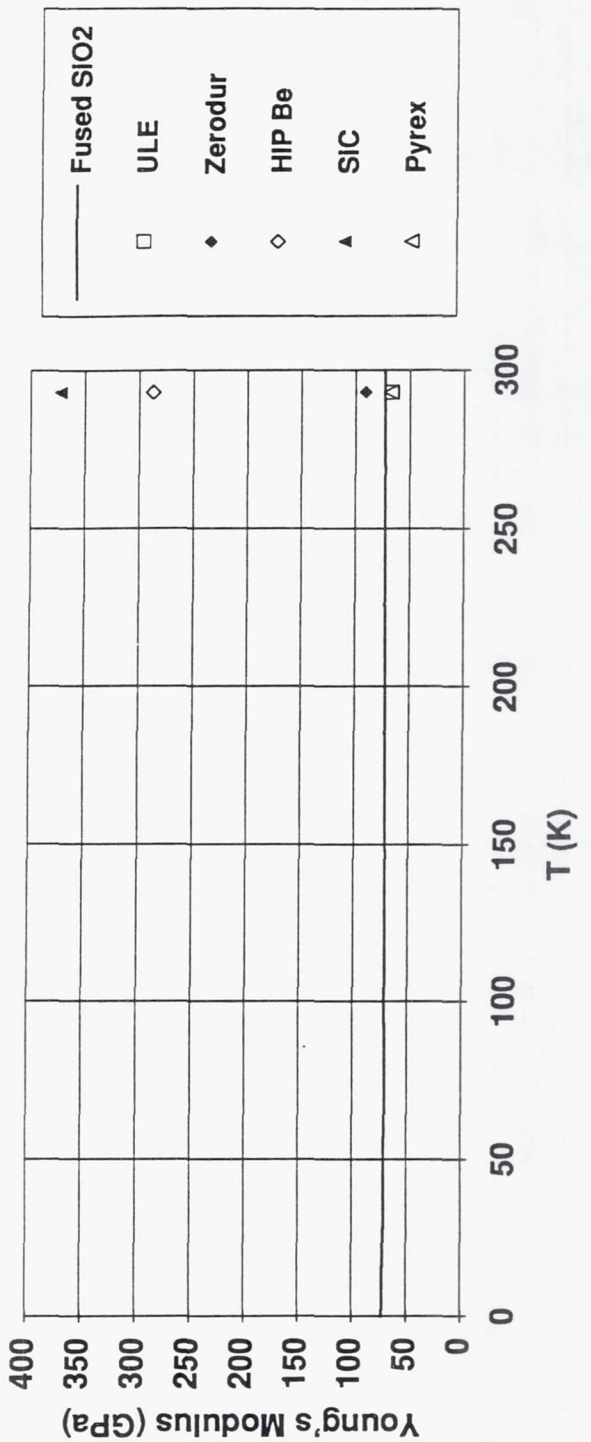

Figure B-8. Young's Modulus of Candidate Mirror Materials.

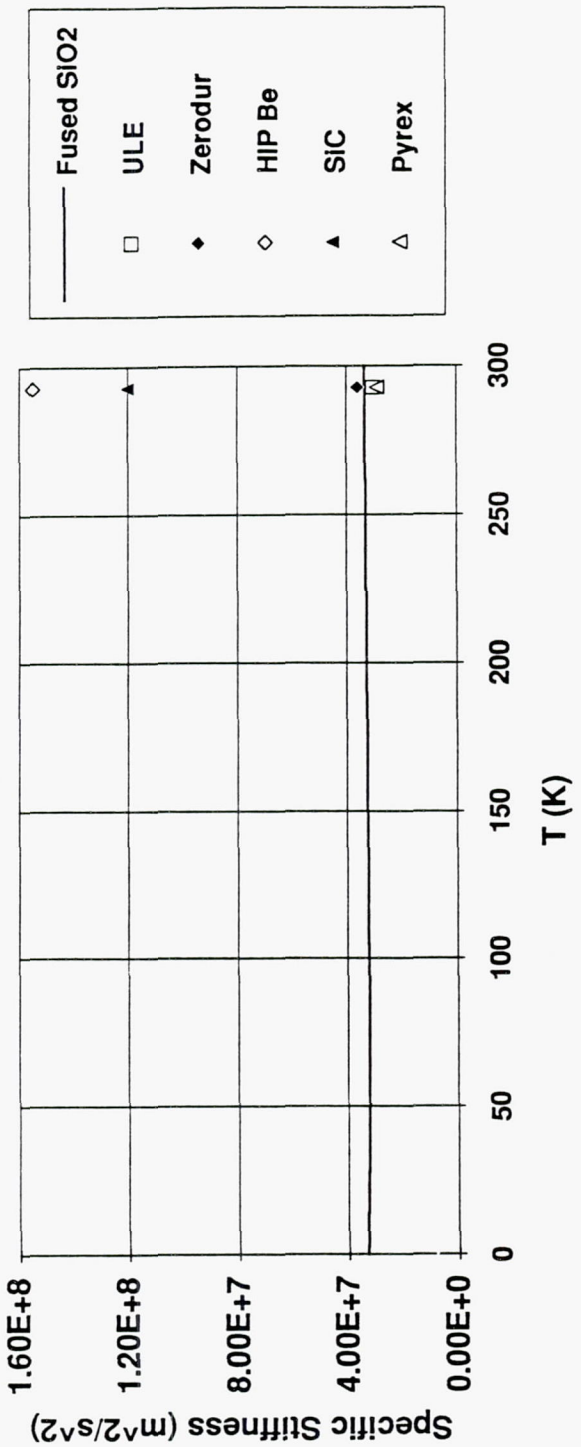

Figure B-9. Specific Stiffness of Candidate Mirror Materials.

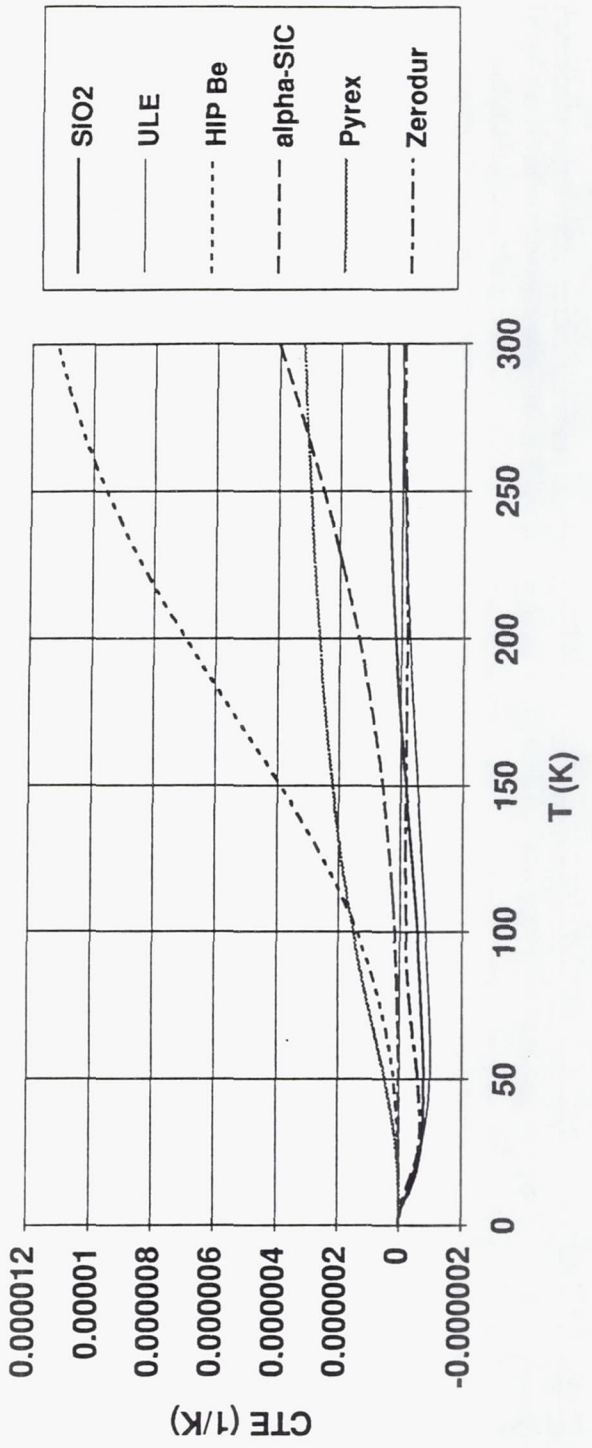

Figure B-10. Coefficient of Thermal Expansion of Candidate Mirror Materials.

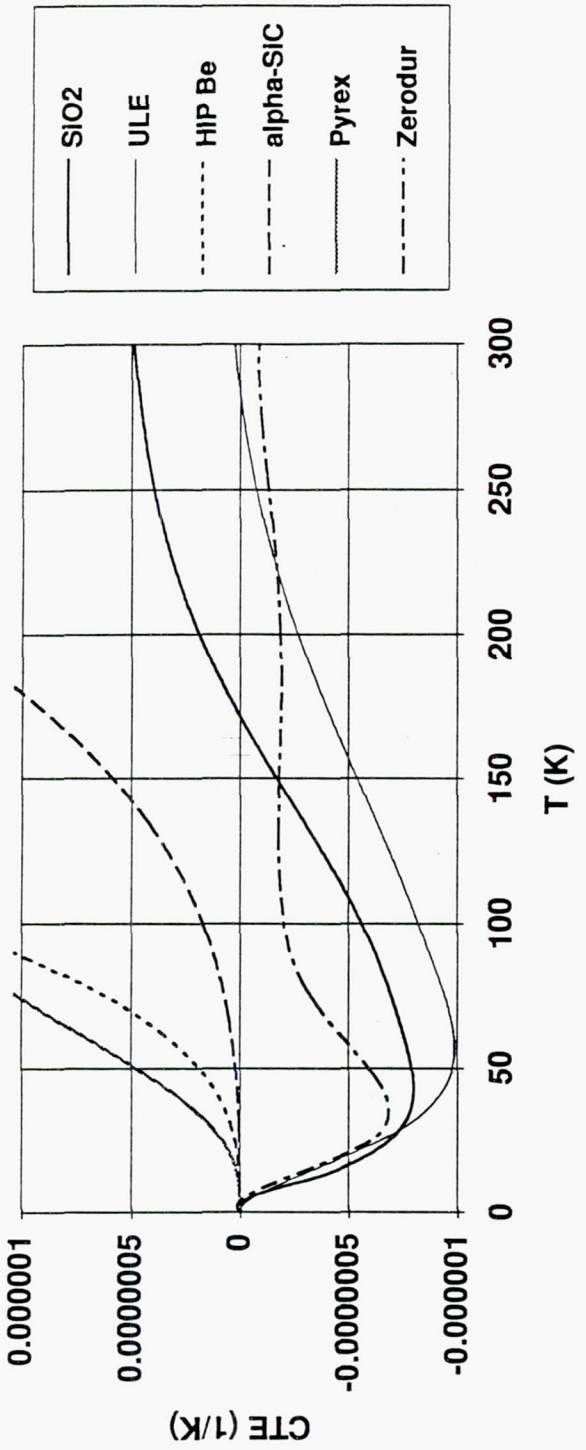

Figure B-11. Coefficient of Thermal Expansion of Candidate Mirror Materials. (Expanded vertical scale of Figure B-10.)

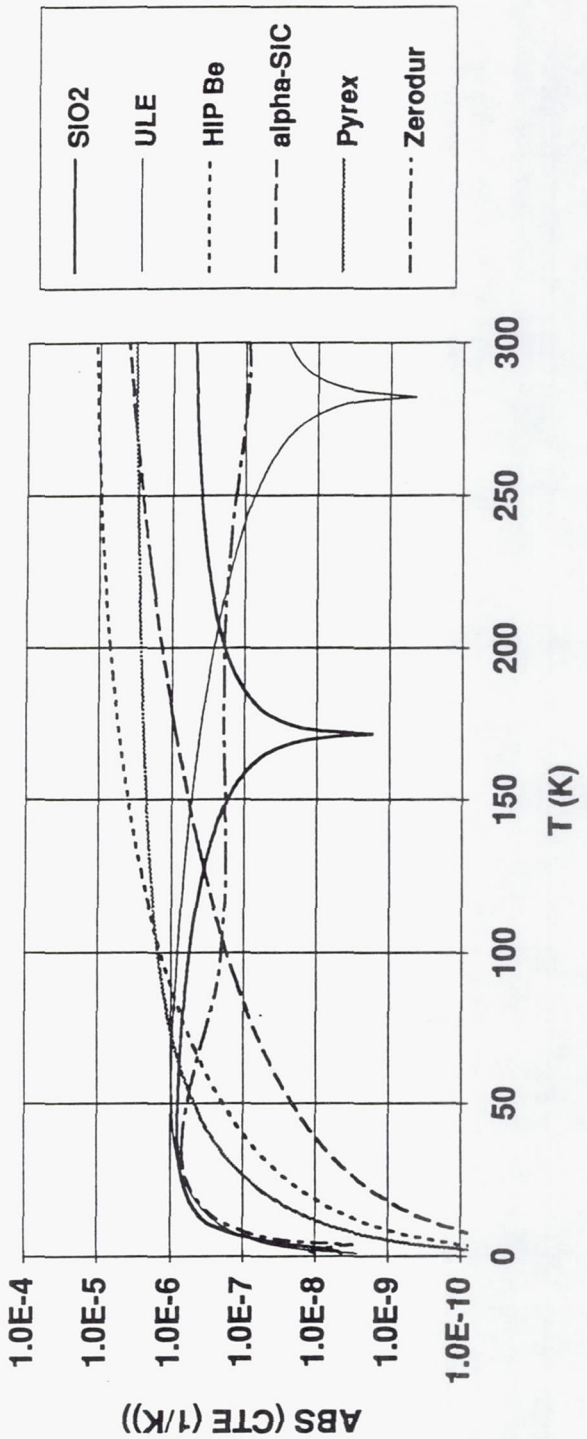

Figure B-12. Coefficient of Thermal Expansion of Candidate Mirror Materials. (Semi-log plot of absolute values of the CTE's shown in Figure B-10.)

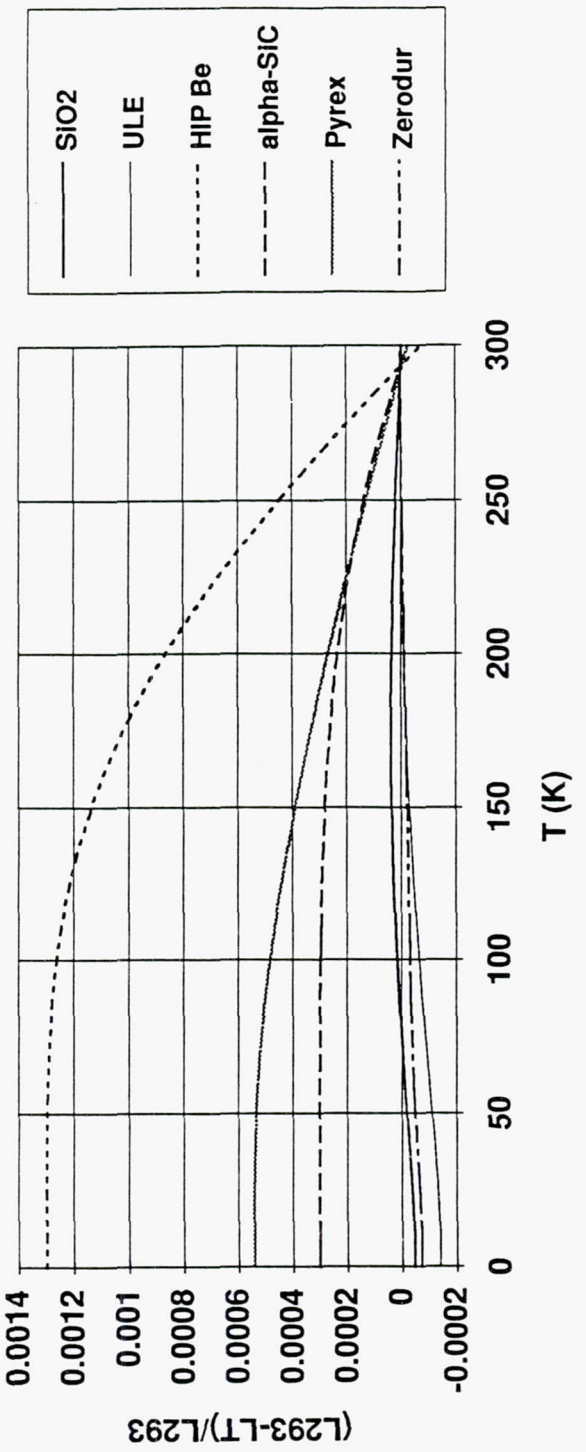

Figure B-13. Integrated Thermal Contraction of Candidate Mirror Materials. Reference temperature is 293 kelvins. Note that fused quartz, Zerodur, and ULE have a net expansion upon cooling to very low temperatures.

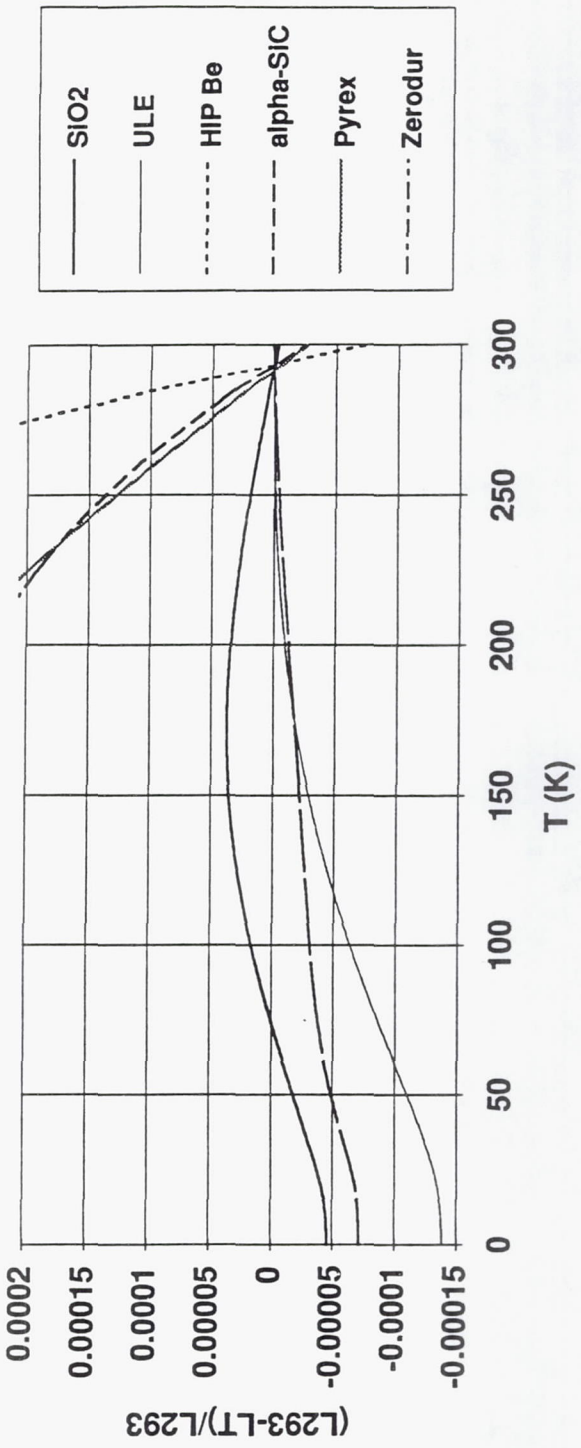

Figure B-14. Integrated Thermal Contraction of Candidate Mirror Materials. (Expanded vertical scale of Figure B-13.)

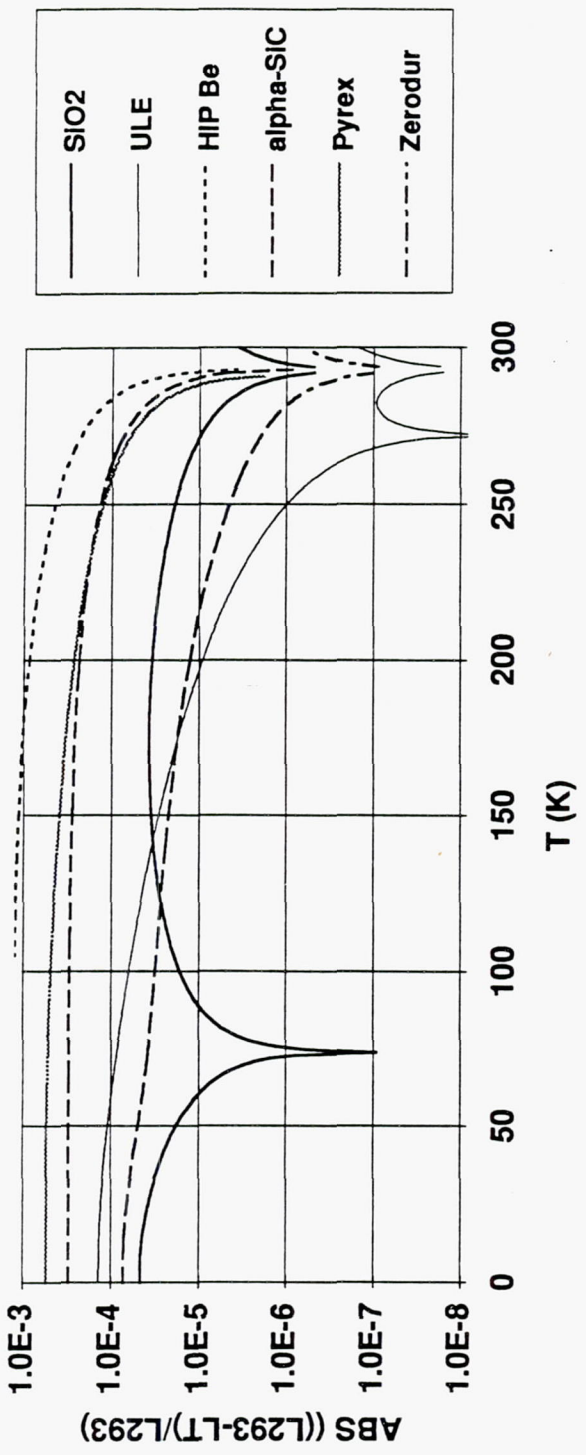

Figure B-15. Integrated Thermal Contraction of Candidate Mirror Materials. (Semi-log plot of the absolute values of the $\Delta L/L$'s of Figure B-13.)

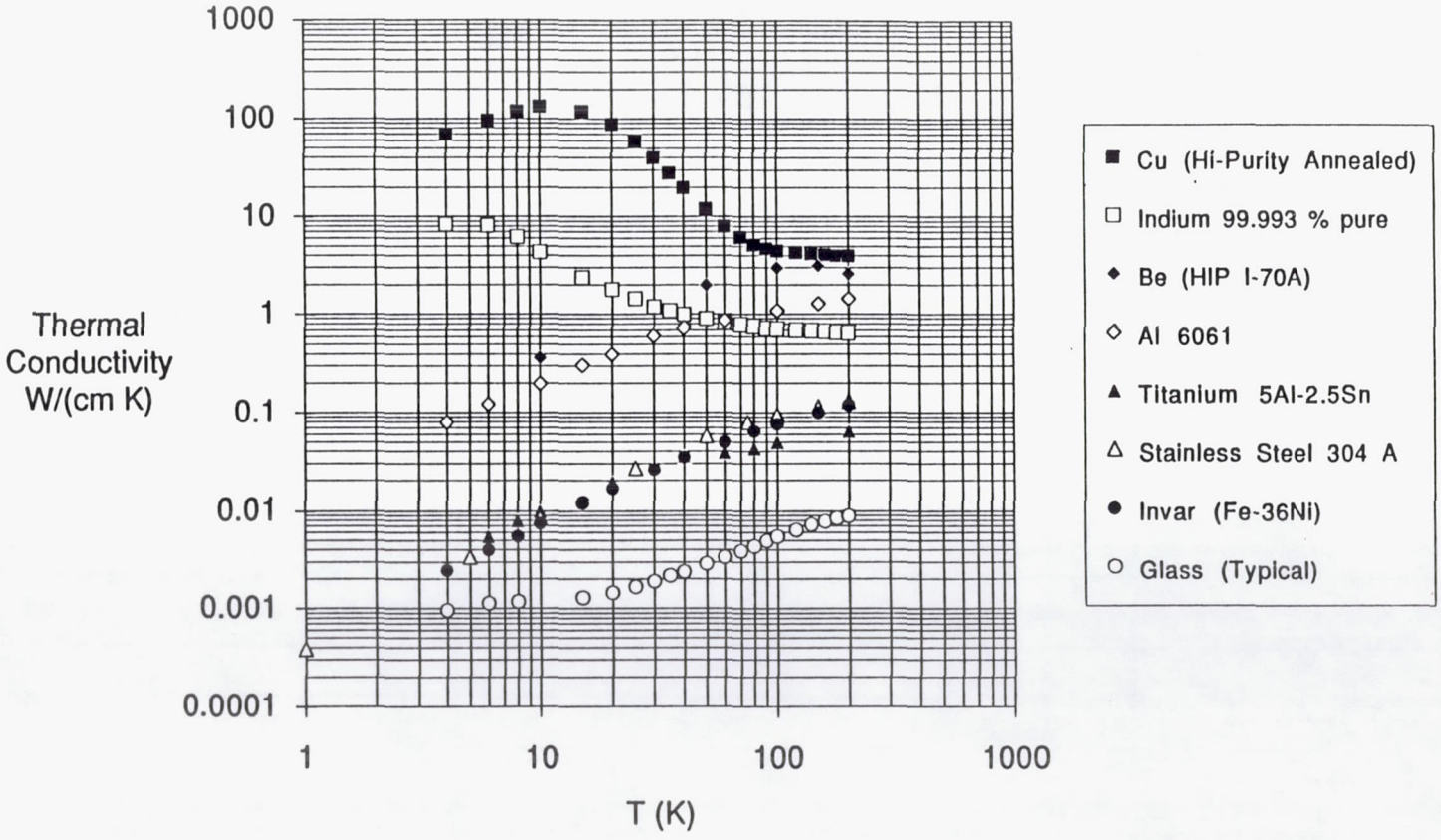

Figure B-16. Thermal Conductivity of Metals and Glass.

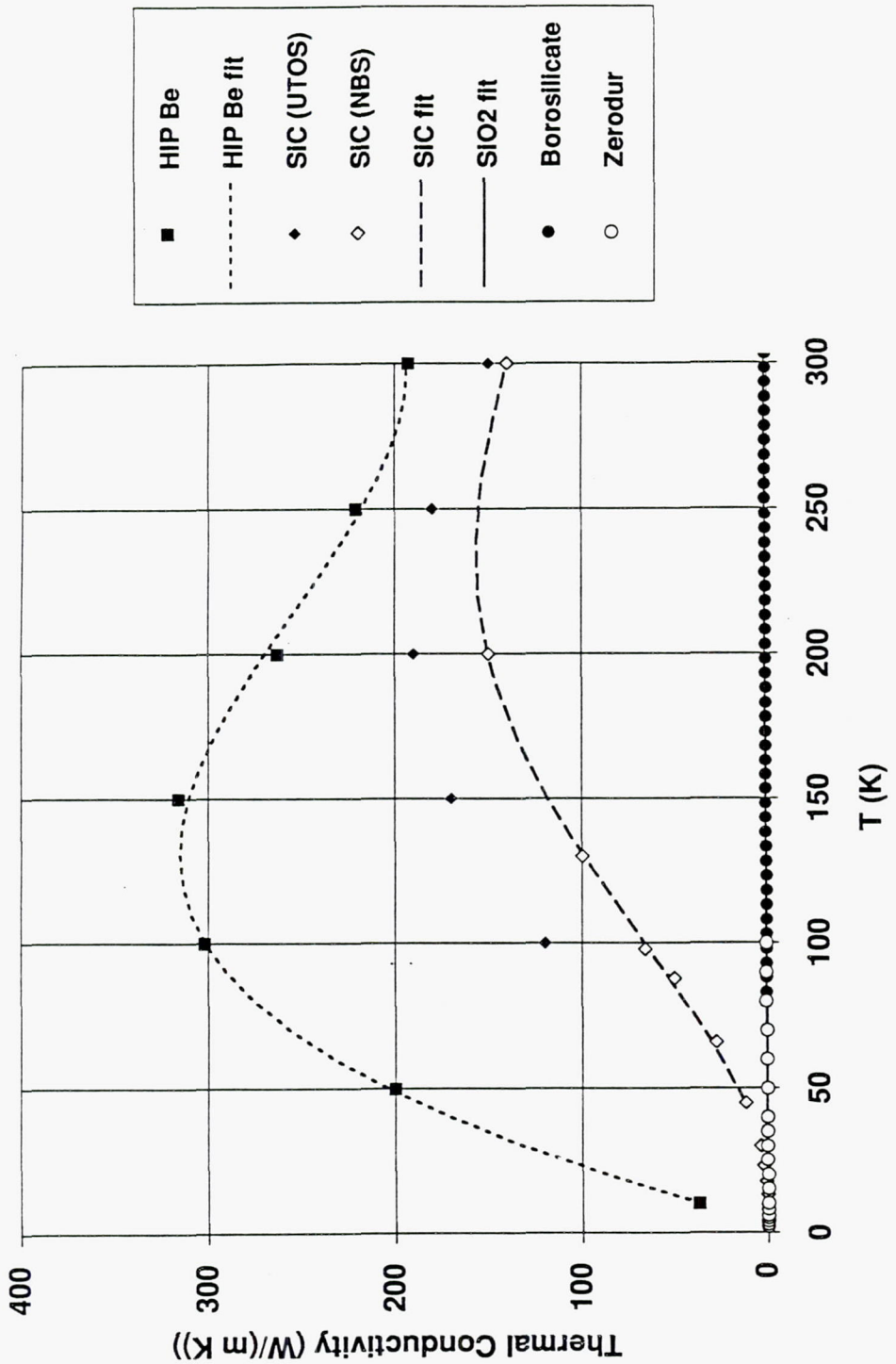

Figure B-17. Thermal Conductivity of Candidate Mirror Materials.

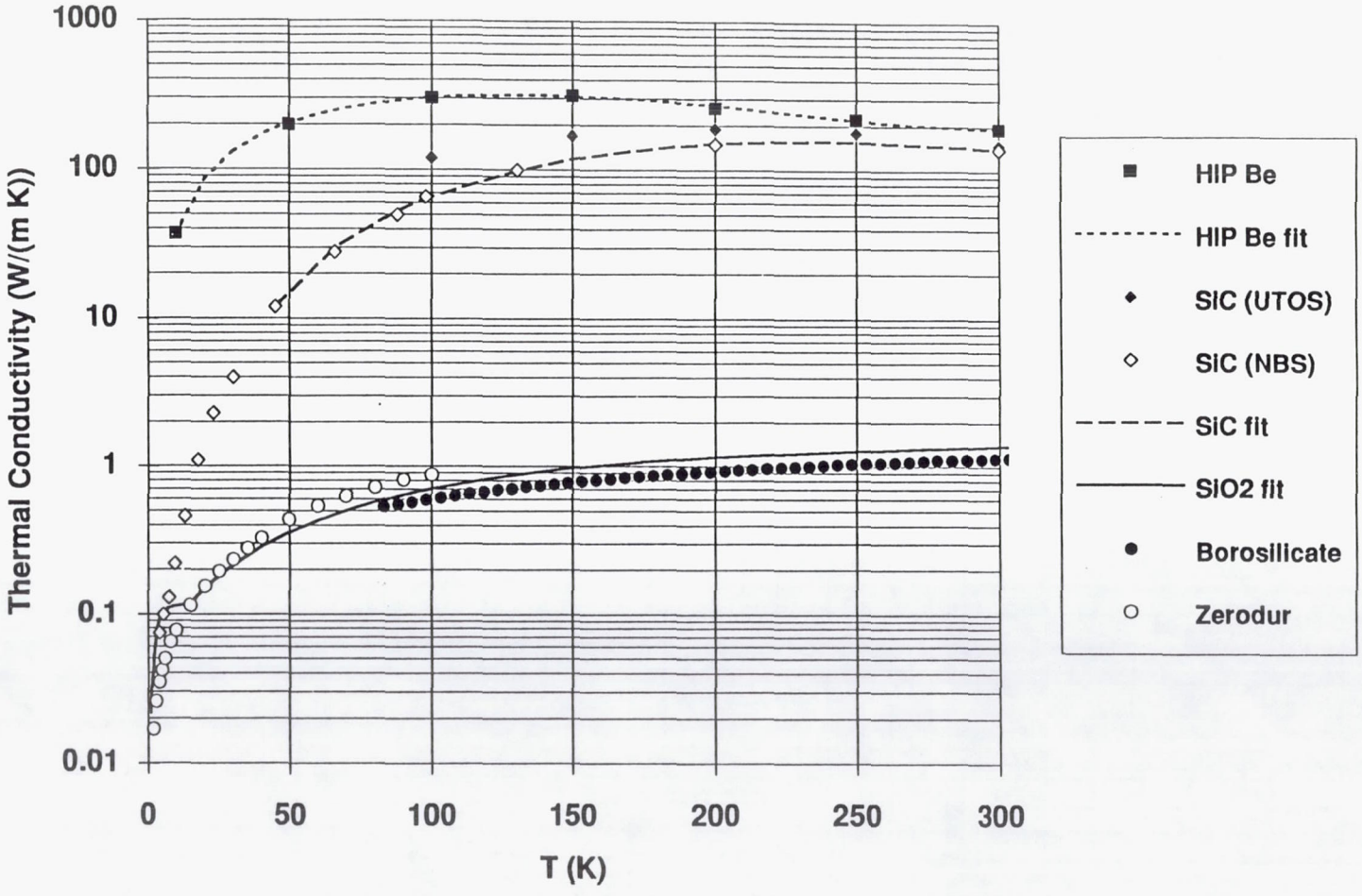

Figure B-18. Thermal Conductivity of Candidate Mirror Materials. (Semi-log plot of Figure B-17.)

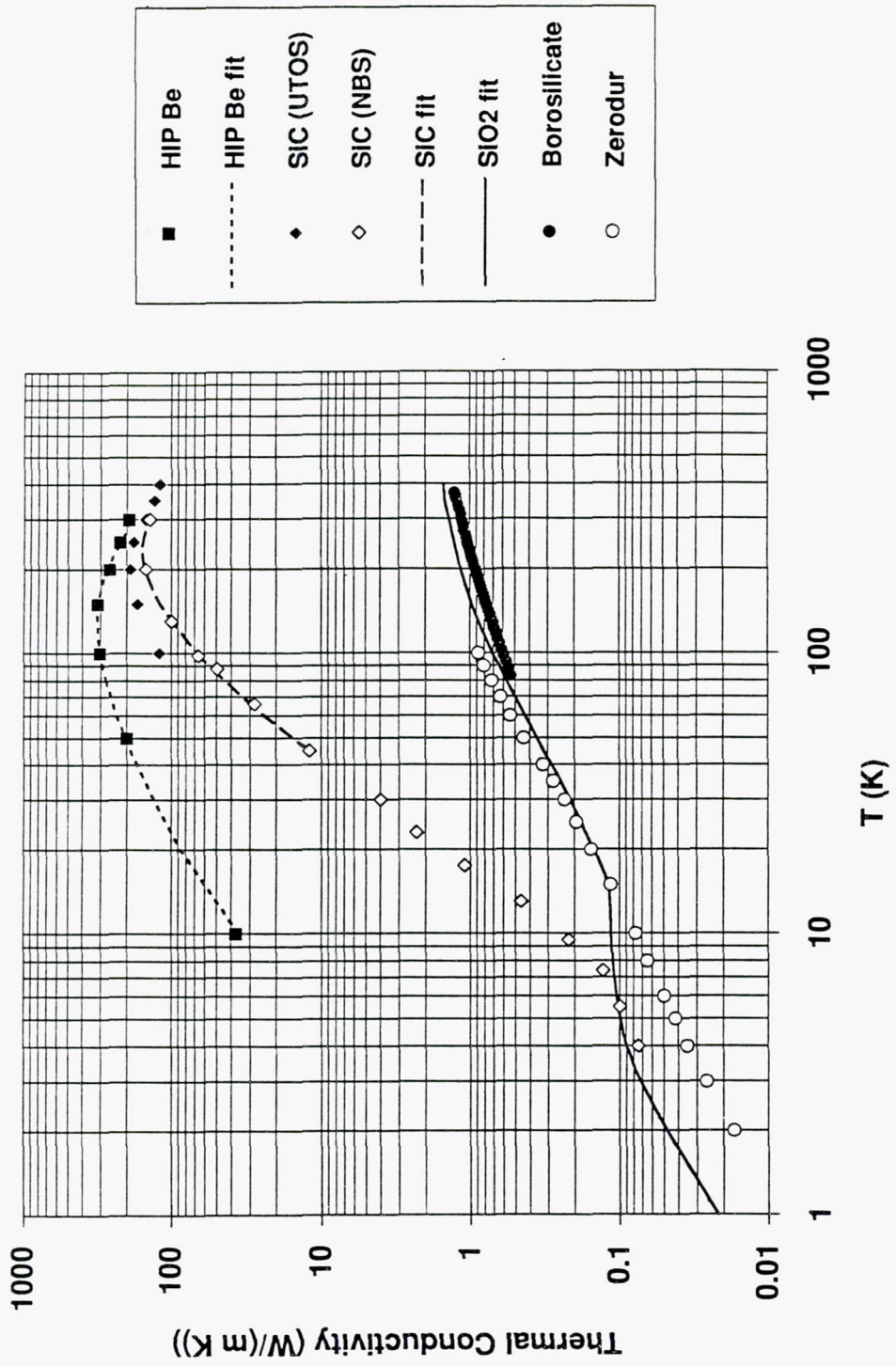

Figure B-19. Thermal Conductivity of Candidate Mirror Materials. (Log-log plot of Figure B-17.)

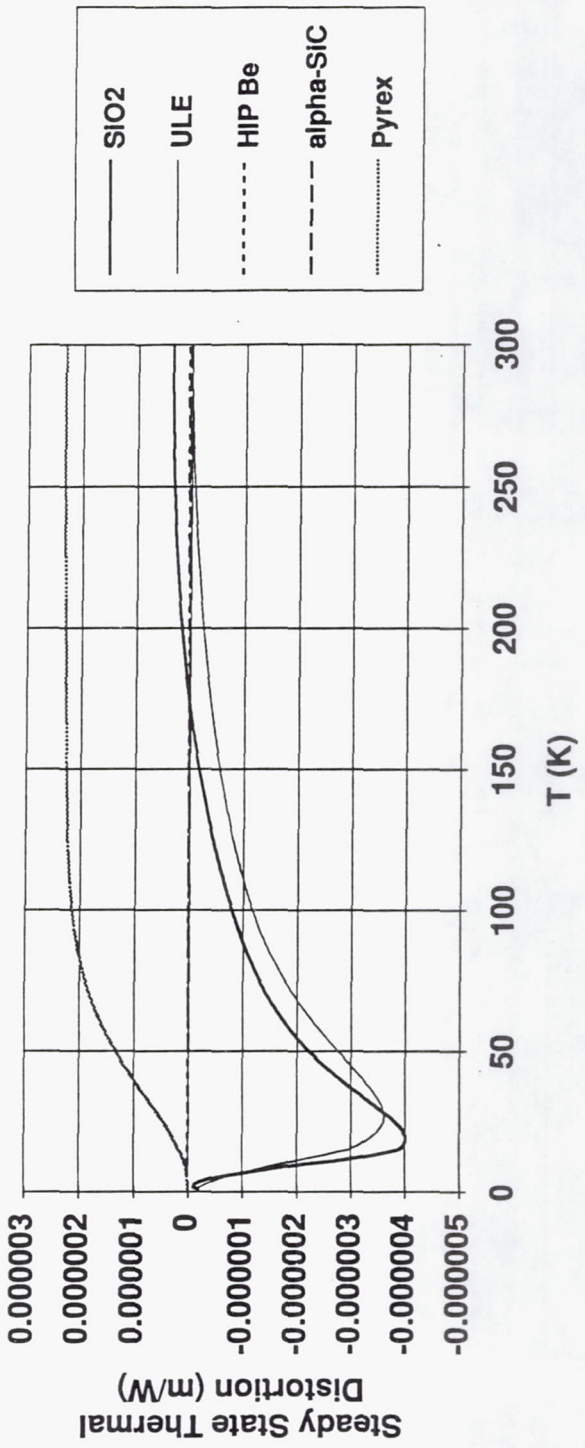

Figure B-20. Steady State Thermal Distortion Coefficient of Candidate Mirror Materials.

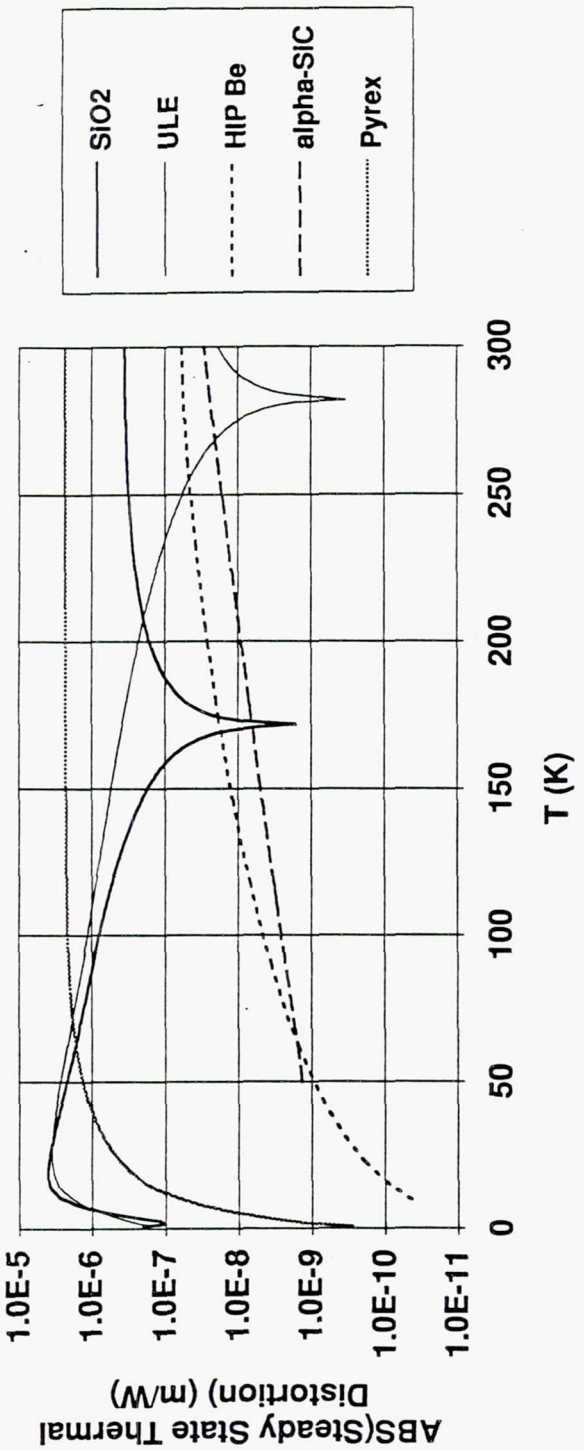

Figure B-21. Steady State Thermal Distortion Coefficient of Candidate Mirror Materials. (Semi-log plot of the absolute values of the SSTD's of Figure B-20.)

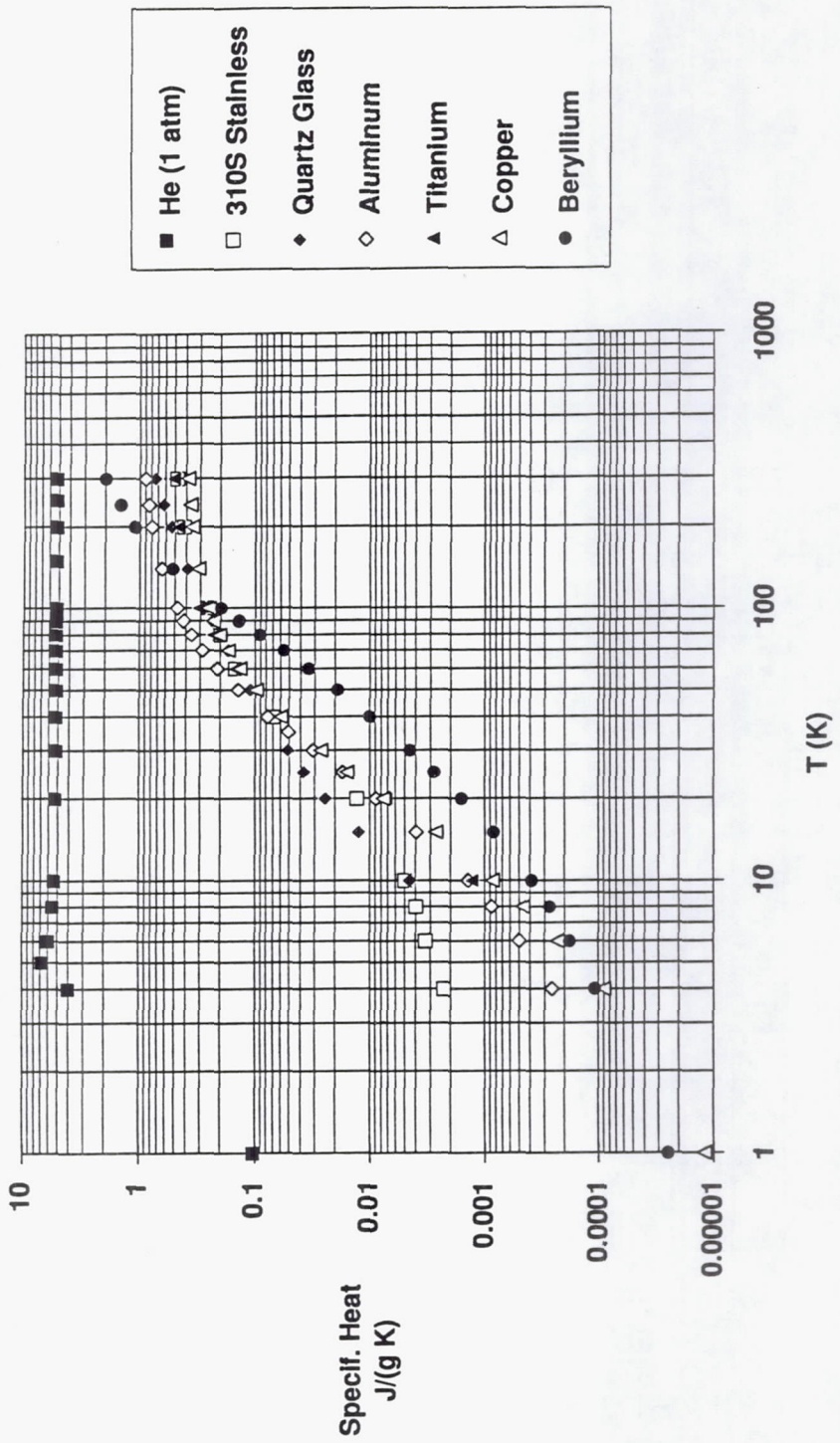

Figure B-22. Specific Heat of Helium, Metals, and Fused Quartz.

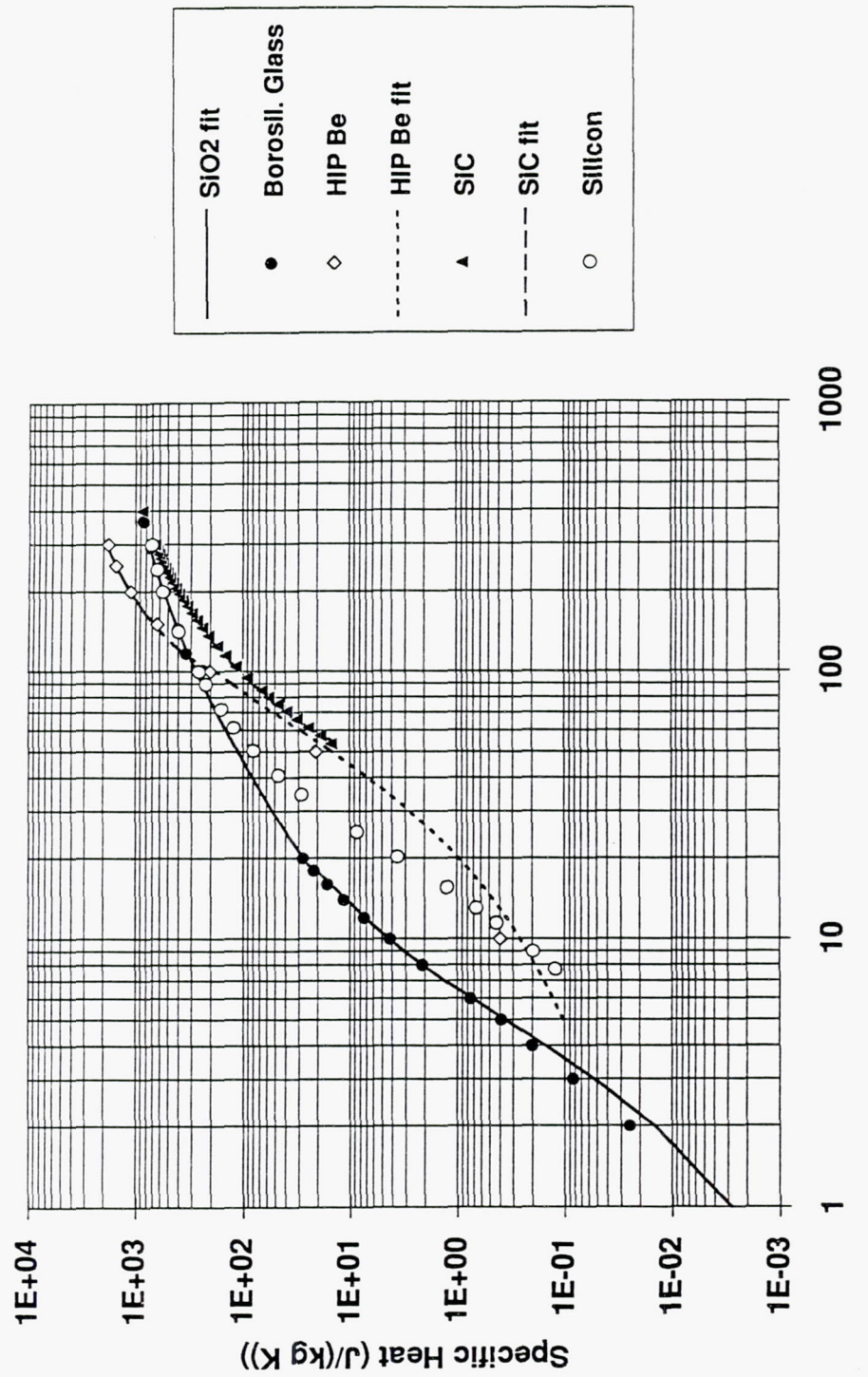

Figure B-23. Specific Heat of Candidate Mirror Materials.

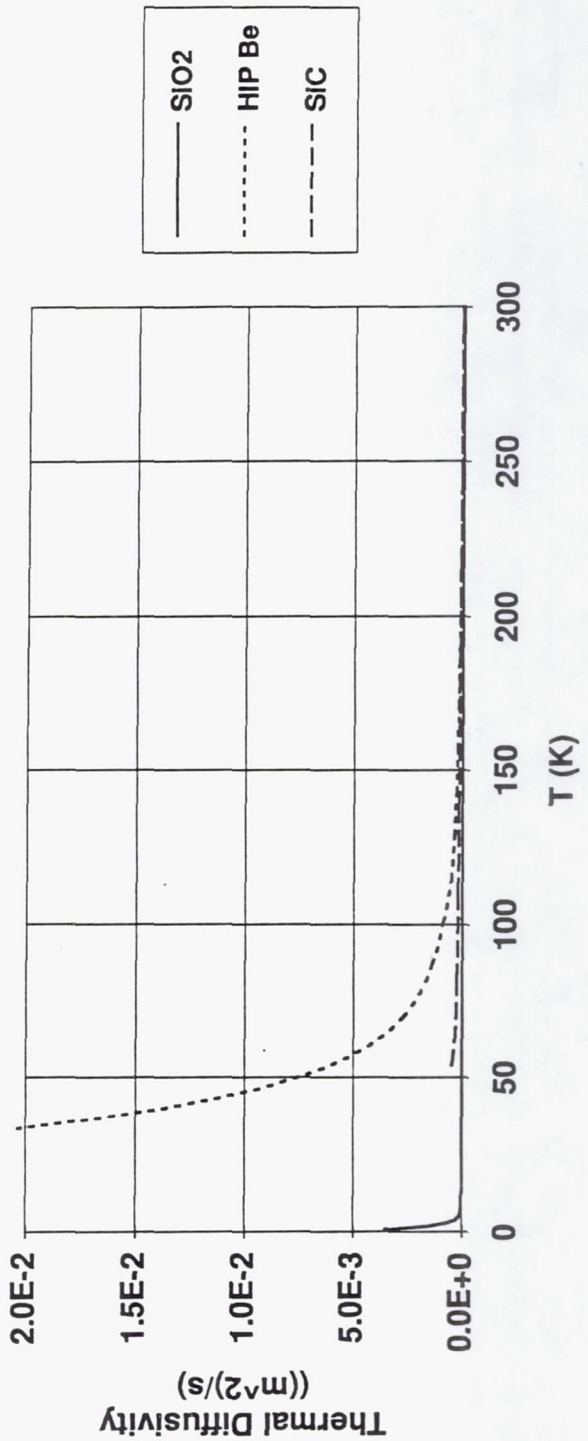

Figure B-24. Thermal Diffusivity Coefficient for Candidate Mirror Materials.

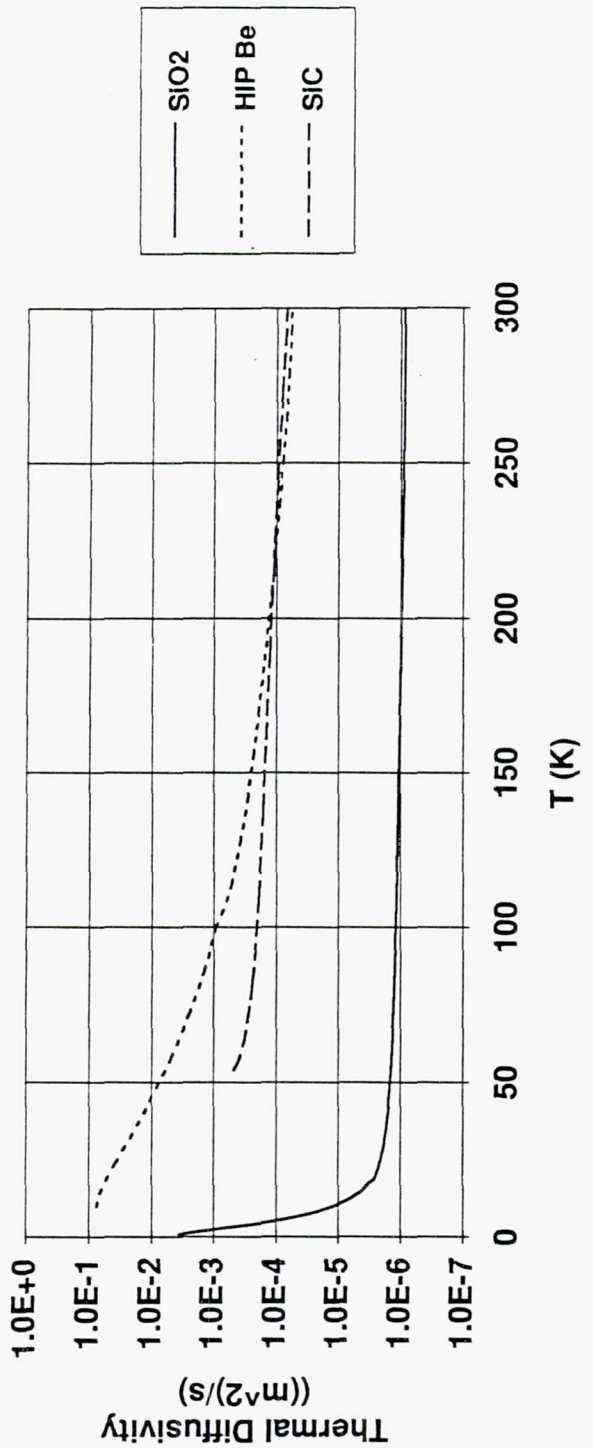

Figure B-25. Thermal Diffusivity Coefficient for Candidate Mirror Materials. (Semi-log plot of Figure B-24.)

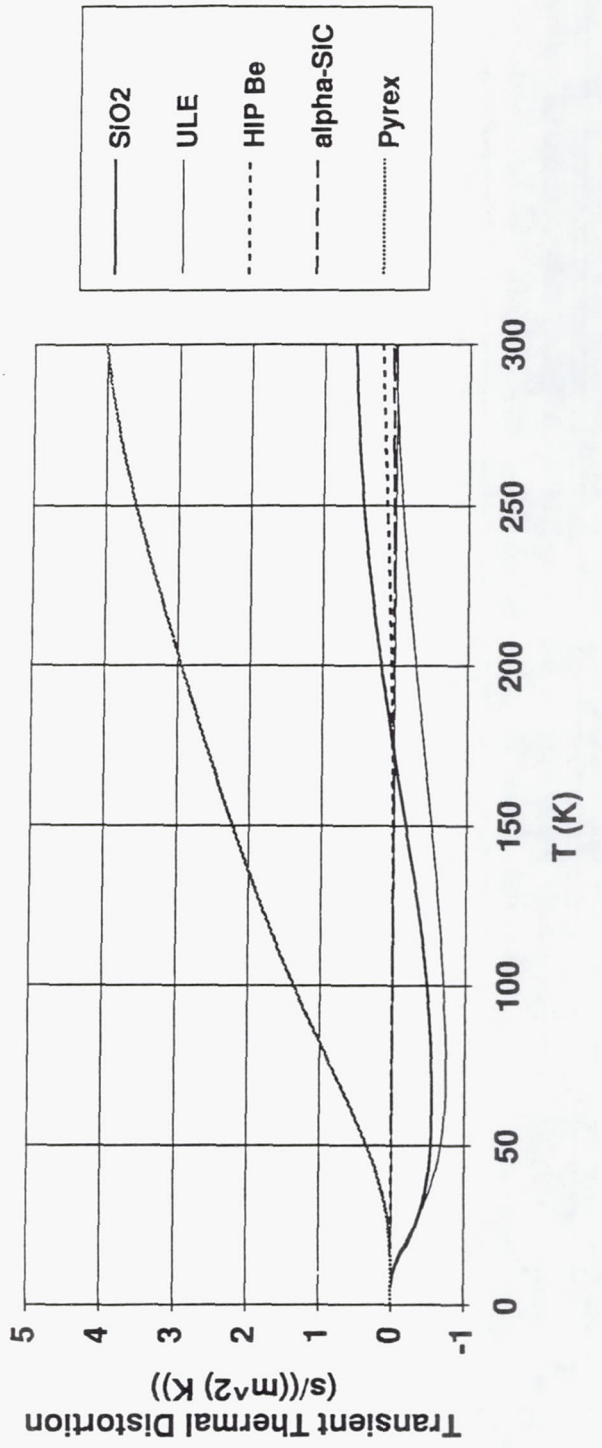

Figure B-26. Transient Thermal Distortion Coefficient for Candidate Mirror Materials.

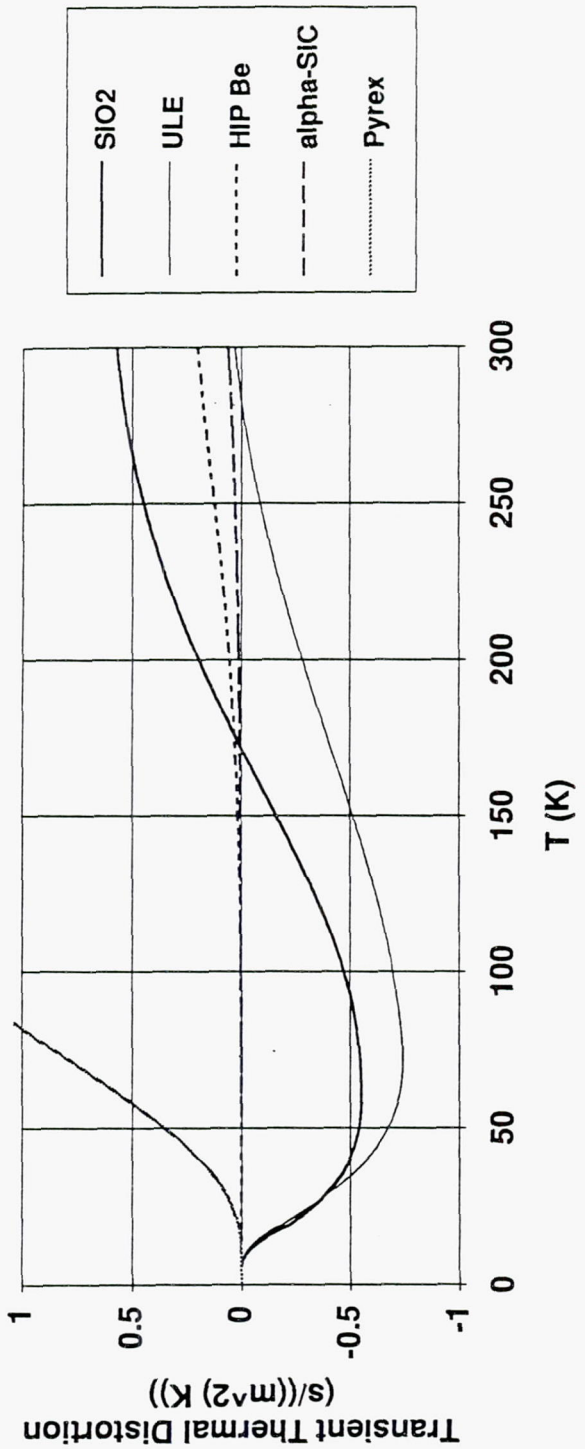

Figure B-27. Transient Thermal Distortion Coefficient for Candidate Mirror Materials. (Expanded vertical scale of Figure B-26.)

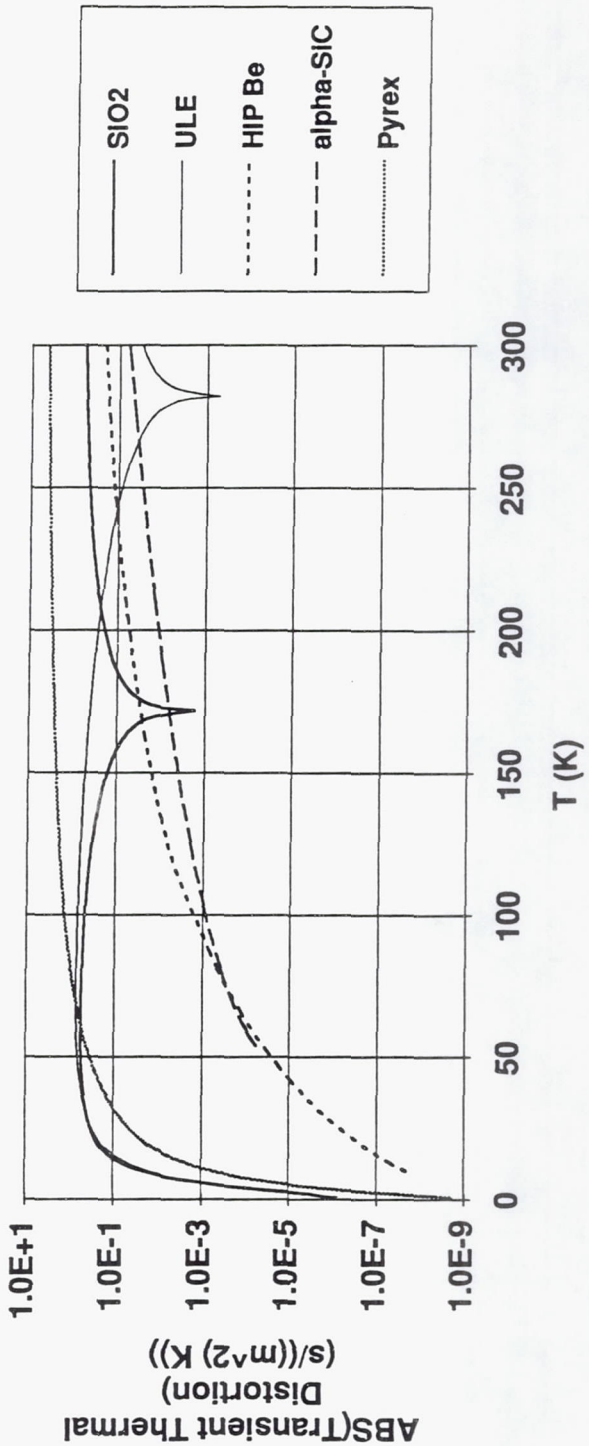

Figure B-28. Transient Thermal Distortion Coefficient for Candidate Mirror Materials. (Semi-log plot of the absolute values of the TTD's of Figure B-26.)